Field Trip Guide for the 70th Annual Meeting of the New York State Geological Association

October 2-4, 1998
Binghamton University
Binghamton, NY

Field Trip Guide for the
70th Annual Meeting of the
New York State
Geological Association

Edited by:

H. R. Naslund

October 2-4, 1998
Binghamton University
Binghamton, NY

Table of Contents

NEW YORK STATE GEOLOGICAL ASSOCIATION

FIELD TRIP TO EASTERN NEW YORK:

BARROVIAN METAMORPHISM IN DUTCHESS COUNTY

3 October 1998

Thomas W. Donnelly
Dept. of Geological Sciences
State University of New York
Binghamton NY 13902-6000

INTRODUCTION

In the late 1800's, the notion of metamorphism was beginning to occupy a distinct place in geological thinking. The first studies linking metamorphic phenomena to distinctive mineralogical assemblages were of contact metamorphic aureoles around shallow igneous bodies. In the English speaking world, the notion of regional metamorphism, with "depth zones" marked by distinctive mineral assemblages is at attributed to George Barrow , who described such zones in 1893 in a Proterozoic meta-sedimentary sequence in the Scottish Highlands. We call these zones "Barrovian Zones" in his honor.

Dutchess County, New York, was mapped by Robert Balk of Mt. Holyoke College during a nine year period in the 1920's and 30's. Balk's paper (1936) is a classic study of the structural geology and stratigraphy of a highly deformed area. Balk's attractive sketch map has been included as Figure 1. His paper was accompanied by a mineralogical - petrological paper by his friend and colleague Tom Barth (1936) of the Mineralogical Institute, Oslo. Although this area has been recognized as perhaps America's pre-eminent Barrovian terrane, these authors interpret the metamorphism as due to igneous activity, including "emanations".

This area remains one of the clearest Barrovian sequences in the world. Unfortunately, possibly because of the eminence of these two papers, later geologists seem to have been somewhat intimidated, and relatively few studies have been undertaken here in subsequent years. Garlick and Epstein (1967) attempted to determine maximum temperatures of metamorphism using oxygen isotopes of metamorphic mineral assemblages. Vidale (1973, 1974) investigated the vein mineralogy and showed that vein-mineral assemblages were a good indication of metamorphic grade. Hames et al (1991) used $^{40}Ar/^{39}Ar$ dating of micas to determine an age of about 445 m.y. for the Taconian metamorphism.; they also found an eastern zone overprinted with younger (390-400 m.y.; interpreted as Acadian) metamorphic modification. Two papers by Whitney et al(1996a and 1996b) have investigated detailed mineralogy, concentrating on the garnets.
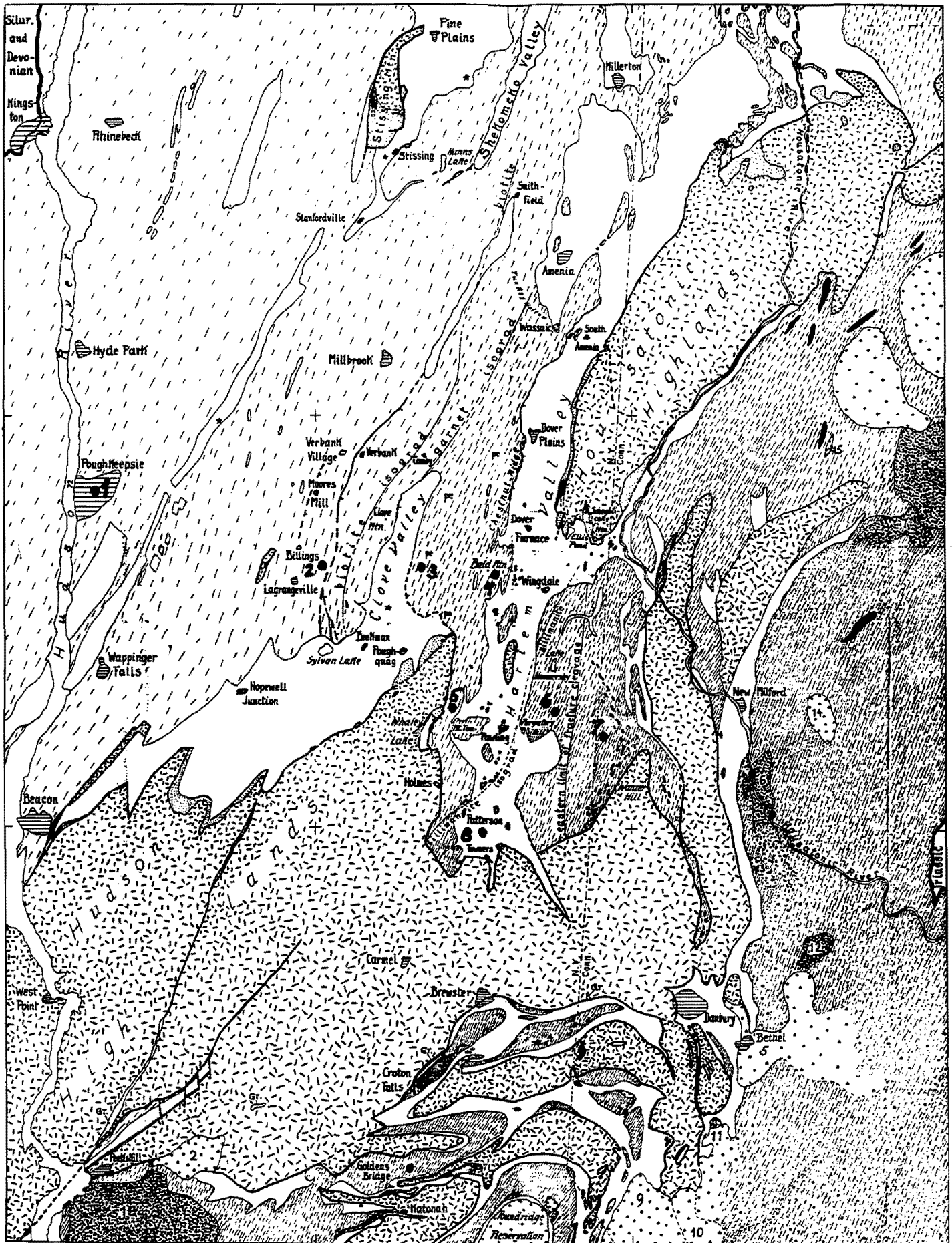
1

Figure 1. Sketch geologic map of Balk (1936). The stops for the trip are shown as numbered black dots.

GEOLOGICAL BACKGROUND

The county is underlain mainly by Cambrian and Ordovician wackes deposited during the geosyncline-filling stage of the Appalachian geosyncline. It is the metamorphism of these sedimentary rocks during the Taconian Revolution (end of Ordovician) that we will be examining on this field trip.

Following is a brief outline history of the geological evolution of the northeastern Appalachian chain, taken from Bird and Dewey (1970). Figure 2 outlines their scheme.

1) Early Stage (550 to 450 m.y.; Cambrian and early Ordovician)

At the beginning of this stage the emergent North American continent subsided in its eastern portion. A vast shallow sea covered the eastern half of North America and left a deposit of quartz-rich beach deposits on top of deeply eroded pre-Cambrian metamorphic and igneous rocks. In this area we see this sequence as the Poughquag quartzites (which we will not see on this trip).

A carbonate platform developed on the eastern margin of this rifted continent. We will see some of the marbles which originated as this platform (Stockbridge marbles).

2) Middle Stage (450 to 534 m.y.; late Ordovician)

During this stage thick wackes accumulated in a "geosyncline" which at this time was adjacent to a passive margin of the Atlantic Ocean ("IAPETUS Ocean"). We now refer to this deposit as a continental margin prism. Bird and Dewey (1970) call it an "exogeosyncline" Subduction beneath a volcanic ridge in western New England (to the east) elevated a tectonic welt, whose erosion shed sediments to the west, in a depression adjacent to the carbonate platform on the eastern edge of the continent. This sequence was deposited initially on the downwarped carbonate platform. These wackes have been known as the "Hudson River Shales" or "Normanskill Shales", and they were the focus of studies a century and a half ago by James Hall that led to the initial concept of geosynclines.

In the later stages of their deposition these fine-grained wackes were tectonically interlayered with blocks of older sedimentary sequences that slid into the depression from the rising welt to the east. The dominantly Cambrian and early Ordovician sediments are sandier than the late Ordovician shales, and the entire sequence is a tectonically interlayered on a scale of a mile or so. Mapping these tectonic units and deciphering their stratigraphy, even in higher metamorphic grades, has been a major accomplishment of many field geologists, mainly from Columbia and Harvard Universities, during this century.

During this trip we will see metamorphosed equivalents of both the younger (mainly autochthonous and finer grained) and older (mainly allochthonous and coarser grained) sediments. Thus, the rocks seen here are not all of the same original composition.

At the final, climactic stage of the Taconian Revolution, paleo-Europe collided with the North American platform and subduction ceased. further tectonic thickening occurred, and granitic melts were generated, mainly slightly to the east of the area visited on this trip.

3) Third and later stages. (437 - 345 m.y.; Silurian to late Devonian)

In the early part of this stage the emergent, tectonically thickened terrane was rapidly eroded to sea level, with debris carried as far west as western New York ("Queenstown Delta"). A vast inland sea became the locus of evaporite deposits, and the quartz-rich sand beneath and around this deposit is represented locally by the Shawangunk sandstone. Renewed convergence to the east resulted in a renewed uplift, and the shed sediments formed the Devonian "Catskill Delta". This second convergence largely of western and southern Europe and western Africa, was completed in latest Devonian and created the super-continent called "Laurasia". This continent remained welded until the rifting at about 200 m.y. which produced the present-day Atlantic Ocean, which formed more or less along the earlier suture line.

3
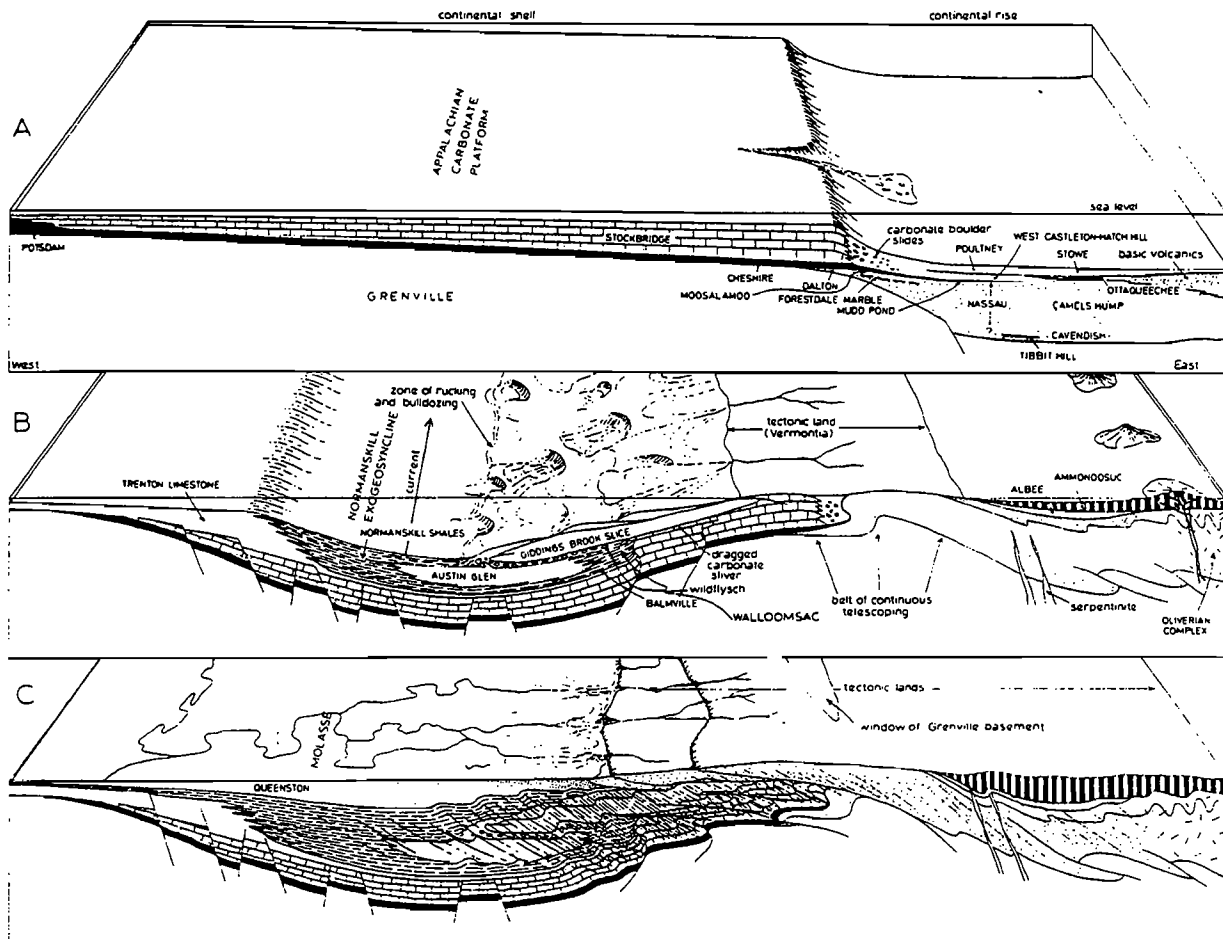
Figure 2. Bird and Dewey's (1970) tectonic evolution scheme, as a series of block diagrams. The continental platform is on the left and the IAPETUS ocean on the right. Note the platform carbonates (Stockbridge), autochthonous continental rise sediments (Austin Glen) and allochthonous slices (Giddings Brook). In the top diagram (A), our area is on the right side. In the second and third diagrams (B and C), our area is approximately in the middle.

Caption for Figure 1. (Explanation of the map)
The short-lined pattern (denser lines to the east) is the clastic Cambrian and Ordovician sedimentary package that is the main focus of the trip. Underlying pre-Cambrian is the random-orientation dash pattern, and overlying it is a narrow belt of densely stippled basal Cambrian Poughquag quartzite. The platform carbonates are unpatterned. Isograds, marking the first appearance of distinctive metamorphic minerals, are shown for the biotite, garnet, and sillimanite grades. There are numerous small plutons scattered especially on the eastern side of the trip; these are shown by a variety of random-orientation patterns.
The stops for the field trip are shown as numbered black dots.

According to the excellent tectonic map of Williams (1978) the rock units seen here are divided into continental shelf carbonate deposits, and continental rise prism clastics. Rock units corresponding to the island-arc welt, the remnants of mid-ocean volcanics and associated sediments, and "exotic" parts of the European continent are all found to the west of the present area.

METAMORPHISM OF THE EARLY PALEOZOIC WACKES AND ASSOCIATED ROCKS

Most of the trop will be devoted to the prograde metamorphism of the "package" of Cambrian and Ordovician tectonic slices during the first major event (end-Ordovician). We see these rocks presently displayed with higher grades of metamorphism to the east, because the later Devonian event raised the rocks more to the east. Subsequent erosion exposed levels that were originally deeper in this direction.

Although they are exposed in this area, time limitations prevent us from examining the pre-Cambrian basement beneath the Paleozoic stratigraphic sequence, and the basal Cambrian quartz-rich shallow water sandy deposits. We will see mainly the wacke sequence, and we will examine one exposure of the marble sequence.

STOPS:

The first two exposures we will be unable to examine, both because of time limitations and the difficulties of handling groups along busy highways. However, these exposures can be profitably examined from the vans. The first is a prominent klippe of dolomite which occurs just west of Newburgh, just before we turn on to highway 9. This dolomite represents the originally platform limestone which was later dolomitized. These dolomites (indeed, many dolomites elsewhere) have abundant silica, either representing original sedimentation or introduced along with the magnesium of dolomitization.

The second exposures to be examined from the van are the layered wackes exposed magnificently along the entrance to the Mid-Hudson Bridge. These are classic Austin Glen (='Hudson River Shales") with beautifully displayed graded bedding. Although the rocks seem to be entirely argillaceous in gross inspection, under the microscope there are revealed abundant tiny dolomitic fragments from the platform. These are the protolith of many of the metamorphic rocks seen later.

First stop [Unmetamorphosed],
Grand Ave and Main Street, Poughkeepsie. We will stop in the small parking lot on this corner. (The large rectangular block is a fine example of a New England two-mica granite). The rocks exposed along Grand Avenue (beware of cars!) are highly tectonized versions of the wacke seen just on the other side of the river. They have not developed a metamorphic mineralogy, and we refer to these as highly tectonized, unmetamorphosed sedimentary rocks. The fine-scale graded bedding is still visible in crumpled fragments. Original sedimentary sulfide has recrystallized as larger pyrite crystals, which weathering has created brown streaks on the outcrops. There is a slight wash of gypsum also present. Some original resistant sandy beds are visible as detached blocks within this melange. These blocks are dark brown because of the weathering of iron-rich dolomite crystals.

Second stop [Biotite Grade],
Wingdale Road, just east of the junction with Highway 55. This stop is our first glimpse of metamorphism. The fine-grained biotite visible in thin section (and in hand specimen if you have good eyes and imagination!) gives the rock a shiny luster. The evidence for metamorphism is mainly the quartz veins, which are themselves deformed by physical deformation as they developed. The ubiquity of these veins in metamorphosed terranes results from the fact that most metamorphic reactions of sedimentary protoliths commonly produce water and SiO_2. Vidale (1974) has studied these vein assemblages in Dutchess County and found that, at increasing higher metamorphic grades to the east, the vein mineralogy includes mica and feldspar, in addition to quartz. Stratigraphic layering is not visible here.

KEY

CHL = Chlorite
Q = Quartz
Mg = Muscovite
CTD = Chloritoid
ST = Staurolite
BI = Biotite
AB = Albite
OR = orthoclase
AS = Alumino Silicate
KY = Kyanite
AND = Andalusite
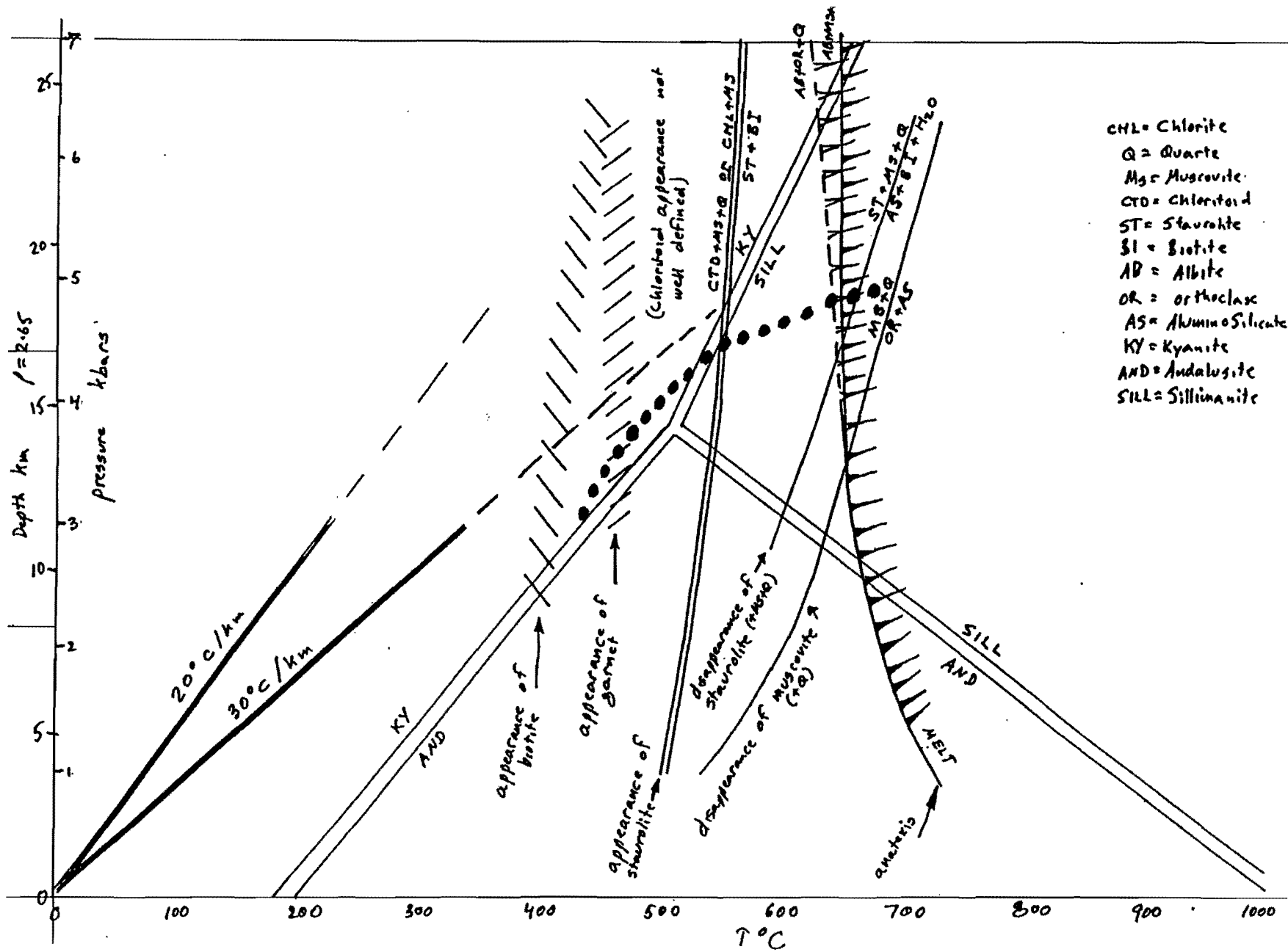SILL = Sillimanite

Figure 3. P - T diagram, showing the alumino-silicate triple point and reaction lines of the ALS system; lower (20°C/km) and higher (30°C/km) thermal gradients, a few important metamorphic mineral reactions, and the beginning of melting (anatexis). Approximate P - T path during metamorphism (estimated, less certain at higher T) shown as black dots (from Whitney et al 1996).

Third stop [Garnet Grade],
Wingdale Road, just beyond intersection to Clove and Clove Valley. Here the rock represents metamorphism of a fine sandy sediment. Both chloritoid and garnet are visible in rocks seen along the highway in outcrop. Chloritoid is an aluminous mineral which is stable apparently within a fairly narrow range of T and P, passing to staurolite at slightly higher grades. There is abundant tourmaline in thin section. Evidently this is detrital, because xenotime, apatite, and thorianite have also been found.

Fourth stop [Staurolite grade],
Wingdale road, vicinity of Bald Mountain, beyond Pheasant Ridge. Here the protolith was more quartz rich and less aluminous. It is evidently one of the sandy Cambrian units. Garnet and Staurolite are both visible in this quartzose, micaceous schist. There are abundant quartz veins.

Fifth Stop [Kyanite grade],
Highway 55, west of Pawling. The protolith is very aluminous. Here kyanite crystals and pale pink garnets are visible. Beware of black spots on this outcrop which are bits of tar spattered during road paving!

Sixth stop [Sillimanite grade, pegmatite],
Quaker Hill Road, east of Pawling. The protolith of this rock is evidently very similar to that seen at the Fifth stop. The rock is very garnet rich, with staurolite visible in thin section. There are many patches of pegmatite here, suggesting that the grade of metamorphism is approaching the beginnings of development of a hydrous silicate melt. Larger pegmatite bodies occur within a few miles of this locality. Tourmaline is sometimes visible in outcrop; it is conspicuous in thin section. Large crystals of staurolite are also visible in thin section. The sillimanite is seen only as fibrolite in mica-rich parts of the thin section.

Seventh stop [Sillimanite Orthoclase grade; gneiss],
Western Connecticut, west of Mizzentop. Here the meta-sediment has become a gneiss, which means extensive recrystallization of a highly weakened rock close to its melting point. There is abundant evidence of venitic separation of a granitic melt. In thin section sillimanite is visible as fibrolitic patches in mica-rich parts of the rock. Both plagioclase and K-feldspar reflect the high grade and partial melting of this rock. Although the rock resembles a granite, the chemical composition is clearly sedimentary.

Eighth stop [marble],
West Patterson. We have passed, without stopping, many seemingly excellent marble outcrops already. However, most of these marbles have been extensively hydrothermally altered , and the calc-silicate minerals are in a very poor state of preservation. This recently exposed outcrop at West Patterson has largely escaped this overprint, and there is excellent diopside, tremolite, and phlogopite in these rocks.

References

Balk, R., 1936, Structural and petrological studies in Dutchess County, New York: Part I. Geologic structure of sedimentary rocks. Geological Society of America Bulletin 47: 685-774

Barth, T., 1939, Structural and petrological studies in Dutchess County, New York: Part II. Petrology and metamorphism of the Paleozoic rocks. Geological Society of America Bulletin 47: 775-850

Bird, J.M. and Dewey, J.F., 1970, Lithosphere plate-continental margin tectonics and the evolution of the Appalachian orogen. Geological Society of America Bulletin 81: 1031-1060

Garlick, G.D. and Epstein, S., 1967, Oxygen-isotope ratios in co-existing minerals of regionally metamorphosed rocks. Geochimica et Cosmochimica Acta, 31: 181-214

Hames, W.E., Tracy, R.J., Ratcliff, N.M. and Sutter, J.F., 1991, Petrologic, structural, and geochronologic characteristics of the Acadian metamorphic overprint on the Taconide zone in part of southwestern New England. American Journal of Science 291: 887-913

Vidale, R., 1973, Metamorphic differentiation layering in pelitic rocks of Dutchess County, New York. In Hoffman, A.W. and others, eds., Geochemical Transport and Kinetics, Carnegie Institution of Washington, Publ. No. 634, p. 273-286

Vidale, R., 1974, Vein assemblages and metamorphism in Dutchess County, New York. Geological Society of America Bulletin 85: 303-306

Whitney, D.L., Mechum, T.A., Dilek, Y., and Kuehner, S.M. , 1996, Modification of garnet by fluid infiltration during regional metamorphism in garnet through sillimanite-zone rocks, Dutchess County, New York. American Mineralogist, 81: 696-705

Whitney, D.L., Mechum, T.A., Kuehner, S.M. , and Dilek, Y., 1996, Progressive metamorphism of pelitic rocks from protolith to granulite facies, Dutchess County, New York, USA: constraints on the timing of fluid infiltration during regional metamorphism. Journal of Metamorphic Petrology, 14: 163-181

Williams, H., 1978, Tectonic lithofacies map of the Appalachian orogen (map; scale 1:1,000,000). Memorial University of Newfoundland, Map 1

	Miles
The route from Binghamton to the start of the trip is as follows: East on 17 to junction with 17K, 2.7 miles east of contact between Silurian and Ordovician. East on 17K to Interstate 84, just west of Newburgh. North on 9W at Newburgh to Mid Hudson Bridge. The road log starts here.	
Turnoff to Mid Hudson Bridge	0.0
jct. Highway 9, east side of Hudson River	1.3
proceed on highway 55 to Church Street; follow Church St. (straight); 55 veers right	2.6
Church St. feeds on to Main St.; continue E. to Raymond St., STOP 1 is parking lot on NE corner The rocks examined at STOP 1 are the outcrops on Raymond St. adjacent to the parking lot. The rocks are highly deformed but not metamorphosed (no quartz veins, no indisputably metamorphic minerals). There are some traces of stratification and there are coarse blocks of more resistant sandstone.	3.3
Lunch can be obtained at one of several fast-food or sub shops a few blocks back; then proceed E to rejoin highway 55; continue E on highway 55 to jct. of County Road 21; turn left on 21	14.0
The next three stops are on county road 21. Be very careful with traffic. Cars tend to drive fast here and sight lines are limited. The road is narrow and parking along the sides is crowded.	
STOP 2 (parking has to be on left side. Careful!) is just before summit of rise on road. Note: Be extremely careful with traffic on this road! The outcrop is very overgrown (Also watch out for abundant poison ivy.). Here the rock is shiny and coarser grained than at STOP 1. There are no traces of stratification. There are many quartz veins.	14.8
Proceed east on 21; at jct. with highway 9 (16.9 miles) continue on 21 up the hill. STOP 3 (park on right side) is just before guard rail on right. Rocks examined are a few hundred feet up the road on the left side. Again be careful with traffic. There is visible garnet (mainly fairly small) and some chloritoid (black, shiny diamond-shaped crystals).	17.7
Proceed eastward on 21. STOP 4 (park on left. Careful!). We will walk back up the hill to examine a good outcrop on the north side of the road. Here there is abundant garnet, common staurolite prisms, and coarse muscovite. There are several quartz veins, some of which are deformed.	21.0
Proceed eastward to Wingdale. There is a good marble here, but we will not examine it on this trip. At mile 23.9 turn right on to combined state highways 22 and 55. Continue south to the village of Pawling. Just at the far edge of Pawling turn right on 55, heading west.	30.8
Continue west on 55, past vivid (but altered) marble outcrops along road. You will pass Harmony Hill Road at mile 32.9. Continue up hill to where outcrops of schist appear on the right side of the road. The exact spot is somewhat difficult to locate, but there is a concrete drain next to the highway at the best place to see kyanite. This is STOP 5 Here there is good kyanite (some with faint blue color) and abundant, small, very pale garnets	34.5

Proceed a few hundred feet further west and turn around by backing into blacktopped driveway. Backtrack to the east; highway 55 turns back to the north at a 270° cloverleaf (mile 38.6). Continue north to Quaker Hill Road. Turn right (east) on Quaker Hill Road.	38.9
Continue on Quaker Hill Road. Just after the junction with Reservoir Road, Quaker Hill Road takes a sharp hairpin turn to the right. Stop on the right side of the road just beyond the turn. STOP 6 The rocks here are coarse grained schist with abundant, coarse garnet. Staurolite is unidentifiable in outcrop but present in many sections. The sillimanite is very fine grained fibrolite. There are several pods of pegmatite, and tourmaline can be found in places.	
Continue up the road. Turn right on Church Rd. at mile 41.8 Observe the magnificent woodwork on the barn here. Proceed southward, swinging eastward to the center of the tiny hamlet of Mizzentop, with its beautiful church and handsome stone public library. At mile 42.3 there is a stop sign. Proceed east from here (same road). Cross into Connecticut (road quality deteriorates noticeably! Note that you have just passed through a narrow strip of real estate that New York got from Connecticut in 1685 when Connecticut said it wanted to keep the bit around Stamford. You do remember your history, don't you? Proceed east into Connecticut (now Wakeman Road). Turn right at stop sign at mile 44.9 on highway 37. Our next stop is a pulloff on the left (again!) at the telephone pole. STOP 7. There is no good outcrop here but there are several large fragments provided by the telephone company. The rock here is a gneiss, with good migmatitic veins.	45.1
Continue south a short distance and turn right at mile 45.3 This is Chapel Hill Rd., but I didn't see a sign. Continue on this road. The crossing into New York is where the road deteriorates. Continue right for several miles, with road gradually swinging left (south) and descending a long hill. At mile 50.8 the road intersects highway 22, heading south. Join 22 here and IMMEDIATELY turn right on to highway 311. Proceed through Patterson to the junction of highway 292. Park on 292 on the left just beyond the junction. STOP 8. This is a fresh marble outcrop, with very good diopside prisms visible in outcrop. There is good tremolite and phlogopite also, but these cannot be seen in outcrop.	52.2
Continue west on 292, going straight at the intersection at mile 55.5 (292 goes right). You are on Mooney Hill Rd., but I didn't see a sign. This road winds for several miles and joins interstate 84. Turn right (west) on 84)	56.0
A few miles along, there is a rest stop on 84. If time permits, walk back up the hill (be careful). Just at the entrance of the rest stop there are magnificent exposures of pre-Cambrian gneisses that are startlingly similar the gneisses seen at STOP 7.	59.4
The trip is now over. Return to Binghamton via 84, 17K, and 17.	

Dutchess Co. Analyses of rocks

	B-2	202-72	13-71	B-4	15-71	95-69	B-5	21A-71	19-71	20B-71	106A-72	136-69	25-71	142A-69	23A-71	24-71
grade	chl	chl	chl	bi	bi	gar	gar	sill	sill	sill	sill	sill	sill	sill-or	sill-or	sill-or
SiO2	65.0	72.9	70.3	66.9	77.4	62.5	62.6	64.5	66.5	66.2	61.1	60.8	64.9	66.1	62.3	62.4
TiO2	0.89	0.49	0.69	0.65	0.48	0.91	0.83	0.73	0.69	0.69	0.81	0.86	0.98	1.06	1.07	0.81
Al2O3	16.2	8.7	13.2	14.3	9.9	16.3	16.5	14.6	15.8	14.8	17.6	17.9	18.4	16.8	18.1	17.0
Fe2O3	1.13	0.48	2.32	1.06	1.31	2.45	0.54	1.61	1.92	1.18	1.39	0.86	2.43	1.52	2.03	2.24
FeO	5.80	2.19	4.04	5.16	2.48	4.36	5.45	4.84	4.44	5.48	6.77	6.45	4.88	5.17	5.60	5.28
MnO	0.04	0.30	0.09	0.10	0.20	0.10	0.12	0.82	0.74	0.16	0.64	0.73	0.07	0.22	0.12	0.26
MgO	1.74	1.65	3.04	3.45	2.09	3.34	3.47	5.00	5.06	4.48	4.53	4.09	2.00	1.88	2.06	2.38
CaO	0.02	4.96	0.18	0.28	0.04	0.91	1.98	1.15	0.55	0.77	0.89	1.08	0.29	0.32	0.79	2.06
Na2O	2.63	0.94	0.04	0.90	0.12	0.99	1.35	1.51	0.98	1.41	0.93	3.23	0.18	0.28	1.11	2.34
K2O	2.80	1.89	2.76	3.09	2.79	5.05	4.56	3.41	2.67	3.79	4.20	3.23	3.77	4.35	3.46	3.33
P2O5	0.12	0.18	0.10	0.20	0.08	0.16	0.14	0.15	0.10	0.12	0.13	0.13	0.15	0.16	0.14	0.16
H2O+	3.23	1.39	2.13	3.32	1.51	2.29	1.61	0.92	0.69	0.87	1.45	1.24	1.66	3.23	2.71	1.12
CO2			0.00		0.00		0.15	0.00	0.00	0.00						0.00

	212-72	B-19	17A-71	B-6	127-72	B-7	137-72	155-72	22A-71	22B-71	138-69	DC94-7	DC-94-1	DC-942?	DC94-3	DC93-4
grade	bi	gar	gar	gar	gar	staur	staur	staur	sill	sill	sill	bi	bi	gar	staur	staur
SiO2	51.8	52.9	58.3	55.4	44.2	56.5	55.2	58.8	57.8	56.9	57.8	65.0	61.8	63.4	59.6	62.5
TiO2	1.20	1.20	0.98	0.99	1.51	0.99	1.27	0.87	1.16	1.23	1.23	0.80	0.84	0.80	1.01	0.65
Al2O3	24.2	25.3	22.2	22.3	28.3	22.5	22.9	20.4	22.7	22.0	21.0	16.3	18.1	16.4	23.5	14.8
Fe2O3	1.80	1.22	3.16	1.30	2.29	1.11	1.73	1.29	3.86	5.24	2.28	7.08	8.14	7.33	8.91	6.63
FeO	7.70	7.83	4.76	6.82	8.02	7.26	5.95	7.59	3.64	3.78	6.48					
MnO	0.14	0.13	0.07	0.14	0.16	0.19	0.25	0.35	0.07	0.15	0.27	0.11	0.15	0.14	0.15	0.75
MgO	2.30	1.67	1.41	2.35	2.60	1.97	2.28	2.38	1.44	2.07	2.28	3.73	4.71	3.87	1.89	8.00
CaO	0.10	0.25	0.20	0.38	0.69	0.49	1.05	1.45	0.81	0.58	0.90	1.54	0.14	1.87	0.23	1.07
Na2O	1.52	2.25	1.31	1.02	1.33	1.66	2.64	3.05	1.38	1.77	2.40	0.59	1.40	1.21	1.10	1.61
K2O	4.35	3.62	3.34	5.45	5.73	5.00	4.49	2.06	5.37	4.72	4.58	3.99	3.76	4.13	3.67	3.92
P2O5	0.12	0.17	0.17	0.20	0.12	0.12	0.15	0.04	0.23	0.15	0.08					
H2O+	4.74	3.94	2.43	3.55	3.89	2.80	2.74	2.24	1.33	2.35	1.82	4.89	4.70	3.53	3.81	1.46
CO2		0.00	0.00		0.00				0.00							

	DC94-8	DC94-9	DC94-1?	YD94-1	YD94-2	YD94-3	YD94-4	YD94-5	stop 2	stop 3	stop 4	stop 5	stop 6	stop 7
grade	staur	staur	sill	unmm	unmm	unmm	unmm	unmm	bi	gar	staur	kyan	sill	sill or
SiO2	60.9	54.2	60.1	66.1	63.2	72.9	65.6	58.4	51.7	52.1	56.4	58.6	54.1	80.2
TiO2	0.91	1.29	1.18	0.83	0.78	0.72	0.80	0.94	1.06	1.26	1.28	0.7	1.12	0.6
Al2O3	21.3	24.8	23.1	13.2	13.7	12.2	12.8	15.4	22.8	28.9	23.5	17.8	29.6	9.27
Fe2O3	8.99	10.23	7.36	4.71	5.39	4.53	4.79	6.14	12.11	8.76	8.74	10.1	8.4	3.7
FeO														
MnO	0.16	0.29	0.16	0.05	0.08	0.04	0.08	0.10	0.67	0.13	0.29	1.57	0.04	0.05
MgO	2.11	2.47	1.90	1.85	2.10	1.62	1.60	2.00	4.92	1.58	2.27	7.2	2.07	0.96
CaO	0.29	0.43	0.95	5.80	6.77	2.45	6.88	8.12	0.62	0.72	1.02	0.89	1.01	1.65
Na2O	0.75	1.21	1.18	1.56	1.77	1.38	1.80	1.62	1.52	1.05	1.25	0.24	1.26	1.7
K2O	3.93	4.71	3.33	2.30	2.35	2.24	2.15	2.85	4.43	4.75	4.82	4.14	4.53	1.83
P2O5				0.15	0.14	0.15	0.14	0.16	0.05	0.27	0.3	0.46	0.21	0.16
H2O+	2.31	2.52	1.80											
CO2														

Analyses "B-x" are from Barth, 1936; analyses "DC94-x" and "YD94-x" are from Whitney et al, 1996;
(row labeled "H2O+" for YD94 and DC94 samples records the LOI)
Analyses "stop x" are our analyses from stops on this trip; remaining analyses from Vidale, 1973

OVERVIEW

This is a trip emphasizing contacts, rock fabrics, and regional structure. It examines rocks of the lowlands/highlands boundary zone spaced along Rt 812 over a distance of about 6.5 miles starting 2.5 mi. NE of Harrisville and ending 4 mi. SW of Harrisville. This trip examines structures, fabrics, and lithologies of Adirondack lowlands rocks and of the Diana complex adjacent to their mutual boundary near Harrisville, NY[1]. The trip starts at the Route 3 bridge over the Oswegatchie River in Harrisville, NY. It proceeds E to where Rt 812 branches N from Rt 3, about 1.1 mi E of Harrisville and continues on Rt 812 to where Stone Road intersects Rt 812, about 1.1 mi N of the Rt 812 / Rt 3 junction. It follows Stone Rd to the north 0.3 mi to stop 1.

Locations and brief characterizations of Field Trip Stops.

Stop 1 - metagabbro/marble contact; on east side of Stone Road, 0.3 miles north of the junction of Stone Road with Rt 812; location: 44° 10.42' N, 075° 20.07' W.

Stop 2 - meta-quartz-syenite/marble contact; on east side of Rt 812, 1.1 mi north of the junction of Rt 812 with Rt 3 NE of Harrisville; location 44° 10.22' N, 075° 19.73' W.

Stop 3 - rusty-calcsilicate gneiss, diopsidic marble contact with Diana syenite gneiss; on the east side of Rt 3, 0.5 mi N of the bridge where Rt 3 crosses the Oswegatchie River in Harrisville; location 44° 09.45' N, 075° 19.02' W.

Stop 4 - Diana syenitic gneiss with abundant mylonitic veins; on the north side of Rt 3, 0.8 mi west from the Rt 3 bridge over the Oswegatchie River in Harrisville; location 44° 08.73' N, 075° 19.94' W.

Stop 5 - Diana syenitic augeniferous gneiss; on both sides of Rt 812, 0.7 mi. south of its junction with Rt 3.

---

[1]There is a muncipal parking lot, with three picnic tables, about 100 m SE of the bridge in Harrisville next to Scanlon's bakery and coffee shop. Possible lunch and rest-stops in Harrisville on Main St. are: Hunter's View Restaurant; Scanlon's bakery and coffee shop; the Village Inn; and Pastamore Restaurant (for pizzas). There is also Greg's grocery-deli store for soft-drinks and fixings for sandwiches.
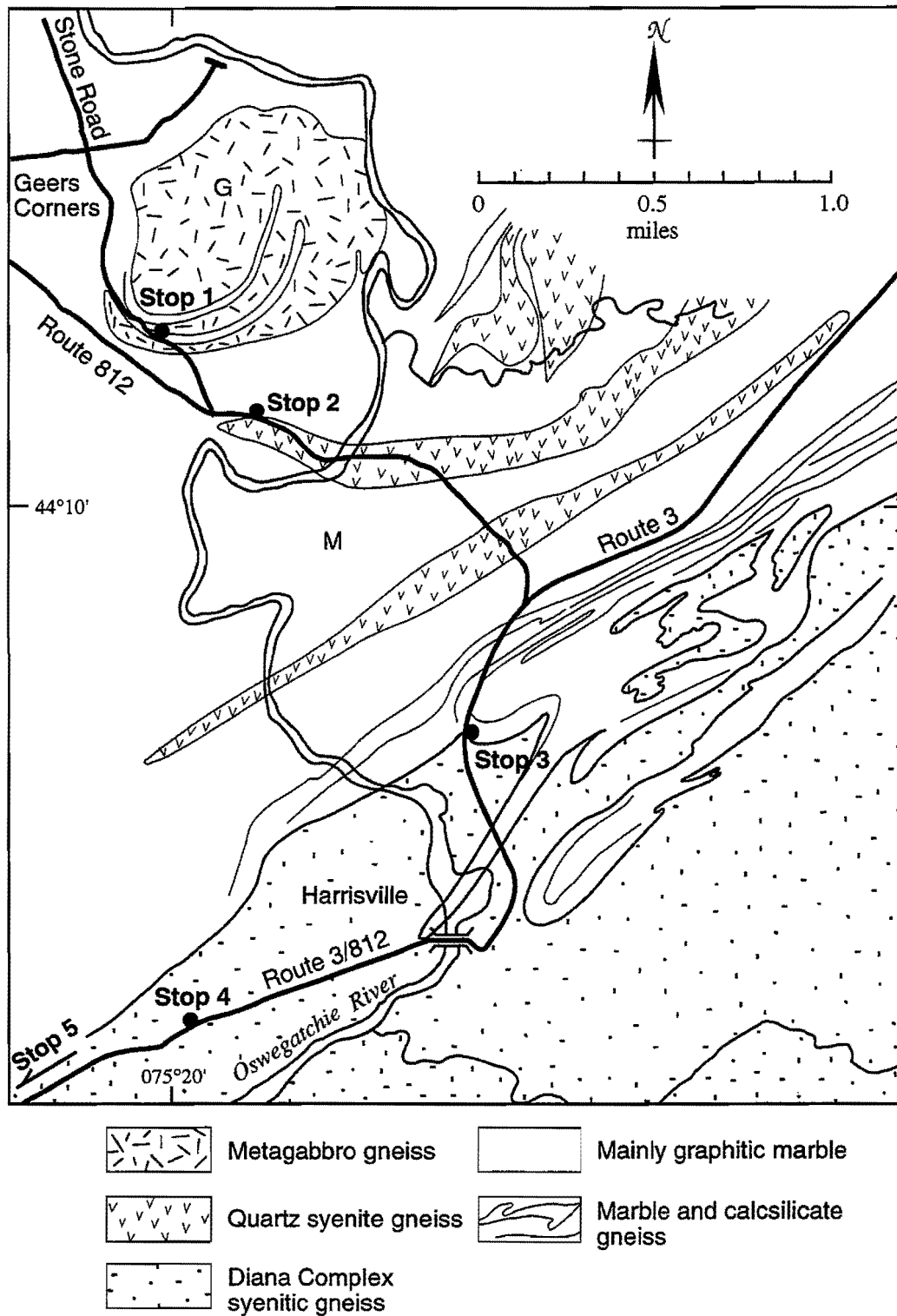
Figure 1. Location of stops for this field trip are distributed along 6.5 miles of Rt. 812 in the vicinity of Harrisville, NY. Geologic sketch map after Wiener (1983).

INTRODUCTION

Regional setting

The focus of this trip is on the contact zone of the Grenville marble and paragneiss with the Diana Syenite Complex in the NW Adirondack Mts. This contact zone extends from Carthage NY to Colton NY, perhaps extending as far as 500 km or more (Lamb, 1993). The trip follows an approximately N-S track along Rt 812 through Harrisville NY, about mid-way between Carthage and Colton (Fig.1). The excellent detailed map and report of Wiener (1983) describes the local geology.

Major lithological subdivisions

Lowlands paragneisses and orthogneisses. The Grenville meta-sedimentary rocks of this area include garnet-quartz-plagioclase-biotite gneiss, biotitic granitic gneiss, calc-silicate gneiss, and related rocks (Smyth and Buddington, 1926; Wiener, 1983). These are intruded by metamorphosed and deformed sills of gabbro and quartz-syenite. This trip will examine gabbro, quartz-syenite and marble, and their contact relations.

'Highlands' orthogneisses. The principal meta-igneous rock of interest SE of the boundary is the Diana syenite (Buddington, 1939; Buddington and Leonard, 1962; Hargraves, 1968; Wiener, 1983). Buddington (1939) interpreted the Diana Quartz Syenitic Complex as a major differentiated sill, over 6 km thick, isoclinally folded with Grenville meta-sediments which it intrudes, and overturned to the SE in the Harrisville vicinity. This trip examines the syenite at three localities, and its contact with the metasedimentary rocks at one locality.

Structural aspects

Much of the syenite is mylonitic to varying degrees, and is cut by fine mylonite veins of variable development. The zone of mylonite development is broad, and extends into the paragneisses to the NW, leading Geraghty et al. (1981) to map a broad zone of Diana Complex and adjacent paragneisses/marbles as the Carthage-Colton mylonite zone.

Major and minor structures. Wiener (1983) mapped numerous major folds and minor cross-cutting folds in this region (see his Fig. 6 for the overall fold pattern and his numerous other figures detailing individual fold structures). He distinguishes four major phases of folding in the Harrisville vicinity, characterized as follows:

First phase folds: NE trending isoclinal folds; overturned to SE; limited to Grenville paragneisses/marbles of the lowlands region; minor folds are reclined, hinges plunge N to NW.

Second phase folds: NE trending isoclinal folds; overturned to SE; this is the generation represented by an abundance of minor folds and by the development of mylonitic foliation especially evident in the Diana complex; minor fold hinges plunge N to NE and SW to W.

Third phase folds: NE trending, overturned to SE; more open in the NW and tighter to the SE (includes Harrisville anticline/syncline and Baldface Hill syncline of this trip); minor fold hinges trend N to NE in the east, N to W in the SW, and SW to W in the NW parts of the Harrisville area.

Fourth phase folds: NW trending open and upright folds (includes Meadow Brook syncline of this trip); minor fold hinges plunge mainly NW.

Interpretations of the highlands/lowlands boundary

Several interpretations have been offered on the nature and origin of the Highlands

(orthogneisses) / Lowlands (paragneisses) boundary. In some interpretations, the Diana syenitic complex is part of the highlands association, in others it is part of the lowlands assembly, and in others it is the boundary zone or straddles the boundary between the two major assemblages. Explanations for this boundary include the following:

- *trace of a fold-thrust nappe* (Geraghty et al., 1981)
- *intrusive boundary*, isoclinally folded and overturned to SE (Wiener, 1983; Buddington 1939; Buddington and Leonard, 1962)
- *major suture* (Mezger et al., 1992; Martignole, 1986)
- variations on *faults, fault reversals, detachment faults* (e.g. Mezger et al., 1992; Isachsen and Geraghty, 1986)

DESCRIPTIONS OF THE GEOLOGICAL STOPS

STOP 1 - Gabbro/Marble Contact

This locality is characterized by multiple sills of gabbro, intruding marble, subsequently metamorphosed and multiply folded.

Meta-gabbro lies along the east side of the road, both north and south of this outcrop. Here at Stop 1 we find gabbro in the central upper region of the outcrop. The gabbro-marble contact rises both north and south from near road-level in the middle of the exposure. Marble foliations trend approximately N70E, 30 N at both ends of the outcrop. Near the south end of the outcrop erosional relief shows excellent internal details of the marble structure. Here there are isoclinal folds of both large (meter) and small (centimeter) scale, with mainly *easterly* plunges in the plane of the foliation. Marble foliations also envelope boudins of more competent marble and of calc-silicates. A more open *north* -plunging fold can be found in the marble near the north end of the outcrop. The gabbro-marble contact is obscured somewhat by surface obstructions and by shearing but can generally be located within a meter or so, defining a gentle basin in the N-S profile along the outcrop. The meta-gabbro has a moderately well-developed foliation. A few hundred meters south near the pipeline clearing it contains large (1 cm.) subequant hornblende porphyroclasts.

According to Wiener (1983) this meta-gabbro lies in a structural basin east of Geers Corners at the intersection of the NE-trending Baldface Hill syncline (third-order fold) and the NW-trending Meadow Brook syncline (fourth-order fold); he (ibid.) interprets the gabbro as having been intruded after the first regional folding phase and mainly before the second phase.

STOP 2 - Marble/Quartz-syenite Contact

This exposure clearly displays the contact between a sill of quartz-syenite and the graphitic marble. A sketch (Fig. 2) shows the view east at this locality. The marble is discordantly and isoclinally folded adjacent to the more gently folded quartz - syenitic gneiss. The intrusive contact shows several prominences and re-entrants; foliation in the

GRAPHITIC
MARBLE

CONTACT

QTZ-SYENITE
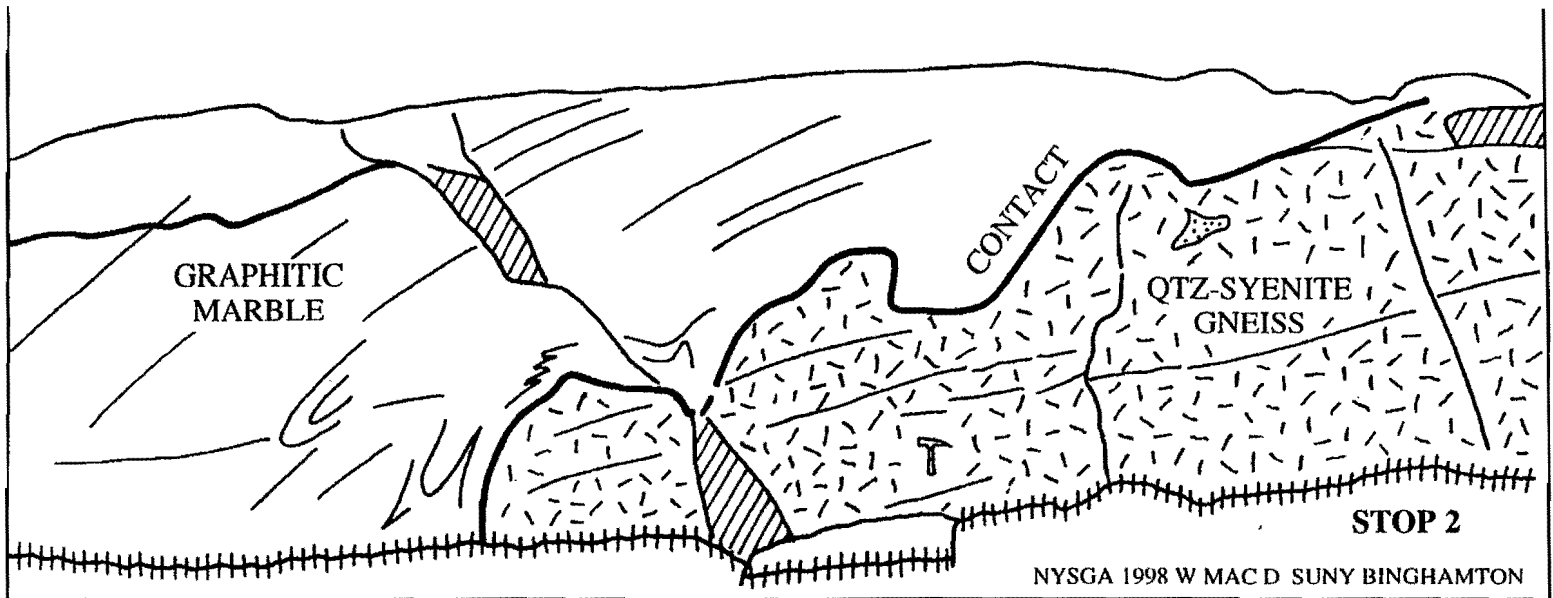GNEISS

STOP 2

NYSGA 1998 W MAC D SUNY BINGHAMTON

Figure 2. Stop 2, view east. Sketch of contact relations between graphitic marble and quartz-syenite.

marble generally follows the irregular syenite contact. Glacial grooves and striae of approx. N-S trend can be found all along the top of the outcrop, but are better preserved in the marble.

This outcrop is at the west end of a large sill of quartz syenite gneiss, one of several which crop out west of Baldface Hill (Wiener, 1983). The marble/syenite contact is quite irregular and is consistent with an intrusive boundary. The fabric of the syenitic gneiss is quite subtle relative to that of the marble. Some graphite crystallization has occurred along fractures in the gneiss. Disseminated sulfides are also found in the marble, contributing to rusty stains. Marble foliation here is defined by color banding, silicate-rich bands, and erosional relief on weathered surfaces. The foliation dips about 45 northwesterly.

These sills of quartz syenite are believed to be genetically related to the Diana syenite complex (Buddington and Leonard, 1962). They were intruded during the second phase of regional folding. These sills appear to be less intensely deformed than the Diana Complex syenite, possibly because they are enveloped by less competent marbles which flowed around them during regional deformations.

STOP 3 - Marble/Diana Syenite Contact

This site reveals isoclinal meta-carbonates and related rocks now down- folded into the Diana syenite. The location is approximately in the common limb between the Harrisville syncline (to the NW) and the Harrisville anticline (to the SE) (Wiener, 1983). The structures here dip NW and are overturned to the SE.

The exposure has three main parts of equal width, from N to S: 1) a zone of rusty calc-silicate gneisses grading into white marbles, 2) diopsidic marble, and 3) Diana syenite. Faults and shear zones of WNW trend and steep NE dip separate these three units. The foliation within the diopsidic marble and Diana syenitic gneiss on either side of the 2-3 shear zone trend NE and dip steeply NW.

Zone 1) The foliation of the rusty calc-silicates is approximately conformable with that of adjacent marbles. Transition across this zone from rusty calc-silicates at the north end of the outcrop to white marble near the contact with diopsidic marble is gradual. The zone 1 - zone 2 contact between light-colored marbles and grey diopsidic marble is quite abrupt and probably is a fault or shear zone .

Zone 2) Adjacent to its north limit, the diopsidic marble shows strongly isoclinal folding (streaks of light grey bands in dark grey marble). Isolated diopsidite clusters and masses, some of which resemble metamorphosed thin-bedded limestone fragments, 'float' in a more massive dark grey matrix of calcite with abundantly scattered dark green granular diopside grains. Some of the light-green diopsidic masses have a darker green 'halo'. Numerous small faults of variable trends cut through the diopsidic marble; some have calcite slickenfibres and others are plated with serpentine (antigorite?).

Zone 3) A fault or shear zone at the S limit of the diopsidic marble separates it from zone 3 which is dominantly Diana syenite. This shear zone (approx. 105, 70N) is strongly discordant to the foliation of the adjacent diopsidic marble which trends approx. 035 and dips 65NW. However, on south side of that shear zone are brown to rusty brown well-foliated gneiss with foliation approx parallel to the shear zone. The contact of these light-brown weathering gneisses with the darker greenish grey massive Diana syenite is transitional over a meter or so. This contact appears to be the intrusive contact between the paragneisses of the lowlands and the orthogneisses of the Diana complex. A very weak foliation in the Diana syenite (defined by sub-parallel lenticular grains of K feldspar) here is about 035, 70 NW, consistent with that in the adjacent diopsidic marble

STOP 4 - Mylonitic Diana Syenite
Diana syenite is the dominating lithologic unit in the roadcuts on both sides of the road. The outcrop on the north side of the road is emphasized here. It is cut by numerous thin mylonite veins, the 'late ductile shear zones' of Wiener (1983). There are also a few small faults and larger shear zones, and some thin meta-dikes(?) of 10 to 20 cm thickness. In the eastern quarter of the outcrop is a tightly folded meta-dike(?). Abundant glacial grooves and striae at the top of the outcrop trend approximately along azimuth 175. The principal features to examine here are the Diana syenite, the mylonites, and the meta-dikes(?).

Diana Syenite
The Diana syenite here is weakly foliated, dark greenish-grey and relatively uniform in appearance. The weak foliation in the Diana syenitic gneiss here is defined by parallel lenticular grains of K feldspar up to about 1 cm long and up to a few mm thick. This foliation is most clearly seen in the weathered rinds along the drill-holes (drill-holes used for blasting the roadcut). The Diana syenitic gneiss foliations trend approximately N50E and dip somewhat variably but approx N50 to 60 NW. A little further south (e.g. stop 5) the foliation becomes more strongly developed and augeniferous. The Diana syenite was intruded early in the second phase of regional deformation and folding, and its protomylonitic foliation developed during the second phase of regional deformation (Wiener, 1983).

Mylonites
This is an excellent outcrop to examine the development of mylonitic zones in the Diana syenite. Mylonitic bands are of several different types:
a) thin, planar, of significant extent (to 5 m or more) mainly 1 to 3 cm thick
b) curved and branching, of irregular thickness and relatively limited extent
c) broad banded zones (to 20 cm) less abundant and typically of limited extent
The mylonites terminate by pinchout, by truncating at high-angle junctions with other mylonites, or by branching from other mylonites at more acute angles. Although the mylonites are clearly later than the foliation in the syenite, there is relatively little offset of the syenite foliation by the mylonites. Internally, the mylonites have a well-developed foliation, with abundant porphyroclasts of rounded subequant sphene and occasional elongate pyroxene. Sulfides occur along the margins of some mylonites. In the syenite
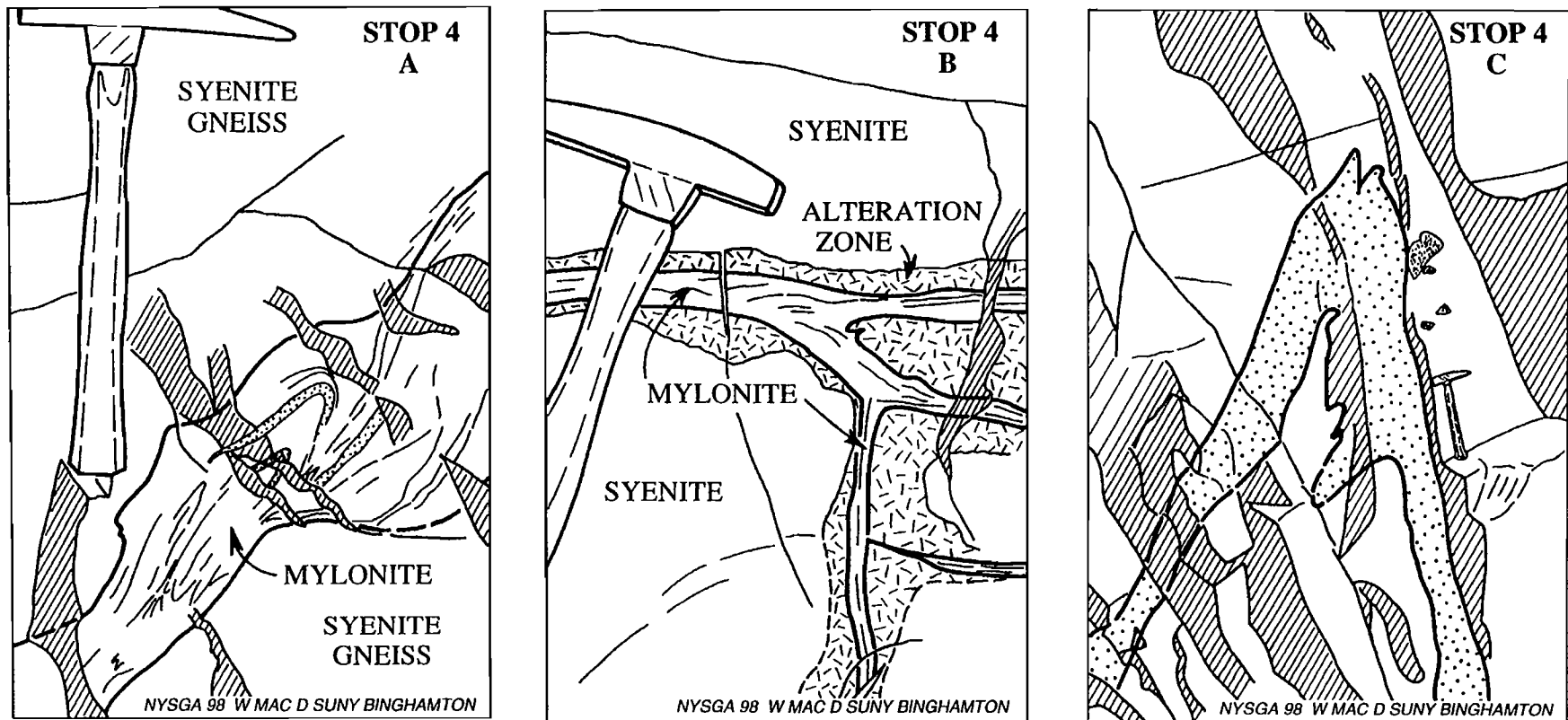
18

Figure 3. Stop 4, north side of road. Sketch A shows small-scale folds within a mylonite zone. Sketch B shows branching and termination of mylonite veins in Diana syenite. Sketch C shows tight fold in meta-dike(?).

adjacent to many mylonites are marginal alteration zones of variable width in which pinkish K feldspar dominates, and mafics are less abundant. Some of the alteration zones are several times as wide as the associated mylonite vein. In some alteration zones, prominent alignment of pyroxene grains or clusters can be seen, plunging moderately to steeply N to NNW.

The mylonites do not appear to have been folded. However, their distribution is symmetric with respect to the regional fold axis of the second phase of regional folding (see Fig. 4 and discussion). A small z-fold is evident about 200 m east of the west end of the outcrop. This small isoclinal fold pair (anticline/syncline) occurs in the fabric of the mylonite; the mylonite zone here is about 10 to 15 cm wide and its boundaries have not been folded. The sense of shear indicates W side up. Such folds in the mylonite are scarce.

Meta-dikes(?)

Several meta-dikes(?) now largely altered to pyroxene cut the syenite. They are mostly relatively thin, 10 to 30 cm thick. A tight fold has developed in one of these, in the eastern third of the outcrop. This kind of fold is not common. The theoretical axial surface plane of this fold trends about N10W and dips 75 W, and lies at a high angle to the foliation of the Diana syenite. The theoretical hinge (found by interpolating the intersection of the limbs) plunges steeply N. As a mylonite adjacent to this fold is not itself folded, it is thought that the mylonites post-date deformation of these 'meta-dikes'.

Discussion

Some structural relationships at this outcrop are summarized in Fig. 4. Here we see that the foliation ('protomylonitic' foliation) of the Diana syenite dips moderately NW. The mylonite veins appear to have a common axis of orientation which plunges 62 toward 347. According to Wiener (1983), this is the common direction of lineations for the second phase of regional deformation. That pole and the associated 95% confidence oval (Bingham statistics) represent the direction of the eigenvector corresponding to the minimum eigenvalue for the distribution of about 30 axes or normals to the mylonite veins. These are for measurements in the western third of this outcrop only. Both pyroxene lineations and the theoretical axis of the tightly folded 'meta-dike' also lie close to this direction. This suggests that although the mylonites are of greatly variable orientations, they are mainly coaxial about an axis near the foliation plane of the Diana syenite and plunging NNW.The pyroxene lineations adjacent to mylonites are therefore near the intersections of the mylonite foliations with the Diana syenite foliation, as might be expected.

STOP 5 - Augeniferous Diana Syenite

Augeniferous well-foliated syenite gneiss is exposed in low outcrops on both sides of the road. A few thin mylonites are visible here. The foliation, wrapping around centimeter-sized feldspar augen, trends approximately N45E and dips 45NW. Dark-cored feldspar augen (greenish) with lighter tan rims and curved cleavage are abundant.
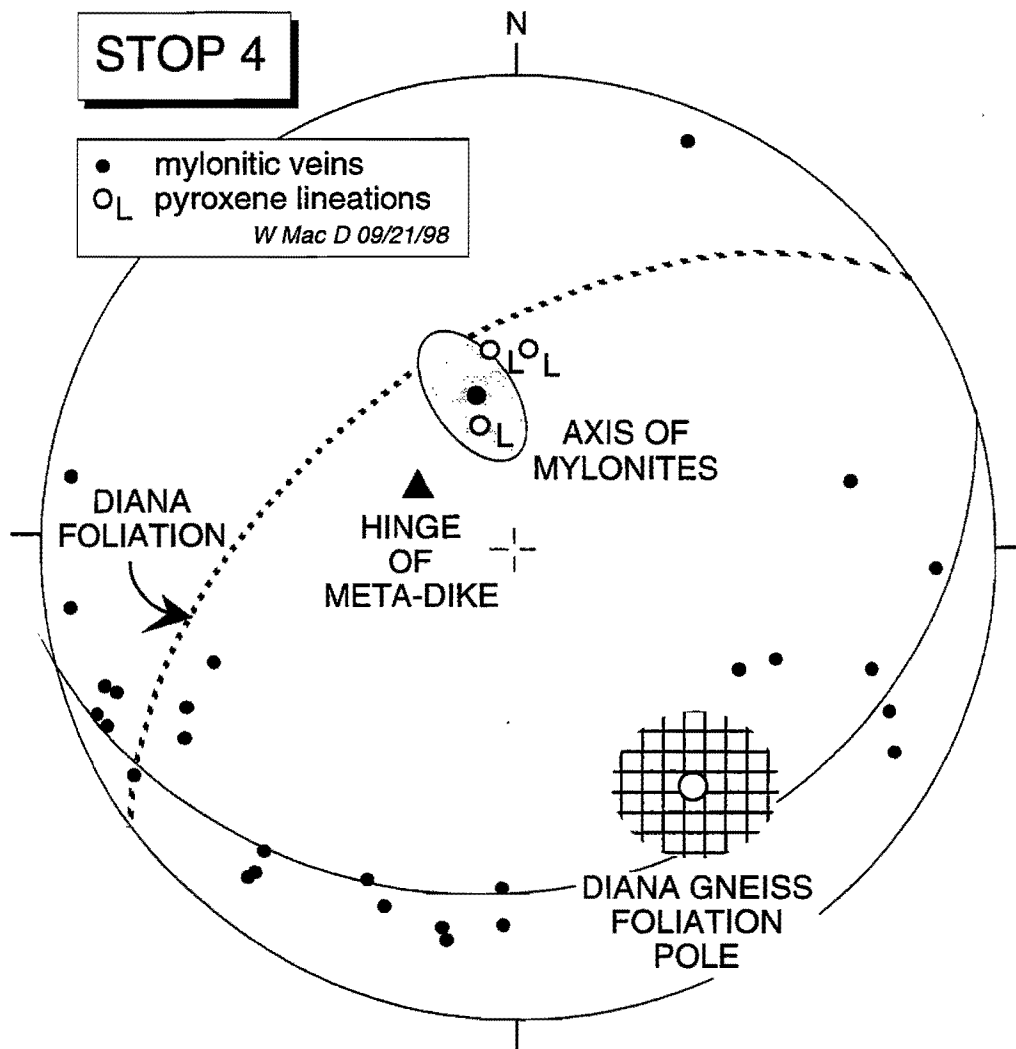
Figure 4. Stop 4. Structural relations here are summarized in this stereographic diagram. The foliation of the Diana syenite dips moderately northwesterly. Cross-cutting mylonites intersect along a common axis plunging 62 toward 347. This is close to the lineations defined by pyroxene lineations, and to the theoretical hinge of the isoclinally folded meta-dike (?).

Foliation in the Diana syenite is best seen in the drill-holes used for blasting, where the syenite weathers to a light brown color. The rock is quite uniform here, and there is no indication of interlayering with other lithologies.

Southward from this outcrop the foliation becomes better developed approaching flaser gneiss, and layers of other rocks, such as shonkinites, develop. Still further south, hornblende granite appears. This apparent regional zonation led Buddington and Leonard (1962) to conclude that the Diana complex is essentially a large isoclinally folded and metamorphosed differentiated sill complex, overturned to the SE such that higher levels of the sill lie to the SE.

BIBLIOGRAPHY

Buddington, A.F., 1939, Adirondack Igneous Rocks and Their Metamorphism: Geol. Soc. America, Memoir 7, 354 p.

Buddington, A.F., and Leonard, B.F., 1962, Regional geology of the St. Lawrence Country magnetite district, northwest Adirondacks, New York: U.S. Geol. Surv. Prof. Pap. 376, 145 p.

Geraghty, E.P., Isachsen, Y.W., and Wright, S.F., 1981, Extent and character of the Carthage - Colton mylonite zone, northwest Adirondacks, New York: Nuclear Regulatory Commission, NUREG/CR-1865, Wash., 83 p.

Hargraves, R. B., 1968, A contribution to the geology of the Diana syenite gneiss complex: Origin of anorthosite and related rocks: p. 343-356 in Isachsen, Y. (Ed.), The Origin of Anothosite and Related Rocks: New York State Museum (Albany, NY), Memoir 18, 466 p.

Isachsen, Y.W. and Geraghty, E.P., 1986, The Carthage-Colton mylonite zone, a major ductile fault in the Grenville province: International Basement Tectonics Association, Salt Lake City, Utah, p. 199-200

Lamb, William M., 1993, Retrograde deformation within the Carthage-Colton Zone as recorded by fluid inclusions and feldspar compositions; tectonic implications for the southern Grenville Province: Contributions to Mineralogy and Petrology, v. 114, n. 3, p. 379-394.

Martignole, J., 1986, Some questions about crustal thickening in the central part of the Grenville Province, in Moore, J.M., Davidson, A., and Baer, A.J., (Eds.), The Grenville Province: new perspectives: Geol. Assoc. Canada, Spec. Paper v 31, p. 327-339.

Mezger, K., van der Pluijm, B.A., Essene, E.J., and Halliday, A.N., 1992, The Carthage - Colton mylonite zone (Adirondack Mountains, New York): The site of a cryptic suture in the Grenville orogen: Jounal of Geology, v. 100, p. 630-638.

Smyth, C.H. Jr, and Buddington, A.F., 1926, Geology of the Lake Bonaparte quadrangle: New York State Museum bulletin , 269, 106 p.

Wiener, Richard W., 1983, Adirondack Highlands-Northwest Lowlands "boundary"; a multiply folded intrusive contact with fold-associated mylonitization: Geological Society of America Bulletin, v. 94, n. 9, p. 1081-1108.

Finger Lakes Gorges Revisited

Peter L.K. Knuepfer
Tim K. Lowenstein
Department of Geological Sciences and Environmental Studies
Binghamton University
Binghamton, NY 13902-6000
email: knuepfr@binghamton.edu
email: lowenst@binghamton.edu

Introduction

The Finger Lakes region of central New York is justifiably world-renowned for its beauty, especially the spectacular deep gorges–the Finger Lakes glens--that characterize tributary streams draining into the central troughs. The origin of the troughs themselves has been the source of debate for as long as geologists have ventured into upstate New York (as summarized by Mullins and others, 1989). The recent geophysical studies by Mullins and his colleagues (Mullins and Eyles, 1996) have resolved much of this controversy, demonstrating that the modern troughs, at least, must have been formed by a combination of glacial scouring and the action of high-pressure sub-glacial meltwater. Seismic stratigraphic relationships suggest that the stratigraphic and morphologic record left behind by this event–including the Valley Heads Moraines (VHM) as well as much of the infill of the Finger Lakes troughs themselves--must have occurred between (and including) VHM time, around 14.9-14.4 ka ^{14}C yr. B.P. (Muller and Calkin, 1993). Late-stage trough-fill sediments were deposited until 13.6 ka ^{14}C yr. B.P. (Wellner and others, 1996), by which time ice had retreated north of the modern Finger Lakes. Our goals on this field trip (Figure 1) are to consider the implications of this record for development of the modern Finger Lakes glens/gorges.

Late-Glacial Evolution of the Finger Lakes Troughs

The spectacular reflection data obtained by Mullins and Hinchey (1989) and discussed in more detail in Mullins and Eyles (1996) have provided a fundamentally
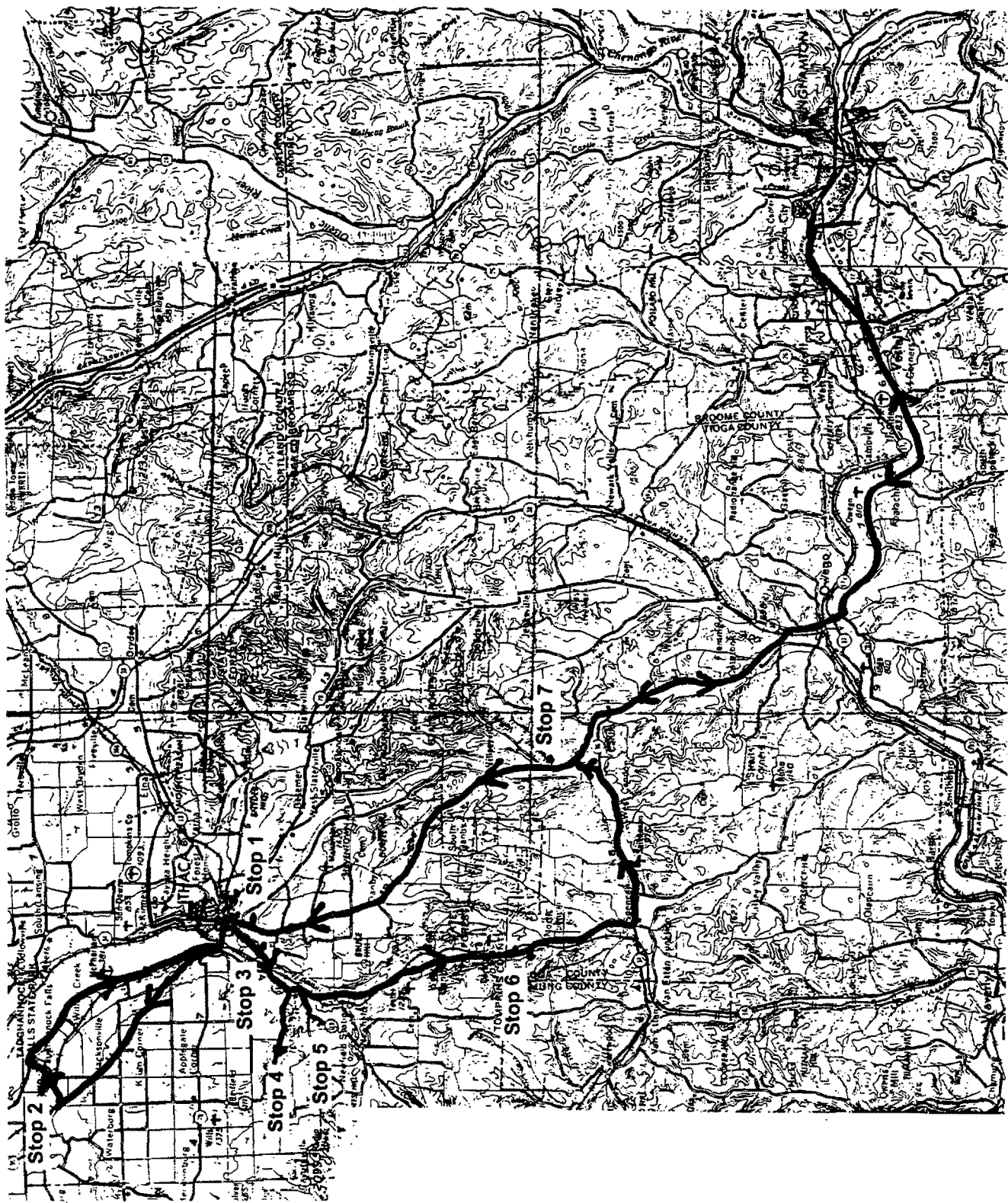
Figure 1. Map showing field trip stops. Base from U.S. Geological Survey 1:250,000 Elmira and Binghamton sheets.

new view on the formation of the Finger Lakes troughs. While an ice-erosion origin for the troughs had long been recognized (Mullins and others, 1989), it wasn't until extensive seismic reflection studies had penetrated the sub-lake stratigraphy that the full nature of sub-glacial erosion could be recognized. We summarize here what we consider to be the most important observations and conclusions of this work, at least as related to our goal of understanding the evolution of the Finger Lakes gorges.

(1) Deep bedrock scour below each of the Finger Lakes is as great as 306 m below sea level (Seneca Lake). The depth of scour, coupled with seismic stratigraphy of the deepest sediments that fill these basins, is most consistent with erosion by high-energy, high-pressure sub-glacial meltwater (Mullins and Hinchey, 1989; Mullins and others, 1996). It is, perhaps, no coincidence that this interpretation is consistent with the argument by Shaw and Gilbert (1990) that subglacial meltwater flood(s) played a major role in development of the drumlin field of the Ontario lowland to the north. Mullins and Hinchey (1989) suggest that the VHM were deposited by the water from this scour event; we'll stop at a large exposure of VHM sediment that will provide an opportunity to discuss this hypothesis.

(2) The oldest sediments preserved in any of the Finger Lakes troughs correlate with and onlap sediment preserved in the Valley Heads Moraines deposits. Assuming synchroneity of the VHM deposits, the best estimate of the age of this event is supplied from the Nichols Brook site in western New York. Muller and Calkin (1993) conclude that ice retreat at this site had begun by 14.4 ka ^{14}C yr. B.P., with radiocarbon dates as old as 14.9 ka ^{14}C yr. B.P. obtained from this site.

(3) Sub-glacial scour apparently removed any pre-existing sediment within the bottoms of the troughs, although some sediment of likely last interglacial age is preserved locally within or near hanging valleys on the margins of troughs. The principal site that has been well studied is the "Fernbank" exposure on the west margin of Cayuga Lake (Maury, 1908; Bloom, 1972; Karrow and others, 1990). Interglacial deposits, assumed to be of Sangamon age, were reported from this location, providing

direct evidence that a Cayuga Lake trough of some sort existed prior to Wisconsin glaciation (Bloom, 1972, 1986). The lack of interglacial sediment as interpreted from seismic stratigraphy from the Cayuga Lake trough proper indicates that the present depth of excavation of the trough is a late-glacial feature.

(4) Sedimentation in the troughs was substantial in late-glacial time, up to 270 m total (Mullins and others, 1996). The bulk of this sedimentation occurred under proglacial lake conditions while ice was retreating northward in the troughs. The deposition initially was largely from the north, consistent with subaqueous outwash (Mullins and others, 1996). A reversal in direction of inwash into the proglacial lakes occurred around 13.9 ka ^{14}C yr. B.P., which Mullins and others (1996) interpret as an indicator of substantial lake-level drop. Perhaps this marks the time of retreat of the ice margin into the Ontario lowlands, although Mullins and others (1996) infer that a sedimentation event immediately prior to this reversal represents deposition from an ice margin that terminated at the north end of the present Finger Lakes. In any event, Mullins and others (1996) indicate that sedimentation in the period 13.9 ka ^{14}C yr. B.P. to 13.6 ka ^{14}C yr. B.P. consisted predominantly of sand and gravel deposits from lateral and southern sources, marking the first significant influx of sediment from these sources into the troughs. Alternatively, one could interpret the available evidence to indicate that prior to 13.9 ka ^{14}C yr. B.P. debris influx from the southern and lateral drainage systems was relatively minimal; we consider this interpretation below. There need not have been a regional change in the influx from lateral tributaries. However, boreholes south of both Canandaigua Lake and Cayuga Lake record the burial of lacustrine sediments by sand and gravel at this time, indicating a lake level comparable to the modern and progradation of deposition from the south. Thus, the lowering of lake level must have been complete by this time.

(5) Post-glacial infill of the lake troughs is relatively minor. Maximum interpreted thickness of post-glacial lake sediments (their Sequence VI) in Cayuga Lake is only about 12 m (Mullins and others, 1996) to perhaps greater than 15 m (Mullins, 1998).

Thus, the modern Finger Lakes troughs, including Cayuga Lake, owe their present morphology and sedimentation to late-glacial and post-glacial processes. However, these interpretations do not bear on the issue of the ultimate origin of the Finger Lakes, failing to address whether the troughs existed prior to the late Wisconsin ice advance. The stratigraphic relationships place strong constraints on evolution of the modern landscape, but to understand something of the broader context of trough development we turn our attention to the gorges themselves and the record they preserve. We will focus our attention on Cayuga Lake and its gorges, the focus of this field trip, as this area has been most intensively studied.

Prior Studies of Finger Lakes Gorges–Interglacial and/or Post-glacial?

Early workers (e.g. Matson, 1904; Tarr, 1904) recognized that post-glacial erosion must be invoked to explain the present deep gorges of the Cayuga Lake basin, incised to a base level controlled by the modern lake level. Fairchild (1899) provided a key framework for this interpretation by mapping the extent of pro-glacial lakes in the Cayuga trough. Progressive northward retreat of the Laurentide ice sheet opened progressively lower outlets for lake overflow (such as Grasso, 1970, and Hand, 1978, have described in detail for the Onondaga Valley lakes in the Syracuse area). This produced a series of distinct lake levels, progressively lower, into which tributaries built deltas (e.g., Fairchild, 1934). Most tributaries preserve morphologic and stratigraphic evidence of these pro-glacial lake deltas. Available exposures into these surfaces that we have visited in the Cayuga Lake trough generally display foreset beds, in some cases overlain by topset beds or even till (e.g. Stops 2C and 5 on this trip). As many as 7 or more delta surfaces are preserved above some of the gorges (Figure 2).

The early observers (e.g. Matson, 1904; Rich and Filmer, 1915) noted that the modern gorges generally are incised into broader valley bottoms, producing in some cases a valley-in-valley morphology (Figure 3). Rich and Filmer (1915) argued that multiple glacial events must have occurred to produce this landscape. They reasoned that tributary valleys evolved (widened) during interglacial times, and were buried by
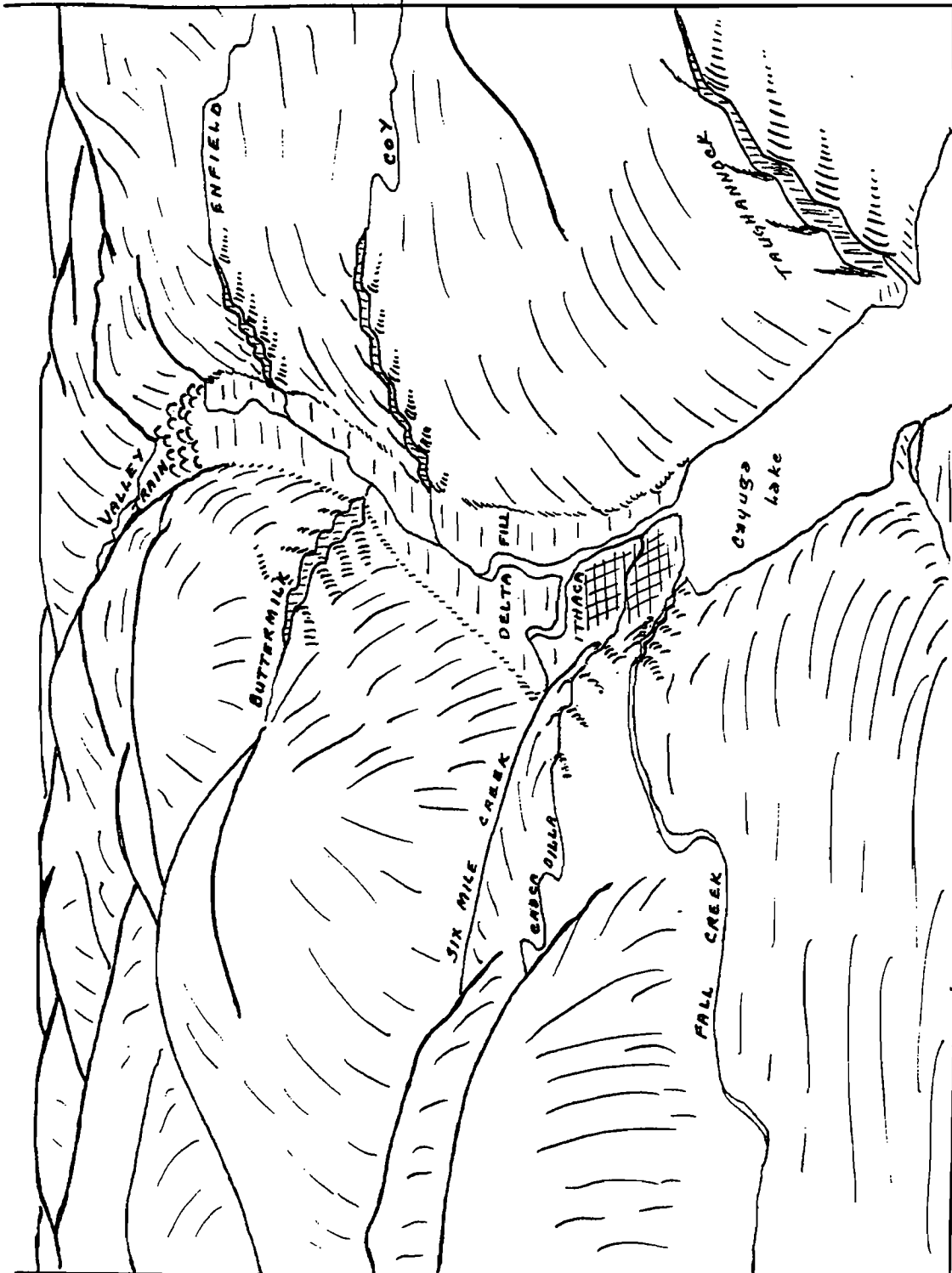
27

Figure 2. Diagrammatic sketch of the Ithaca region looking south. From Morisawa, 1950.

drift when ice covered the landscape. The main north-south Cayuga trough was deepened during each glacial period, and glacial retreat was followed by incision of now-hanging valleys to the newly established base level. Thus, they argued that the overall valley form of the upland valleys is inherited from pre-latest glacial (interglacial?) times, with post-glacial incision forming the modern gorges. The "classic" example cited in their work is the valley of Six Mile Creek. Von Engeln (1929) interpreted weathered gravels below till as evidence for deposition during advance of the last glacial maximum. Muller (1957) essentially confirmed this interpretation by dating wood in proglacial lake sediments at greater than 35,000 years. Subsequent dating of this and other sites in Six Mile Creek indicate that a proglacial lake, presumably impounded by the advancing Laurentide ice sheet, occupied a pre-existing valley at 41,900 ^{14}C yr. B.P. (Bloom, 1972).
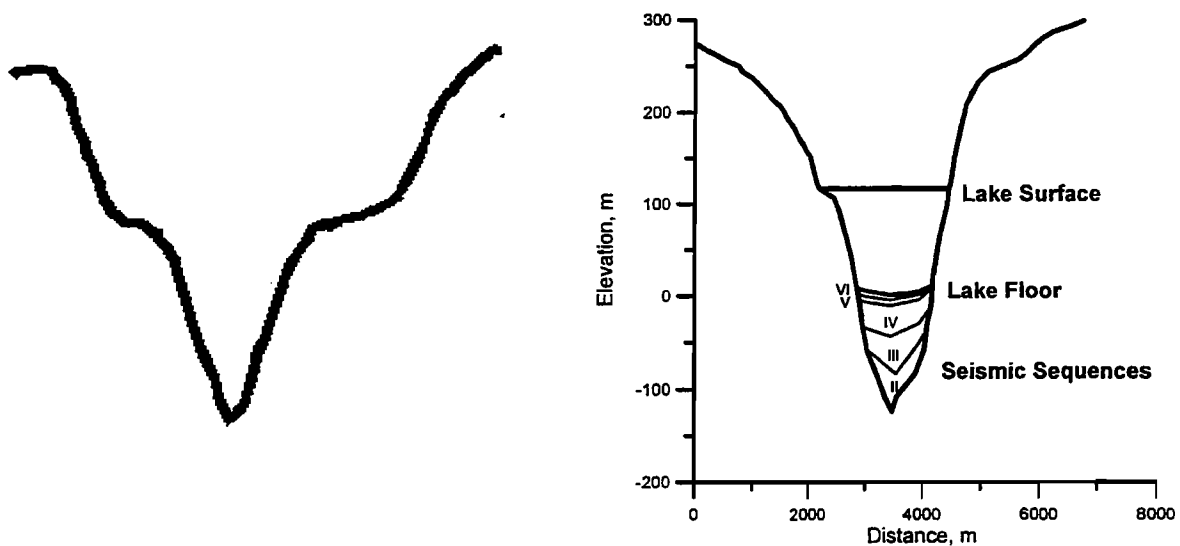

Figure 3. "Valley-in-valley" profiles. Left profile is typical of those found in rapidly incising valleys in the eastern Central Range of Taiwan (e.g., Willemin, 1993) and shows a canyon incised into a broader, higher valley below drainage divides. Not to scale. Right profile shows the shape of the Cayuga Lake trough as obtained from the Ludlowville 7.5' topographic map with sub-lake morphology and seismic stratigraphy generalized from Mullins and Hinchey, 1989. The bedrock incision below the lake floor is not as dramatic an example of "valley-in-valley" as the tectonically induced incision in Taiwan, but the overall character of valley incision is similar.

The morphology of Enfield Glen and other gorges also is cited as evidence for interglacial (or at least pre-latest glacial) development of tributary gorges. The relatively broad, open upper and middle portions of Enfield Glen have been described elsewhere (e.g. Cornell University, Dept. of Geology, 1959) as being re-excavated sections of an interglacial valley (Figure 4). Although this is a reasonable morphologic argument, we have been unable to find exposures of pre-latest glacial deposits to confirm this.

The available evidence and interpretations provide a convincing argument that the Finger Lakes gorges have a complex history, and that tributary gorges (or at least valleys) existed prior to the LGM. The modern gorges clearly are a post-glacial feature. But how and why did excavation occur, and how long has it taken to excavate (and preserve) this spectacular landscape?

Implications of Recent Work

The sites of the modern gorges were covered by ice when Valley Heads Moraine deposition was occurring at 14.9-14.4 ka ^{14}C yr. B.P. Upon ice retreat from the Valley Heads position, ice dammed meltwater escape to the north, the VHM deposits limited meltwater escape to the south, and local divides and cols controlled meltwater escape to the east and west. Thus, a series of proglacial lakes was impounded (Fairchild, 1934), with local streams (such as Enfield Creek) forming deltas into these lakes (Figure 5). As the ice retreated north, lake levels dropped, and delta positions dropped and advanced valleyward (Figure 5). Cayuga Lake and other Finger Lakes had apparently reached levels close to modern by 13.6 ka ^{14}C yr. B.P. Thus, base-level fall that triggered lowered deltas and tributary valley incision must have occurred within about no more than 1300 years. Indeed, Mullins and others (1996) imply that gorge incision was accomplished only after sedimentation from lateral and southern sources is recorded in the Finger Lakes cores and seismic records, i.e. in the interval 13.9-13.6 ka ^{14}C yr. B.P. This seems unlikely; other seismic stratigraphic evidence indicates a largely ice-free Cayuga Lake trough by 13.9 ka ^{14}C yr. B.P. (Mullins and others, 1996), which means lake levels already would have lowered in response to ice retreat.
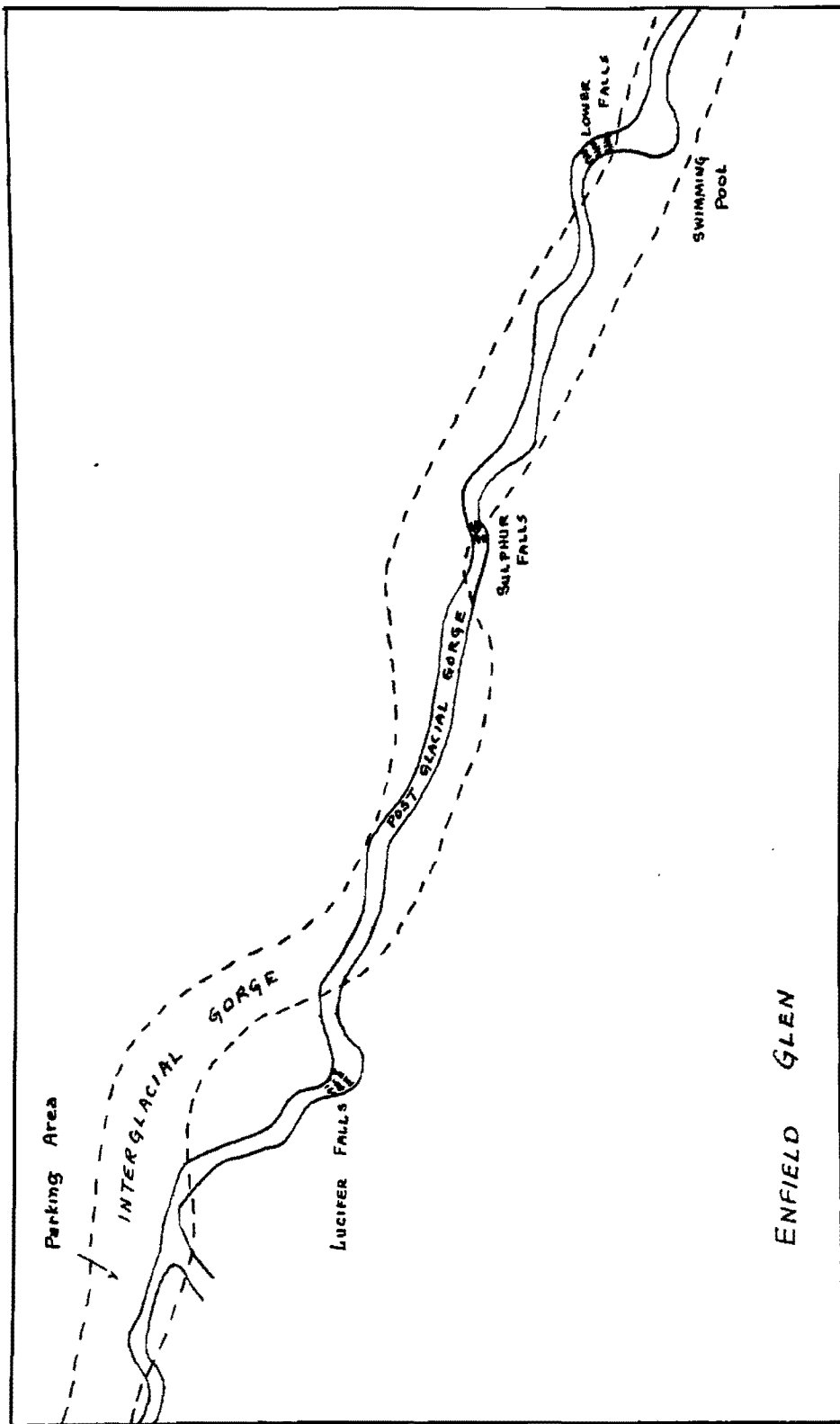
Figure 4. Inferred interglacial gorge of Enfield Creek, Enfield Glen, Robert Treman State Park. Similar figures are published in many guidebooks; this version is by Morisawa, 1950.
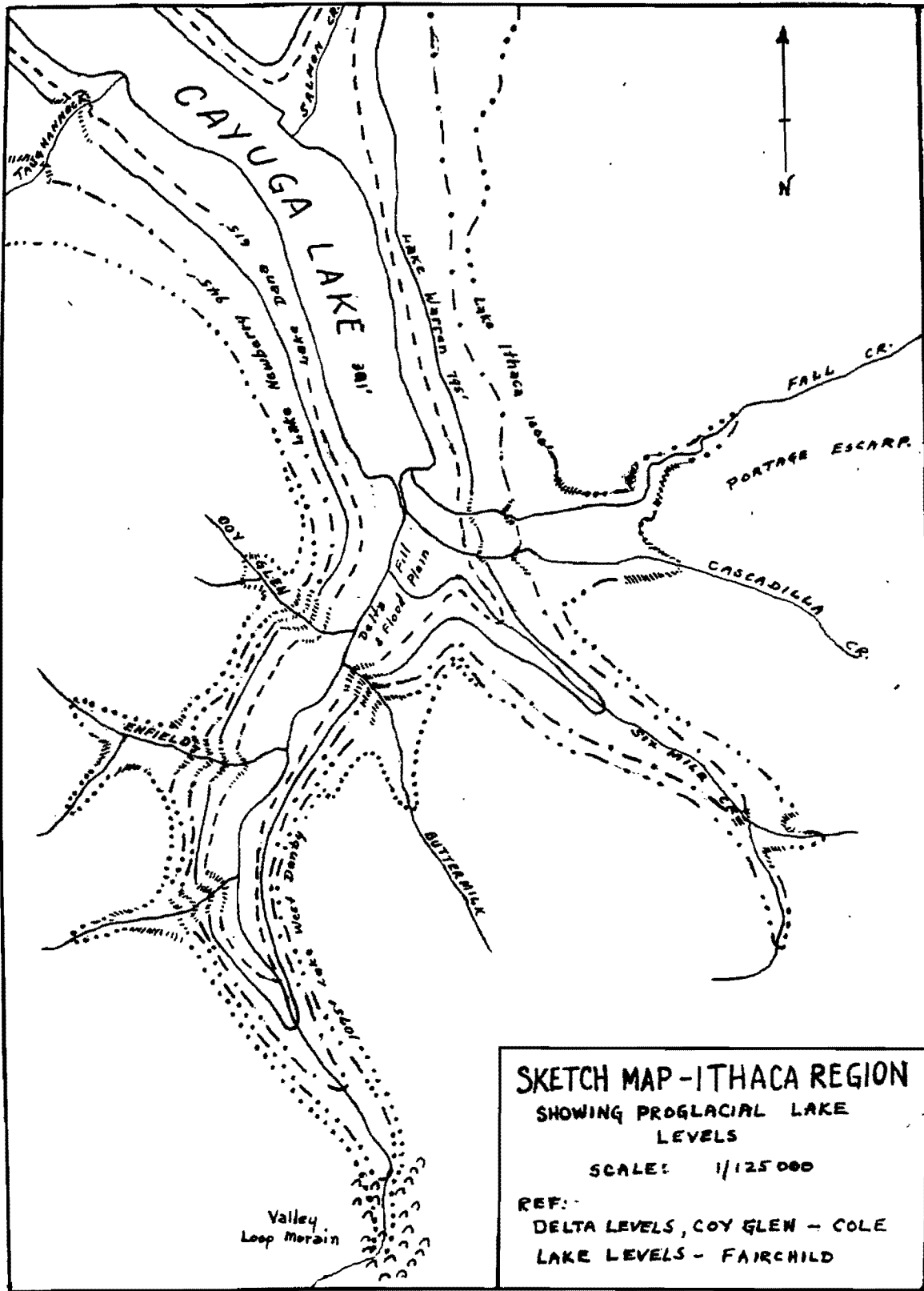
Figure 5. Proglacial lake levels and approximate delta distributions in the Ithaca region. From Morisawa, 1950.

Regardless of how short the time period was, formation of the deltas of the Finger Lakes, and at least some significant incision, was accomplished within a very brief interval of late-glacial time.

The implications of these dates are extremely important for understanding modern geomorphic processes and evolution of the Finger Lakes gorges. The base-level fall that produced the potential for gorge incision was rapid, but occurred in stages. Each drop in lake level was accompanied by trough-ward migration of the delta front and drop in level. Each change in delta level, then, must have been accompanied by formation of a knickpoint within the tributary channel, where the creek dropped from a previously established delta level to the new level. The final drop formed the modern prograding delta level for streams such as Taughannock Creek that drain directly into the lake. Streams like Buttermilk Creek that drain into southern inlet channels (in this case, Cayuga Inlet) actually have undergone minor post-glacial base-level *rise* as progradation of the inlet channel deposits has altered local base level.

The key point here is that knickpoint development is intricately tied into base-level fall, and the potential height (and, to some extent, position) of waterfalls was established during the late-glacial base-level drop. In this context, it is worth noting that incision and knickpoint retreat in individual streams have occurred very differently in response to this common base-level drop. The main waterfalls at Buttermilk Creek have retreated little from their positions established at and near the gorge mouth, whereas retreat of Taughannock Falls appears to be far more substantial (Figure 6). It is beyond our current purpose to speculate about the factors that have controlled this differential retreat.

Finally, we argue that the bulk of geomorphic work–base-level drop and subsequent knickpoint development and retreat–must have been substantially accomplished contemporaneously with initiation of the modern gorges during lake-level lowering. This clearly must be the case in streams such as Buttermilk Creek and Falls Creek, where the main knickpoint has not retreated significantly. For many of these
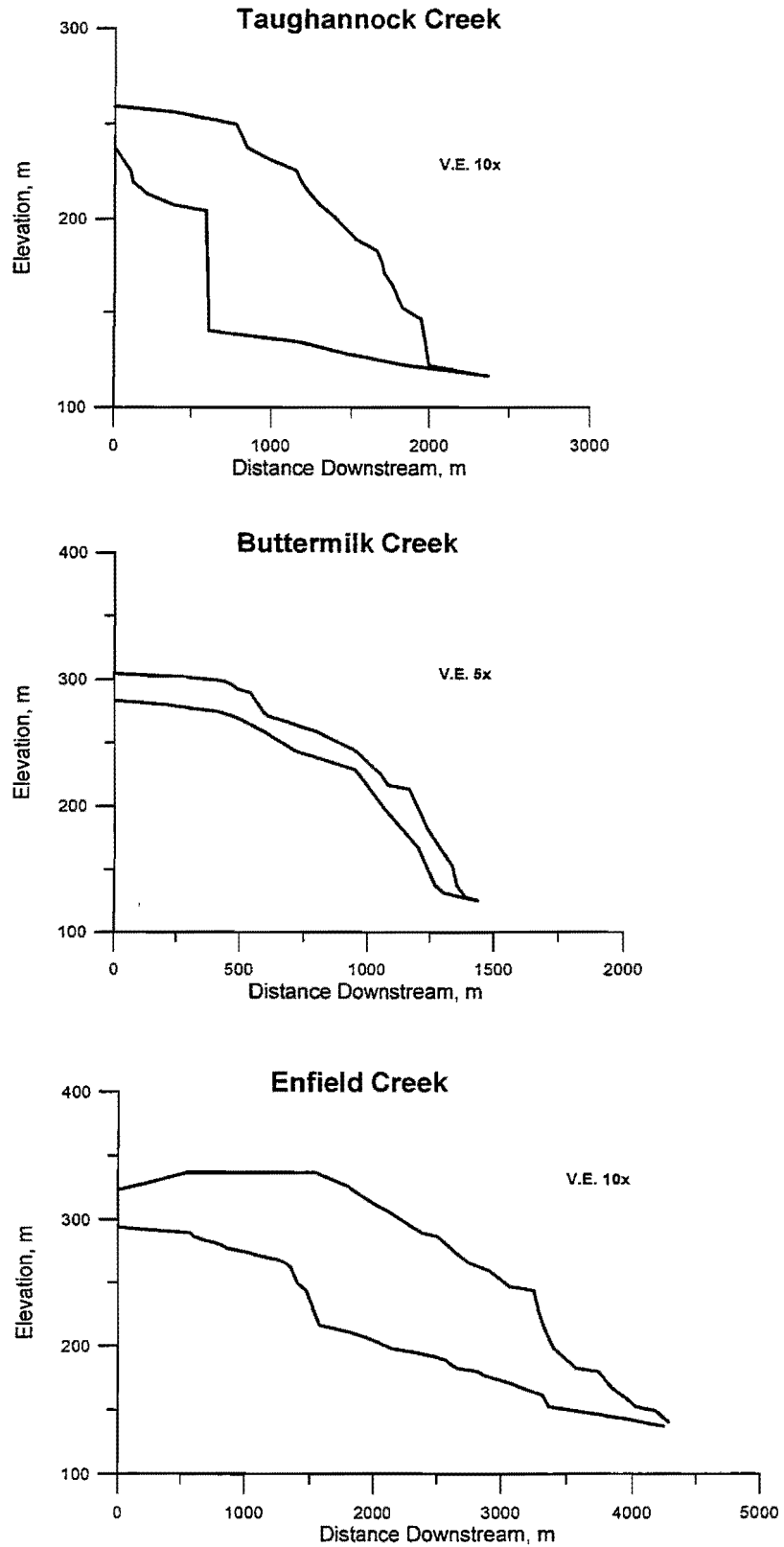
33

Figure 6. Long profiles of creek (lower line) and gorge crest (upper line), Enfield and Buttermilk Creeks from Ithaca West 7.5' topographic map, and Taughannock Creek from Ludlowville 7.5' topographic map. Note differences in degree of stream incision, distribution of incision, and preservation of delta sufaces.

streams, then, the discharge during late-glacial time must have been substantially more efficient in producing erosion than has been the case through the Holocene. We speculate that there was little vegetative cover on hilltops during the latest Pleistocene glacial retreat. Direct paleoclimatic data are lacking from this area, but pollen studies from other areas in the Northeast (esp. Wallface Pond in the Adirondacks—Whitehead and Jackson, 1990—and Tannersville Bog in the Poconos—summarized by Gaudreau and Webb, 1985) indicate that vegetation conditions during and immediately after ice retreat were comparable to modern tundra environments, although scattered spruce probably was present. This lack of vegetation, coupled with the lack of soils on freshly deglaciated uplands, likely would have resulted in high runoff/infiltration ratios and more effective discharge in upland basins. These may well have been the key conditions for rapid incision of streams tributary to the Cayuga Lake trough and other Finger Lakes basins.

References Cited

Bloom, Arthur L., 1972, Schedule and Guidebook, Friends of the Pleistocene 35th Annual Reunion: Cornell University, 20 p.

Bloom, Arthur L., 1986, Geomorphology of the Cayuga Lake basin: Field Trip Guidebook, 58th Annual Meeting, New York State Geological Association, p. 261-279.

Cornell University Department of Geology, 1959, Geology of the Cayuga Lake Basin: Guidebook for the 31st Annual Meeting, New York State Geological Association, 36 p.

Fairchild, Herman L., 1899, Glacial Lakes Newberry, Warren and Dana, in central New York: American Journal of Science, Fourth Series, v. 7, p. 249-263.

Fairchild, Herman L., 1934, Cayuga Valley lake history: Geological Society of America Bulletin, v. 45, p. 233-280.

Gaudreau, Denise C., and Webb, Thompson, III, 1985, Late-Quaternary pollen stratigraphy and isochrone maps for the northeastern United States, in Bryant, Vaughn M., Jr., and Holloway, Richard G., eds., Pollen Records of Late-Quaternary North American Sediments: American Association fo Stratigarphic Palynologists Foundation, Dallas, p. 247-280.

Grasso, Thomas X., 1970, Proglacial lake sequence in the Tully Valley, Onondaga County: Guidebook, 42nd Annual Meeting, New York State Geological Association, p. J-1 - J-23.

Hand, Brice M., 1978, Syracuse meltwater channels: Fieldtrip Guidebook, 50th Annual Meeting, New York State Geological Association, p. 286-314.

Karrow, P.F., Warner, B.G., Miller, B.B., and McCoy, W.D., 1990, Reexamination of an interglacial section on the west shore of Cayuga Lake, New York [abs.]: CANQUA-AMQUA Joing Meeting, Programme and Abstracts, p. 22.

Matson, George C., 1904, A contribution to the study of the interglacial gorge problem: Journal of Geology, v. 12, p. 133-151.

Maury, Carlotta Joaquina, 1908, An interglacial fauna found in Cayuga Valley and its relation to the Pleistocene of Toronto: Journal of Geology, v. 16, p. 565-567.

Morisawa, M., 1950, Falls and glens near Ithaca, N.Y.: unpublished field trip guide, Columbia University.

Muller, Ernest H., 1957, Filled bedrock gorges in the drainage basin of Cayuga Lake, New York [abs.]: Geological Society of America Bulletin, v. 68, p. 1771.

Muller, Ernest H., and Calkin, Parker E., 1993, Timing of Pleistocene glacial events in New York State: Canadian Journal of Earth Sciences, v. 30, p. 1829-1845.

Mullins, Henry T., 1998, Environmental change controls of lacustrine carbonate, Cayuga Lake, New York: Geology, v. 26, p. 443-446.

Mullins, Henry T., and Eyles, Nicholas, eds., 1996, Subsurface Geologic Investigations of New York Finger Lakes: Implications for Late Quaternary Deglaciation and Environmental Change: Geological Society of America Special Paper 311, 89 p.

Mullins, Henry T., and Hinchey, Edward J., 1989, Erosion and infill of New York Finger Lakes: implications for Laurentide ice sheet deglaciation: Geology, v. 17, p. 622-625.

Mullins, Henry T., Hinchey, Edward J., and Muller, Ernest H., 1989, Origin of New York Finger Lakes: a historical perspective on the ice erosion debate: Northeastern Geology, v. 11, p. 166-181.

Mullins, Henry T., Hinchey, Edward J., Wellner, Robert W., Stephens, David B., Anderson, William T., Jr., Dwyer, Thomas R., and Hine, Albert C., Seismic stratigraphy of the Finger Lakes: a continental record of Heinrich Event H-1 and Laurentide ice sheet instability, in Mullins, Henry T., and Eyles, Nicholas, eds., 1996, Subsurface Geologic Investigations of New York Finger Lakes: Implications for Late Quaternary Deglaciation and Environmental Change: Geological Society of America Special Paper 311, p. 1-35.

Rich, John Lyon, and Filmer, Edwin A., 1915, The interglacial gorges of Six Mile Creek at Ithaca, New York: Journal of Geology, v. 23, p. 59-80.

Shaw, J., and Gilbert, R., 1990, Evidence for large scale subglacial meltwater flood events in southern Ontario and northern New York State: Geology, v. 18, p. 1169-1172.

Tarr, R.S., 1904, Hanging valleys in the Finger Lake region of central New York: American Geologist, v. 33, p. 271-291.

von Engeln, O.D., 1929, Interglacial deposit in central New York: Geological Society of America Bulletin, v. 40, p. 469-480.

von Engeln, O.D., 1961, The Finger Lake Region; Its Origin and Nature: Cornell University Press, Ithaca, 156 p.

Wellner, Robert W., Petruccione, John L., and Sheridan, Robert E., 1996, Correlation of drillcore and geophysical results from Canandaigua Lake valley, New York: evidence for rapid late-glacial sediment infill, in Mullins, Henry T., and Eyles, Nicholas, eds., 1996, Subsurface Geologic Investigations of New York Finger

Lakes: Implications for Late Quaternary Deglaciation and Environmental Change: Geological Society of America Special Paper 311, p. 37-49.

Whitehead, Donald R., and Jackson, Stephen T., 1990, The Regional Vegetational History of the High Peaks (Adirondack Mountains) New York: New York State Museum Bulletin No. 478, 27 p.

Willemin, James H., 1993, Tectonic geomorphology and patterns of late Quaternary uplift, eastern Central Range, Taiwan: Ph.D. dissertation, State University of New York at Binghamton.

Road Log

Cumulative Mileage	Miles from Last Point	Route Description
0.0	0.0	Start at Lot C, Anderson Center, Binghamton University campus. Exit north and turn left onto Vestal Parkway, then immediately right onto Hwy. 201. Continue north on Hwy. 201 through the Johnson City traffic circle and exit west onto Hwy. 17. Travel west on Hwy. 17 to Owego.
20.8	20.8	Exit onto Hwy. 96 north through Owego to Candor, NY.
31.8	11.0	Continue directly north on Hwy. 96B toward Ithaca.
49.4	17.6	View area on left overlooking Cayuga Lake trough. Recent construction has impaired the view of geologic features.
50.1	0.5	Turn right onto Ithaca College campus and right toward football stadium. **STOP 1. Overview.** The Ithaca College campus is built on hanging deltas of Six Mile Creek and commands a spectacular view of the Cayuga Lake basin. Features that can be seen on a clear day include the oversteepened margins of Cayuga Lake trough to the north and hanging deltas of Coy Glen and Enfield Glen to the west and southwest. Similar hanging deltas characterize most of the streams that drain into the Finger Lakes troughs and the filled troughs to the south of the lakes. This stop affords us the opportunity to set the stage for features to be observed and discussed during the remainder of the trip.
50.3	0.2	Retrace steps to Hwy. 96B.
50.5	0.2	Turn right (north) on Hwy. 96B and descend South Hill into Ithaca. Continue on Hwy. 96B to its junction with Hwy. 13.
52.0	1.5	Junction Hwy. 13 north, Meadow St. in Ithaca. Turn right.
52.3	0.3	Turn left on Hwy. 96 to the "octopus" and continue up the hill past the Paleontological Research Institute and Thompkins County Hospital, through Jacksonville, and nearly to Trumansburg.
61.9	9.6	Turn right on Taughannock Park Rd. Note increasing incision of Taughannock Creek as we drive downstream. Note also our position on a relatively flat surface, one of the highest hanging deltas of Taughannock Creek.
63.1	1.2	Junction with Falls Rd.; turn right and cross bridge.
63.2	0.1	Turn into parking lot on left. **STOP 2A. Upper Taughannock Falls.** We walk onto the old rail bridge above (upstream of) Taughannock Falls. Although incision of Taughannock Creek has been increasing as we drove downstream from Hwy. 96, here is the first significant knickpoint in the channel—a drop of some 15 m.

Cumulative Mileage	Miles from Last Point	Route Description
		The view downstream is instructive: the lake-ward terminus of the high delta on which we have parked is clearly visible about 0.8 km (0.5 mi) downstream. Some of the incised meanders of the gorge upstream of the main Taughannock Falls also are visible.
63.9	0.7	Return to Taughannock Park Rd. and turn right. Stop at Falls Overlook parking area on right. **STOP 2B. Taughannock Falls Overlook.** The view area affords an excellent perspective of the main Taughannock Falls. Here the creek drops some 65 m through late Devonian Genesee Group sediments. The top of the falls is formed in resistant siltstone of the Sherburne member (Grasso and others, 1986); the notch at the lip of the falls has remained little changed since a rockfall in the late 1880s or early 1890s. One question to consider is how much the waterfall has retreated upstream. A possible clue is afforded by the retreat of the amphitheater in which the modern waterfall is located. Another possible clue is the position of the delta front, downstream of this position, that corresponds to the elevation of the crest of the waterfall. Bloom (1972) has suggested that the broad valley downstream of the waterfall is indicative of re-excavation of an interglacial valley. We are unaware of any exposed pre-latest Pleistocene unconsolidated sediments anywhere within the lower gorge. A related issue is how much of the incision we see here has occurred in post-glacial time, and how much may have occurred while the ice was retreating northward through the Cayuga Lake trough (and other Finger Lakes troughs) and providing the dams for progressively lowering lakes (and accompanying deltas). **STOP 2C. Gravel Quarry.** Cross Taughannock Park Rd. from the Falls Overlook parking area and walk onto the unpaved road on the left side of the small parking area. Walk about 100 m into an old quarry. This quarry is cut into the front edge of the most prominent high hanging delta of Taughannock Creek. Recent working of the northeast wall of the quarry has resulted in a spectacular exposure of the delta-front foreset beds. Sediments include well stratified sands and gravels with occasional clayey and silty interbeds.
63.9	0.0	Return to vehicles. Drive down Taughannock Park Rd. to Hwy. 89. Note the small delta surfaces across which we drive. The youngest delta, of course, is the active delta complex on which much of the developed area of Taughannock Falls State Park is located. This is one of the

Cumulative Mileage	Miles from Last Point	Route Description
		largest deltas on Cayuga Lake. If we use the analog from Canandaigua Lake and the evidence that Mullins and others have provided, we can assert that this delta probably began to form in latest glacial time, after base level for Taughannock Creek had dropped to approximately its modern position. Again, we can consider how much of the incision of bedrock occurred during this drop in lake levels, and how much is post-glacial.
64.7	0.8	Junction Hwy. 89. Turn right (south) to Ithaca.
74.2	9.5	Junction Hwy. 13 south in Ithaca. Turn right on Hwy. 13 south.
76.5	2.3	Entrance to Buttermilk Falls State Park on left. Turn in to Buttermilk Falls and park. **STOP 3 (LUNCH). Buttermilk Falls and Buttermilk Glen.** Time permitting, we'll walk up the lower park of Buttermilk Creek. Much of the incision is represented by the two main waterfall in the lower creek; this contrasts sharply with the situation at Taughannock Creek. Delta surfaces are not as well preserved here, but again hanging deltas do occur. Why is there such a difference in incision pattern? Was there no pre-last glacial channel to re-excavate here? Joint systems play a minor role in erosion by Buttermilk Creek, but spectacular potholes are excavated into the rocks at the gorge bottom. We may meet vans at the parking lot above the gorge, or we may continue from the lower entrance to the State Park. The road log assumes the latter.
78.0	1.5	Return to Hwy. 13 and turn left (south). Turn right at Hwy. 327.
81.0	3.0	Drive to upper entrance to Robert Treman State Park and turn left. Note an entrance to an abandoned gravel quarry on the right 0.2 miles before the entrance to the park. This quarry, formerly operated by the Town of Enfield, exposed foreset beds of the uppermost Enfield Glen hanging delta. These beds were overlain by a poorly consolidated, thin (less than 2 m exposed) till. We interpret the deltaic sediments as marking the input of Enfield Creek sediments into the highest level of the pro-glacial Cayuga Trough lake, with a nearby ice margin overriding the sediments during a brief interval of re-advance.
81.75	3.75	Park at entrance to Enfield Glen. **STOP 4. Enfield Glen.** No tour of the Finger Lakes gorges around Ithaca would be complete without a stop to tour the upper part of Enfield Glen. The parking area and picnic ground are in a relatively broad valley containing an

Cumulative Mileage	Miles from Last Point	Route Description
		alluvial floodplain over bedrock. Note that bedrock is exposed in the valley walls and in tributary channels such as Fish Kill just upstream from the mill. Poorly exposed colluvium mantles other slopes of this valley wall. As we walk into Enfield Glen, note the abrupt change to a narrow gorge deeply incised into well jointed bedrock. Here jointing has played a key role in facilitating excavation of bedrock by the stream. We walk down to Lucifer Falls, below which the valley again opens into a much wider, bedrock-walled gorge. The traditional interpretation is that the wide gorge sections indicate reoccupation of a buried interglacial gorge, whereas the bedrock gorge represents post-glacial incision into the Devonian bedrock (e.g. von Engeln, 1961). The reason for post-glacial diversion through a bedrock gorge is assumed to be a mass of Wisconsin glacial sediment choking the interglacial valley, such that Enfield Creek was diverted and flowed across (and incised into) bedrock. Again, to what extent has the incision occurred in post-glacial times (which is what the "conventional" interpretation would imply) and how much occurred during ice retreat up Cayuga Lake trough? If the stream achieved a base level approximately at the modern Cayuga Inlet altitude, then virtually all of the base-level fall that has driven incision occurred during late glacial time. How much knickpoint retreat has occurred? How can we assess this?
85.5	3.75	Return to Hwy. 13. Note delta surfaces as we drive back down the hill.
87.3	1.8	Turn right (south) on Hwy. 13. Continue on Hwy. 13 to Millard Hill Road; Landstrom Gravel Pit on the right. Turn onto Millard Hill Road and into the parking lot of the Landstrom Pit. **STOP 5. Landstrom Gravel Pit.** *Get permission at the office before entering.* This pit is excavated into the lowermost delta of Enfield Creek and represents the last depositional event before Enfield Creek had stabilized at more or less its current base level. Note the similarity of overall stratigraphy to what we viewed at Stop 2C. Here we have a higher clay content and the development of clay balls and climbing ripples (which may or may not be visible on the day of the field trip).
87.3	0.0	Return to vehicles.
87.8	0.5	Drive north on Hwy. 13 to Decker Road, junction Hwy. 34/96 south. Turn onto Hwy. 34/96 toward Spencer. We soon climb into the Valley Heads Moraine complex of West Danby, NY. This is one of the longest and southernmost valley-filling reaches of Valley Heads Moraines in central New York.

Cumulative Mileage	Miles from Last Point	Route Description
96.8	9.0	Pull off to left side of road at entrance to gravel mining operation. **STOP 6. Gravel Pit.** Walk past the gate and down the hill, noticing poorly exposed well rounded gravels on right. Note hummocky morainal topography visible ahead on to the left. Turn right at road at bottom of hill and enter main gravel workings. Here the Valley Heads Moraine is comprised of well rounded, sorted, and weakly stratified sands and gravels. This is typical of VHM deposits in those exposures we have visited in central New York, as well as in exposures discussed by Yang (1992). Clearly water played an active role in abrasion and deposition in this glacial-marginal environment! We'll discuss the implications of this for development of the VHM and its relationship to the Cayuga Lake trough, the hanging deltas, and the exposures we've already seen.
101.7	4.9	Return to vehicles and drive south to Spencer, NY. Turn left onto Hwy. 96 toward Candor. Note asymmetric valley walls. As is typical of valley walls in east-west valleys in the glaciated Appalachian Plateau, the south-facing walls have relatively gentle slopes and the north-facing walls are steep and truncated. Coates (1966) interprets these as till shadows: south-facing walls have thick lodgement till deposits resulting from loss of basal stress as the glacier descended into the valley, whereas the south wall has thinner, compressed till due to high pressure as the south-traveling basal ice "piled up" against the valley.
108.3	6.6	Turn left (north) onto Gridleyville Crossing Road.
109.4	1.1	Turn left (north) onto Hwy. 96B.
·110.2	0.8	Turn right into Robinson's quarry. Note that you shouldn't enter here without permission. The pit managers request that all visiting geologists wear hard hats **STOP 7. Robinson's Gravel Pit.** *Get permission at office before entering pit.* As a final stop, we look at deltaic deposits <u>not</u> associated with the pro-glacial lakes of the Cayuga trough. Here we are downstream of the Valley Heads Moraine of Willseyville Creek. The landform is a kame surface, and we interpret the sediments as primarily deltaic foreset beds. However, they dip back toward the valley wall rather than toward the valley center, suggesting a complex mode of origin. Local slump features and contorted bedding attest to the kame origin of this deposit.
146.1	35.9	Return to vehicles. Drive south on Hwy. 96B back through Candor and on Hwy. 96 south through Owego. Turn east on Hwy. 17 and retrace steps to Binghamton University.

DEVONIAN FLUVIAL TO SHALLOW MARINE STRATA, SCHOHARIE VALLEY, NEW YORK

John Bridge and Scott Jarvis

Department of Geological Sciences, Binghamton University,
Binghamton, New York 13902-6000

Introduction

The Middle to Upper Devonian Catskill clastic wedge in New York State is part of a foreland-basin fill that has relatively thick non-marine deposits to the east and thinner marine deposits to the west. The overall succession of strata is indicative of marine regression: however, there is ample evidence in coastal and fluvial strata of periodic marine transgressions. There are several superimposed scales of cyclicity in these strata, at least three of which can be readily distinguished:

(1) 10- to 100-meter thick, asymmetrical coarsening-upward to fining-upward sequences, representing on the order of hundreds of thousands to millions of years, that have been interpreted as recording relative sea-level changes associated with eustasy, tectonically induced changes in sediment supply and subsidence rate, and possibly climate change (e.g., Dennison and Head, 1975; Dennison, 1985; House, 1983, 1985; Johnson et al., 1985; Ettensohn, 1985; Brett and Baird, 1986; Van Tassell, 1987; Willis and Bridge, 1988; Dennison and Ettensohn, 1994).

(2) Meter- to 10-meter thick fining-upward or coarsening-upward sequences of sandstone and shale (representing thousands to hundreds of thousands of years) that have been interpreted to have been formed by lateral migration, abandonment and filling of channels; progradation and abandonment of channel-mouth bars, crevasse splays and tidal flats; and filling of coastal bays (e.g., Johnson and Friedman, 1969; McCave, 1968, 1969, 1973; Miller and Woodrow, 1991; Bridge and Willis, 1994). Although these sequences could have been caused by autocyclic processes such as channel switching (avulsion), allocyclic causes such as eustatic sea-level changes must also be considered (Van Tassell, 1987; Bridge and Willis, 1994).

(3) Centimeter- to decimeter-thick, sharp-based sandstone stratasets capped by shale that are commonly interpreted as the deposits of individual floods in rivers and floodplains, or storm events at sea (e.g., Gordon and Bridge, 1987; Craft and Bridge, 1987; Halperin and Bridge, 1988; Willis and Bridge, 1988; Bridge and Willis, 1994; and many others).

The validity of these interpretations of the different scales of facies sequence hinges on describing them in detail, and being able to correlate them between different outcrops. Physical tracing of strata between outcrops is made difficult by the wide spacing of outcrops (and cores), variable dip of strata, lateral changes of facies, lack of distinct marker horizons, and the absence of seismic profiles. Biostratigraphic correlation is very crude because biozones extend for on the order of a million years (100 m of strata) and only recently has it been possible to correlate marine
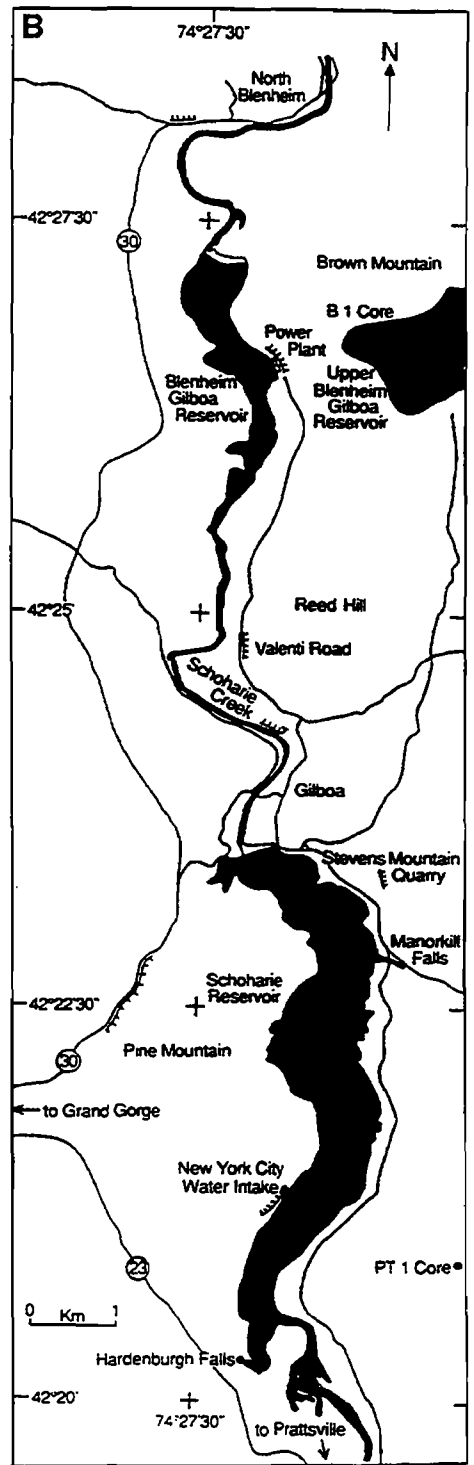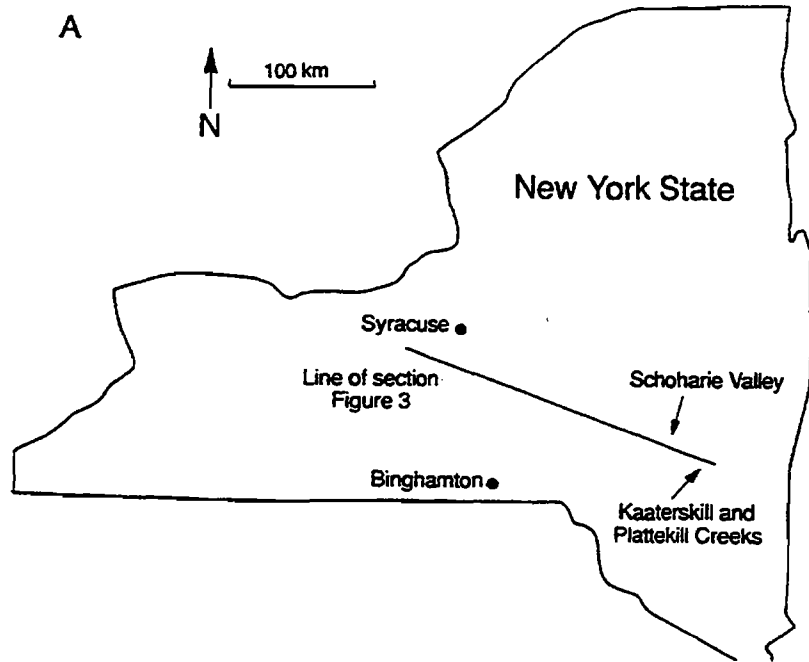
Figure 1. (A) Location of study areas in New York State. (B) Location of outcrops and cores studied in Schoharie Valley. Map drawn from USGS 1:24,000 maps of Gilboa and Prattsville, NY.
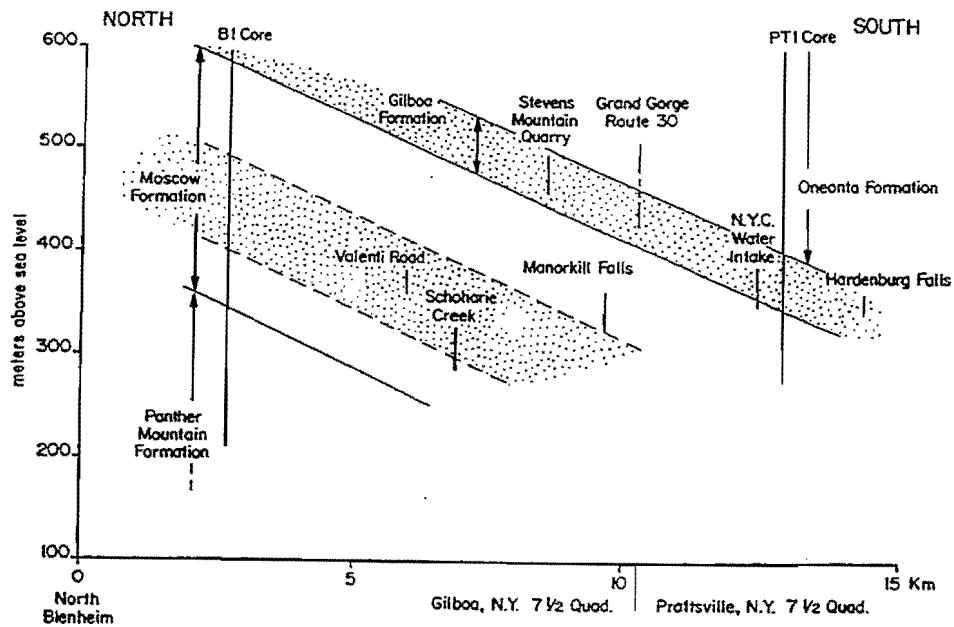
Figure 2. Stratigraphic section oriented N-S showing positions of outcrops and cores, and correlation of formations and other distinctive lithostratigraphic units within Schoharie Valley. Line of section approximately follows Blenheim-Gilboa and Schoharie Reservoirs. (Fig. 1). Correlations were made based on a regional dip to the S. of approximately 1.5° and matching of distinctive sequences which are on the order of tens of meters thick. Sandstone-dominant parts are stippled.

Figure 3. Stratigraphic section oriented approximately ENE-WSW (see Fig. 1 for location) showing correlation of formations in Schoharie Valley with marine formations to the west and fluvial formations to the east. Revised from work of Cooper (1933, 1934), Fletcher (1963, 1967), McCave (1968.

45

and non-marine rocks using miospores. Stratigraphic correlation of 10 meter thick to 100 meter thick sequences in marine strata is accomplis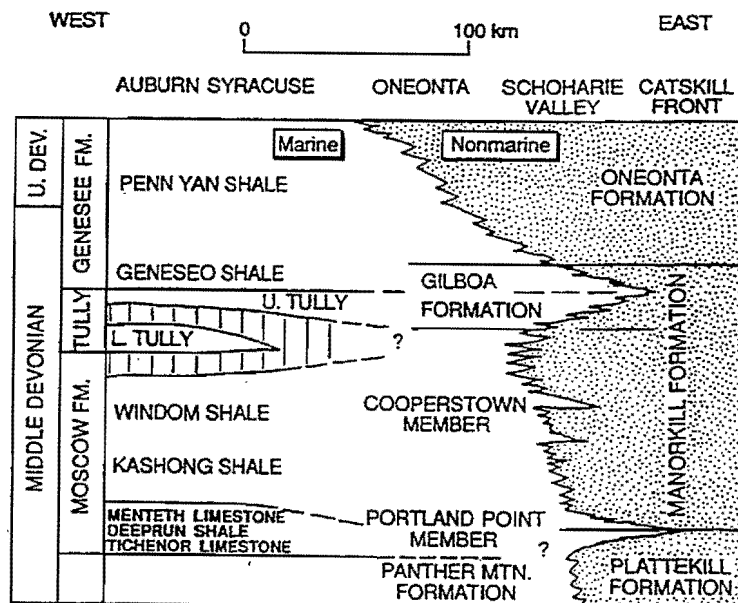hed using laterally extensive black shales and limestones (Sutton et al., 1962; Sutton, 1963; Woodrow and Nugent, 1963; McCave, 1969, 1973; Rickard, 1975, 1989; Brett and Baird, 1985, 1986, 1990). However, their correlation with coastal and non-marine rocks remains uncertain (Halperin and Bridge, 1988; Bridge and Willis, 1994). In coastal and fluvial strata, it is difficult to correlate 10 meter thick and thinner stratasets for more than on the order of kilometers. This inability to correlate any but the thickest sequences across the basin makes it difficult to interpret these deposits in a sequence stratigraphic context, and difficult to assess whether the controls on their formation are local, regional or global.

Examples of the different scales of sequence in fluvial, coastal and shallow-marine deposits will be examined in the Schoharie Valley (in the vicinity of Gilboa, Grand Gorge and Prattsville). Bridge and Willis (1994) studied selected outcrops and cores through the interleaved fluvial and marine deposits of the Schoharie Valley (Figure 1), in order to expand upon previous descriptions and interpretations of these strata (e.g., Johnson and Friedman, 1969; McCave, 1968, 1969, 1973; Miller and Woodrow, 1991). Attention was focussed on the influence of wave, tidal and fluvial currents in shaping the coastal region, and on how these currents and coastal morphology changed during marine transgressions and regressions. Basin-scale controls on deposition were evaluated by considering coeval fluvial deposits to the east (Willis and Bridge, 1988) and offshore marine deposits to the west (Brett and Baird, 1985, 1986, 1990).

Ten-meter thick sequences were correlated between cores and outcrops over distances of up to 10 km (Figure 2; Bridge and Willis, 1994). Stratigraphic subdivision of these rocks (Figure 3; modified from Rickard, 1975, 1989) is due mainly to the work of Cooper (1930, 1933, 1934) and Cooper and Williams (1935). Some formations were defined based on fossils in fully marine deposits, but key zone fossils are absent in coastal and fluvial deposits. Nevertheless, the formations defined by Cooper can generally be recognized in Schoharie Valley. Outcrops to be visited span the upper Moscow Formation (Manorkill Falls), the Gilboa Formation (Route 30 near Grand Gorge, Hardenburgh Falls; Stevens Mountain Quarry), and the lower Oneonta Formation (Route 30 near Grand Gorge). These Formations are mid to late Givetian in age. This stratigraphic interval includes a major transgression and regression, upon which are superimposed smaller scale changes in relative sea level.

Hardenburgh Falls

Description

The Hardenburgh Falls outcrop (Figure 4) is assigned to the middle-upper part of the Gilboa Formation, and is equivalent to the middle part of the Stevens Mountain Quarry section (Figure 2). The lowest 6 meters of this exposure (Figure 4) comprise gray sandstones, dark gray siltstones and shales. The mudstones are sparsely fossiliferous and typically bioturbated. The fine to very-fine grained sandstones are sharp-based, cm- to dm-thick sheets and lenses. Thinner ones contain wave-ripple cross strata and are capped by wave ripple marks (2-D, 3-D, and interfering types). Thicker, coarser grained sandstones have hummocky-swaley cross strata and/or planar strata in their lower parts, and abundant intraformational shale fragments and disarticulated shelly
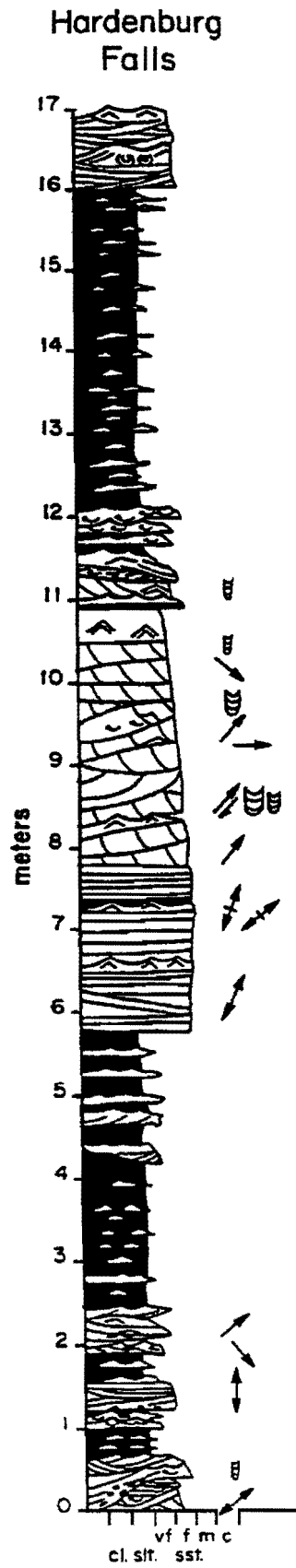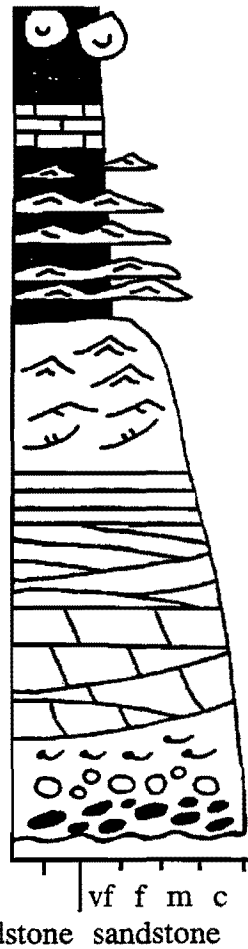
Hardenburg Falls

Figure 4 (A). Sedimentological log from Hardenburgh Falls. The sandstone body in this outcrop is equivalent to sandstone body (b) of Figure 5. Symbols explained in Figure 4 (B).

47

LEGEND

Load structures

Mudstone

Calcareous mudstone

Lenticular/wavy bedding with
wave or current ripple marks

Flaser bedding

Small-scale cross-strata
with wave ripples

Small-scale cross-strata
with current ripples

Planar-strata

Hummocky/swaley cross-strata

Medium-scale planar cross-strata

Medium-scale trough cross-strata

Shell breccia
Extraformational pebbles
Intraformational breccia
Erosion surface

vf f m c

mudstone sandstone

	Fish fragments		Calcareous nodules
	Vertical and horizontal burrows		Mudcracks
	Meniscate burrows of various sizes	=	Fissile
	Chondrites		Blocky texture
	Spirophyton		Disrupted
	U-shaped burrows		Pseudoanticlines
	Branching burrows		Unidirectional paleocurrent direction (N to top of page)
	Tree trunk cast		Orientation of parting lineation
	Plant fragments		Oscillatory paleocurrent directions
	Root casts		
	Rhizoconcretions		

Figure 4 (B).   Legend for Figures 4-7. Set thicknesses of medium-scale cross strata are cm to dm thick, and the cross strata are normally at the angle of repose; however, they are locally lower angle and transitional to hummocky-swaley cross strata.

fossils. Near the base of the section (e.g. Figure 4, meter 2) relatively thick sandstone stratasets have unidirectionally dipping low-angle to high-angle, medium-scale cross strata with easterly paleocurrents, and extraformational pebbles. At the base of the section, amalgamated sandstone stratasets fill N-S oriented channels that are up to decimeters deep and meters wide. These relatively coarse grained strata contain rounded extraformational chert and quartzite pebbles.

Shell accumulations include the brachiopods *Spinocyrtia, Mucrospirifer, Mediospirifer, Orthospirifer, Cupularostrum,* the bivalves *Goniophora, Actinopteria, Palaeoneilo,* and crinoid ossicles. Most of the disarticulated shell fragments lie concave down along stratal surfaces and show little evidence of breakage or abrasion of fine detail. Some shell concentrations are markedly monospecific (e.g *Cupularostrum).* Small, centimeter-diameter vertical burrows occur in the tops of sandstone strata.

The 5.5 meter thick, medium- to fine-grained sandstone body in the middle of this section has a sharp base that is overlain by planar strata and swaley cross strata with horizons of wave ripples draped by shale. Asymmetrical wave ripples indicate a NE-SW oscillation with a preferred migration to the SW. The overlying medium-scale trough cross strata dip to the NE mainly (with a rare, oppositely directed set) and contain superimposed wave- and current-ripple marks. Medium-scale planar cross strata with a SE dip, occurring above the trough cross strata, climb up low-angle surfaces that dip to the NW. Vertical, meniscate burrows of varying diameter occur throughout the sandstone body. Several stratasets of shell-rich sandstone with hummocky cross strata and wave ripples occur immediately above the sandstone body.

Interpretation

Interbedded mudstones and sandstones with hummocky cross strata, planar strata, wave-ripple marks and associated cross strata, and abundant shelly-fossil concentrations are interpreted as nearshore marine deposits formed below fair-weather wave base (e.g. Dott and Bourgeois, 1982; Hunter and Clifton 1982; Swift et al., 1983). Sandstones were formed during storms by either dominantly wave currents or by combined wave and unidirectional currents (Craft and Bridge, 1987; Southard et al., 1990, Duke et al., 1991), whereas mudstones represent fair-weather deposits or those accumulated below storm-wave base. Amalgamated sandstone stratasets indicate deposition mainly above fair-weather wave base. The preferred easterly paleocurrent orientation of some low- and high-angle cross strata, and the association of increasing grain size with increasing inclination of these cross strata, suggest onshore directed currents (asymmetrical wave, and/or flood tidal) that in places were strong enough to change hummocky bedforms to dunes (e.g. Nottvedt and Kreisa, 1987; Arnott and Southard, 1990; Myrow and Southard, 1991; Cheel and Leckie, 1992). The shallow channels may be cut by either storm-induced or tidal currents (e.g. Cacchione et al., 1984; Craft and Bridge, 1987).

The sandstone body in the middle of this exposure is interpreted as the deposits of a tidal-channel mouth bar that prograded into a storm-wave dominated sea. The vertical variation in sedimentary structures indicates wave currents or combined wave and unidirectional currents lower down, but dominantly unidirectional currents higher up. Paleocurrents associated with wave ripples are generally alongshore (NE-SW). The alongshore to landward-directed trough

49

cross strata (NE-E) are probably associated with sinuous-crested dunes formed by tidal flood currents, and ebb tidal currents were relatively unimportant. Planar cross strata migrating to the SE may represent wave-formed swash bars or tide-formed straight-crested dunes (e.g. Hayes and Kana, 1976; Boothroyd, 1978; Fitzgerald, 1984; Sha and De Boer, 1991). Superimposed wave- and current-ripples indicate periods of reduced wave- and tidal-current strength. The sparse fauna and low degree of bioturbation, but dominance of the *Skolithos* ichnofacies, is typical of sandy deposits in coastal areas (Howard and Reineck, 1981).

The relatively sharp base and top of this sandstone body could be interpreted as due to diversion of a channel into this area followed by abandonment, reduction in sand supply, and marine transgression. However, an alternative explanation could be one of progradation of a sandy shoreface during a relative sea-level fall (a forced regression), followed by modest erosion of the top of the sandstone body during marine transgression. These alternatives are discussed below.

Stevens Mountain Quarry

Description

Stevens Mountain Quarry exposes a large proportion of the Gilboa Formation (Figure 2). Attention will be directed to the 2 to 6 meter thick sandstone bodies that occur in the upper 30 meters of the quarry (Figure 5). These fine-to medium-grained sandstone bodies have sharp, erosional bases with tool and flute marks, overlain by intraformational breccia comprising shale clasts, plant fragments and shelly fossils (bivalves, brachiopods, *Tentaculites* and crinoid fragments). Relatively thin (2 to 3 meters) sandstone bodies are composed of amalgamated, dm- to m-thick stratasets containing swaley cross strata and planar strata. The erosional bases of individual stratasets are commonly overlain by transported shell fragments. These sandstone bodies vary little in grain size throughout their thickness: however, they tend to be capped with concentrations of shells, intraformational shale fragments and rounded extraformational pebbles (e.g. Figure 5A, 15-17m, Figure 5B, 7-9m and 12-15m). As the thickness of these sandstone bodies increases, stratasets of medium-scale cross-stratified sandstone begin to dominate their upper parts (e.g. Figure 5B, 19-23m). This kind of sandstone body may fine upwards, coarsen upwards or show little vertical variation in grain size. Like the thinner examples, they are capped by concentrations of shells, intraformational breccia and extraformational pebbles. The thickest sandstone bodies are medium grained and composed almost entirely of medium-scale cross strata, with lenses of planar strata. Erosional reactivation surfaces in cross sets are common. In places, asymmetrical ripple marks on reactivation surfaces and cross stratal surfaces indicate a paleocurrent direction opposite to the medium-scale cross strata (e.g. Figure 5A, 33-39m, Figure 5B, 29-34m). Stratasets in these sandstone bodies may be inclined at several degrees relative to the basal erosion surface (i.e. large-scale inclined strata) and sandstone-filled channels may occur in their upper parts. Immediately above some sandstone bodies, sandstone stratasets may have unidirectionally dipping low-angle and angle-of-repose cross strata, abundant shell accumulations and intraformational and extraformational pebbles. Such stratasets may also be markedly lenticular and fill channels up to dm deep and meters wide (as at the base of Hardenburgh Falls). Laterally extensive horizons of sandstone load casts occur immediately beneath some sandstone bodies.

50

Stevens Mountain Quarry North
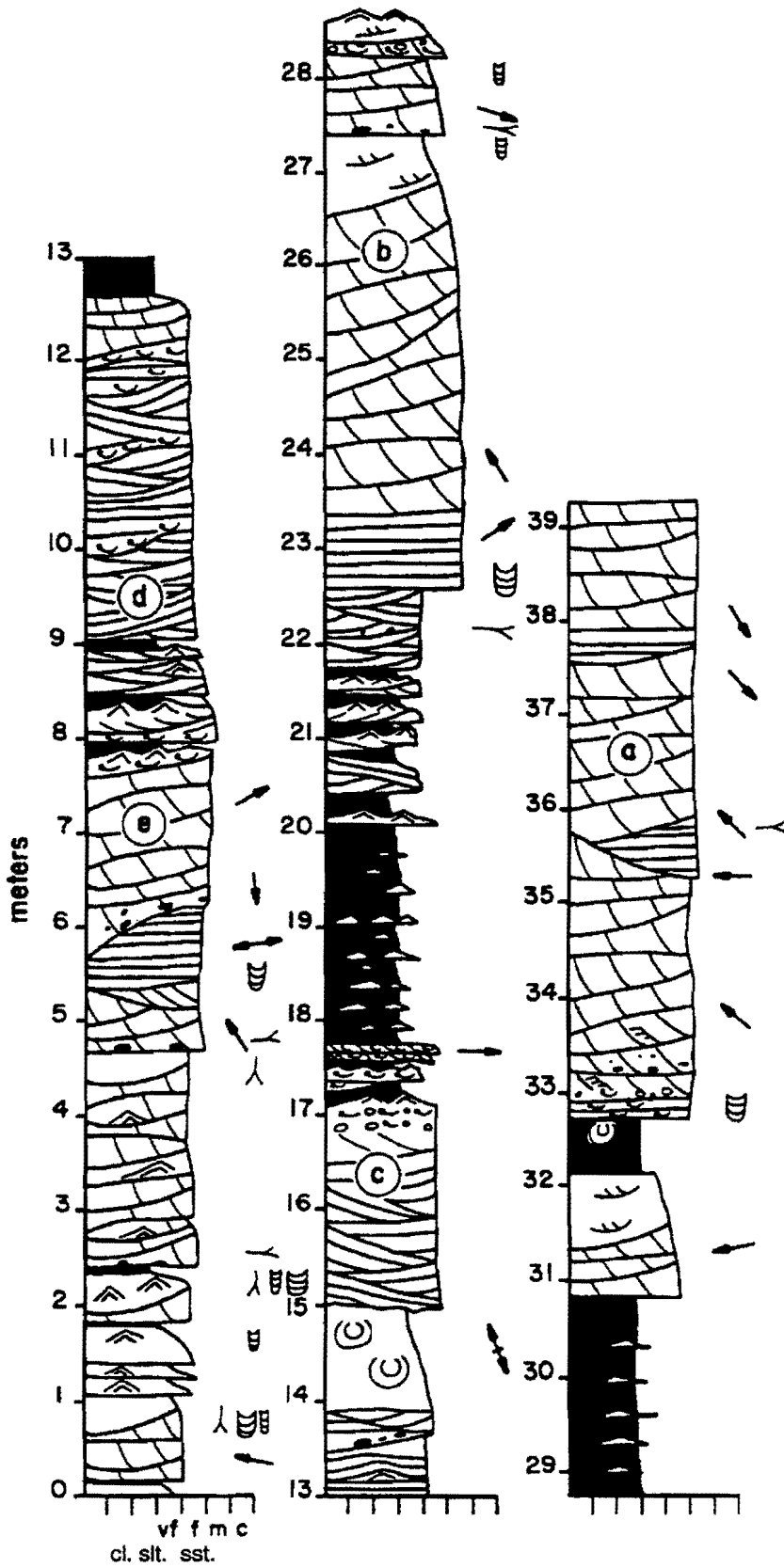
Figure 5 (A). Sedimentological log from the north end of Stevens Mountain Quarry.
Sandstone bodies designated (a) through (e) are identified on both logs
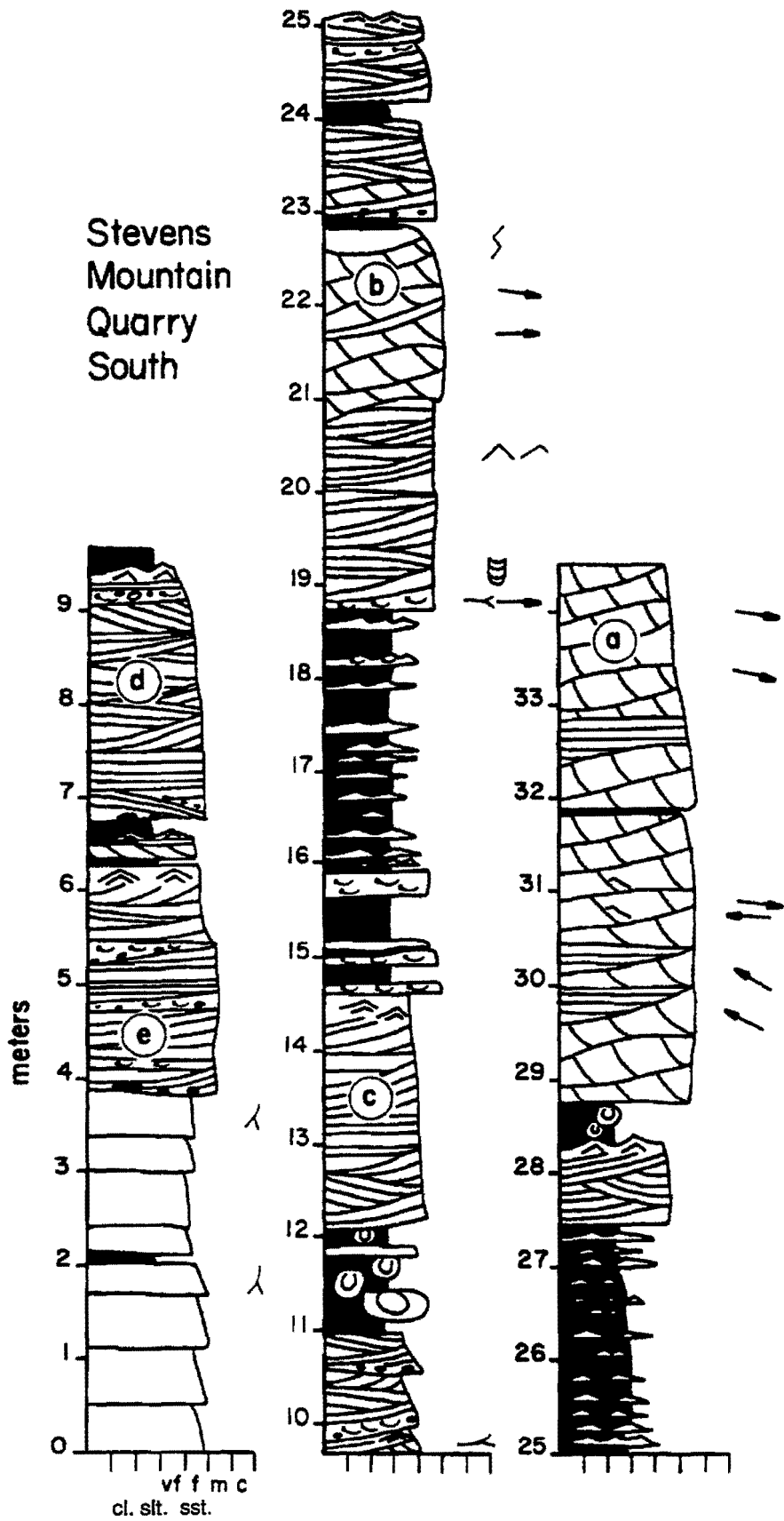in order to illustrate lateral variations.

Figure 5 (B). Sedimentological log from the south end of Stevens Mountain Quarry. Sandstone bodies designated (a) through (e) are identified on both logs in order to illustrate lateral variations.

Paleocurrent directions from medium-scale cross strata in and above the upper parts of all sandstone bodies are generally in an easterly direction (range from NNE to SE). Medium-scale cross strata in the lower parts of the thickest sandstone bodies are generally oriented approximately 180 degrees to those higher up. Tool marks at the base of sandstone bodies give paleocurrents to the W and NW or to the E and SE.

Skolithos burrows (mm to cm diameter) are common in tops of sandstone stratasets. *Arenicolites* and *Chondrites* also occur. Large (up to 0.1m diameter) vertical, sand-filled meniscate burrows are characteristic of thicker sandstone bodies. Some sandstones are so bioturbated that primary sedimentary structures are difficult to discern (e.g. base of quarry). Fossils in the shell accumulations include brachiopods (*Spinocyrtia, Mucrospirifer, Tropidoleptus carinatus, Cupularostrum (Camarotoechia), Mediospirifer, Orthospirifer mesastrialis)*, bivalves *(Goniophora, Grammysia, Actinopteria, Cypricardella, Palaeoneilo), Tentaculites* and crinoid ossicles (Cooper and Williams, 1935).

The thickness and sedimentary characteristics of sandstone bodies and mudstone intervals change laterally over hundreds of meters (compare sandstone bodies e and b in Figures 20A and B). Also, the thickest sandstone bodies dominated by angle-of-repose cross strata occur at the top of the quarry, whereas relatively thinner ones with mainly swaley cross strata and abundant shelly fossil accumulations occur lower down.

Interpretation

The thickest cross-stratified sandstone bodies with erosional bases overlain by intraformational breccia with shelly fossils, large-scale inclined strata and channel-fills, and opposing paleocurrent directions, are interpreted as deposits of laterally migrating tidal channels (see also Johnson and Friedman, 1969). Dominance of ebb-directed paleocurrents lower in sandstone bodies and flood dominance in the upper parts (in places associated with channel fills) is typical of strongly asymmetrical tidal currents in tidal inlets, estuaries, and tide-influenced deltaic distributaries. Variable dip angles of medium-scale cross-strata, erosional reactivation surfaces and superimposed current ripples are further evidence of strong tidal-current asymmetry. They indicate growth of sinuous-crested dunes to 'full vortex' stage during the dominant tidal current, slackening of the current and modification of dune geometry, then erosion of the dune by the subordinate tide. Such features are commonly reported from mesotidal and macrotidal settings (e.g. Terwindt, 1981; Boersma and Terwindt, 1981; Dalrymple, 1984; DeMowbray and Visser, 1984). General absence of tidal-bundle sequences and rarity of current ripples on reactivation surfaces are due to an erosional or nondepositional subordinate flood-tidal current and a dominant ebb-tidal current that may have been reinforced by a fluvial current.

Sandstone bodies in which lower parts have swaley cross strata, planar strata and wave ripples but upper parts have angle-of-repose cross strata, suggest wave currents or combined wave and unidirectional cants lower down but dominantly unidirectional currents higher up. Interpretation of the depositional environment of these sandstone bodies hinges critically on their lateral transition to thicker sandstone bodies dominated by angle-of-repose cross strata and thinner

sandstone bodies dominated by amalgamated swaley cross strata. In some locations, sandstone bodies have sharp erosional bases, but in others they occur at the top of coarsening-upward sequences with interbedded hummocky cross-stratified sandstones and shales immediately beneath. These features suggest deposition on channel mouth bars that were prograding into a marine, storm-wave dominated area. Such bars may have been on the seaward side of tidal inlets (i.e. ebb-tidal deltas) associated with estuaries or barrier-beach shorelines, or associated with tide-influenced deltaic distributaries. Landward-directed (NE to SE) trough cross-strata are most likely associated with sinuous-crested dunes formed by tidal flood currents, but also perhaps with asymmetrical shoaling wave currents.

The relatively thin sandstone bodies dominated by amalgamated swaley cross- stratified strata are interpreted as more distal parts of channel mouth bars, that were completely dominated by storm waves. The lack of mud suggests deposition above fair weather wave base. The common occurrence of load casts near the base of these sandstone bodies suggests rapid deposition of sand on mud. Such soft-sediment deformation features are common offshore from Mississippi delta distributaries (e.g. Coleman and Prior, 1982). Paleocurrent indicators in the bases of sandstone bodies suggest a dominantly offshore directed unidirectional current, as is common in similar Frasnian rocks in the Catskill Region (Craft and Bridge, 1987; Halperin and Bridge, 1988; Bishuk et al., 1991) and in many other ancient storm-dominated shelf deposits (Leckie and Krystinik, 1989). Offshore-directed currents may be associated with coastal set-up during storms (e.g. Craft and Bridge, 1987, Halperin and Bridge, 1988; Leckie and Krystinik, 1989; Duke, 1990; Duke et al., 1991). However, fluvial and tidal currents may also have had an influence. Lenticular, pebbly and shelly sandstone strata, locally in channels, at the top of these sandstone bodies are evidence for relatively strong shoreward directed currents, possibly due to tidal flood, "storm-tides", or asymmetrical shoaling-wave currents (e.g. Cheel and Leckie, 1992). Thus, these coarse, shelly strata on top of sandstone bodies are associated with rapid abandonment of the channel-mouth bar, reduction in sand supply, and marine transgression (see, for example, Boyd and Penland, 1988; Boyd et al., 1989; Sha and DeBoer, 1991; Penland et al., 1988).

Bioturbation is characteristically rare in coastal sand bodies such as these (Howard and others, 1975; Howard and Reineck, 1981). Large, vertical meniscate burrows are similar to those reported in fluvial and coastal channel deposits elsewhere (Thoms and Berg, 1985; Miller, 1979; Bridge, Gordon and Titus, 1986), and may be due to upward escape of bivalves. The brachiopod-bivalve fauna is typical of Devonian nearshore communities (McGhee and Sutton, 1985; Sutton and McGhee, 1985).

The vertical variations in sandstone body characteristics within the upper 30 meters of Stevens Mountain quarry suggest a decreasing marine influence, with progressively more proximal channel bar deposits higher up. This trend is continued upwards into the non-marine Oneonta Formation.

Manorkill Falls

Description

   The Manorkill Falls section (Figure 6) exposes the upper part of the Moscow Formation where a pronounced grain-size fining occurs (Figure 2). When the water level in Schoharie Reservoir is unusually low, up to 10 meters of sandstone is exposed (below the log in Figure 6). Many sandstone casts of tree trunks (part of the famous Gilboa fossil forest) are seated in the gray-green disrupted mudstones immediately above these sandstones. The casts stand upright within the lowest, decimeter-thick sandstone strataset of a 2-m thick sandstone body (Figure 6, 3.5-5.5 m). Within this upward-fining sandstone body, sheet-like stratasets contain mainly medium-scale cross strata with easterly paleocurrents. Reactivation surfaces with ripple marks are superimposed on these cross strata. Sandstone stratasets between meters 6 and 7 have low-angle (swaley?) cross strata, wave-rippled upper surfaces, and rare shelly fossils (bivalves, brachiopods, crinoid ossicles, bryozoa). The distinctive wedge-shaped sandstone body between meters 7 and 8 has low-angle bedding surfaces that dip in the direction the sandstone body thins. Upper surfaces of these large-scale inclined strata are covered with symmetrical and interfering wave-ripple marks. Ichnofossils are abundant and diverse throughout these sandstone bodies, and include *Skolithos, Meunsteria, Arenicolites and Diplocraterion*.

   The overlying mudstone-dominated sequence (meters 8-24, Figure 6) contains relatively undisrupted and fissile mudstones that grade up into intensely disrupted mudstones with desiccation cracks, root casts, burrows, and calcareous rhizoconcretions. Interbedded sandstone stratasets are mainly wave-ripple cross stratified, but may have planar or hummocky-swaley strata at the base. Between meters 18 and 21 (Figure 6) such stratasets occur in E-W oriented, fine-grained channel fills. Some upward-fining sandstone stratasets have medium-scale and small-scale stratasets with easterly paleocurrents (e.g., 16-18 m; Figure 6) Rare transported shelly fossils and tree trunk casts occur again near the top of the section. At the top of the measured section, a 6 meter thick sandstone body has stratasets inclined at up to 5 degrees relative to its basal erosion surface (i.e. large-scale inclined strata). Stratasets lower down in the sandstone body have planar and swaley stratification with superimposed ripple marks. Higher up, stratasets of medium-scale cross strata fill channel forms.

Interpretation

   The mudstones at the base of the measured section record floodbasins with soils that supported a forest of trees. The sandstones that overlie these deposits, including those that buried and preserved the bases of tree trunks, show evidence for landward progradation of wedges of sand into standing water. This and the fossil content indicate a back-shoal washover origin. The overlying fissile mudstones with wave-rippled sandstone indicate deposition in quiet standing water that was periodically agitated by waves, possibly an interdistributary bay or back-barrier lagoon. A return to subaerial conditions is signalled by the occurrence of desiccation cracks, root casts, and calcareous paleosol nodules. Overlying mudstones and sandstones with evidence of landward-directed unidirectional paleocurrents, wave currents, periodic exposure and fine-grained channel fills may have been deposited on sandy to muddy tidal flats that changed upwards to
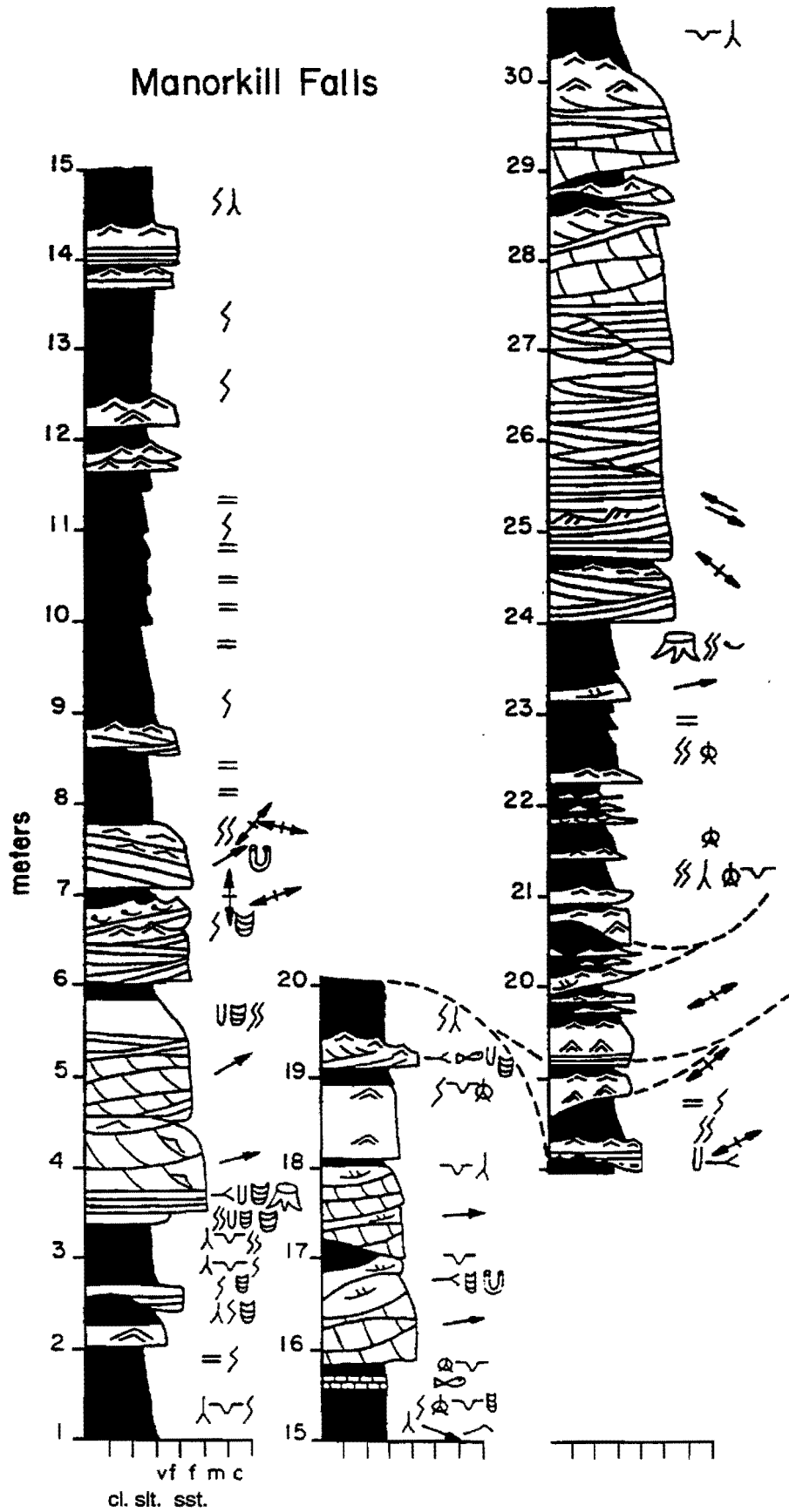
Figure 6.   Sedimentological log of Manorkill Falls Section, east side of Schoharie Reservoir.

subaerial plains. The landward-directed paleocurrents may be associated with tidal floods and/or storm overwash. The sandstone body at the top of this section is interpreted as a tidal-channel mouth-bar deposit.

Gilboa

At the side of the road at the northern tip of Schoharie Reservoir, immediately to the west of Schoharie Creek, there is an exhibit of sandstone casts of tree trunk casts that were recovered during excavations associated with the construction of the dam. There are a number of places in this area where such tree trunk casts can be seen in situ. One of these is Manorkill Falls.

Route 30 near Grand Gorge

Description of lower part

This road cut just north of Grand Gorge (Figure 1) exposes the upper Gilboa and lower Oneonta Formations, the overall sequence recording marine regression. The lowest 28 m of the section (Figure 7) comprises the Gilboa Formation. This Formation is composed of 2 to 6 m thick sandstone bodies separated by mudstone-dominated intervals.

The sandstone bodies have sharp bases with erosional sole marks, overlain in places by intraformational breccia composed of shale clasts, plant fragments, and shelly fossils (bivalves, brachiopods, crinoid fragments, and *Tentaculites*). The thinner sandstone bodies (2-3 m) are composed of amalgamated, decimeter to meter thick stratasets of swaley cross strata and planar strata. Erosional bases of individual stratasets are commonly overlain by transported shell fragments, and wave-ripples are rarely preserved beneath the thin shales draping the stratasets. Grain size of these sandstone bodies varies little through their thickness, except at the top where concentrations of shells, intraformational and extraformational pebbles occur.

As the thickness of these sandstone bodies increases, medium-scale cross strata begin to dominate their upper parts (e.g. meters 14-28). The thickest sandstone bodies are almost entirely composed of medium-scale cross strata. Medium-scale cross strata show opposing paleocurrent directions, especially in the upper parts of sandstone bodies. Symmetrical and asymmetrical ripple marks (draped with shale in places) superimposed on medium-scale cross strata also indicate divergent paleocurrents. These sandstone bodies may fine upwards, coarsen upwards, or show little vertical variation in mean grain size. They may also be capped with pebbly and shelly beds.

The dark gray, sparsely fossiliferous shales are typically bioturbated and interbedded with gray, centimeter to decimeter thick sandstone sheets and lenses. The thinner sandstones have wave-ripples and associated cross strata. Thicker, coarser grained ones have hummocky-swaley cross strata and/or planar strata in their lower parts. Sandstone load casts occur immediately beneath some sandstone bodies.
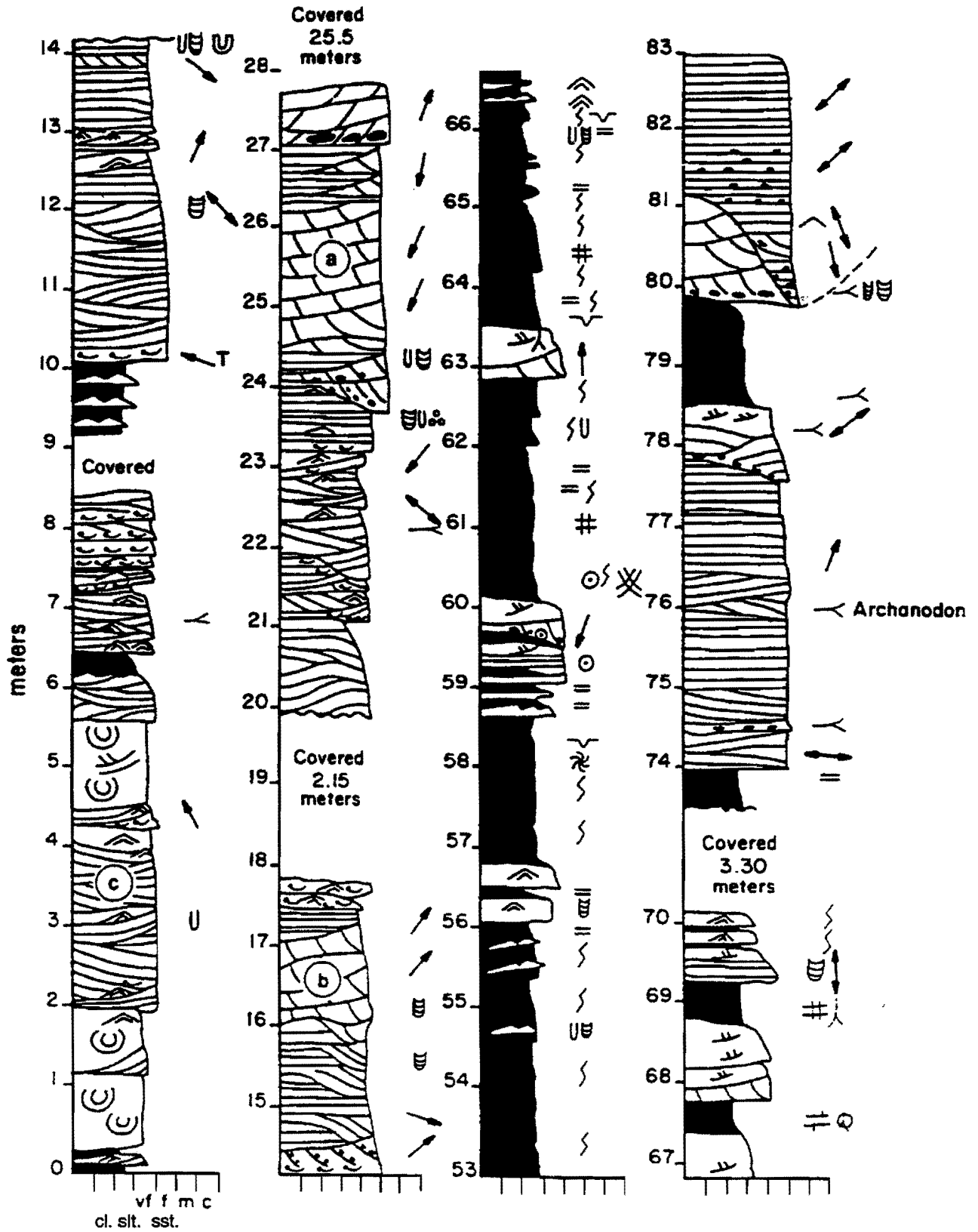
Figure 7.   Sedimentological log of Rt. 30 roadcut, north-east end of Grand Gorge. Sandstone body (b) corresponds to that in Figure 5.

Skolithos burrows (mm to cm diameter) are common in the tops of sandstone stratasets. *Arenicolites* and *Chondrites* also occur. Large (up to 0.1 m diameter) vertical, sandstone-filled meniscate burrows are characteristic of thicker sandstone bodies. Shelly fossils include brachiopods (*Spinocyrtia, Mucrospirifer, Tropidoleptus carinatus, Cupularostrum, Mediospirifer, Orthospirifer mesastrialis*), bivalves (*Goniophora, Grammysia, Actinopteria, Cypricardella, Paleoneilo*), *Tentaculites*, and crinoid ossicles. Most shell fragments are disarticulated, lie concave down along bedding planes, and show little evidence of breakage.

Interpretation of lower part

The thickest, cross-stratified sandstone bodies are interpreted as deposits of laterally migrating tidal channels (Johnson and Freidman, 1969; Miller and Woodrow, 1991; Bridge and Willis, 1994). Ebb-directed paleocurrents are dominant in the lower parts of sandstone bodies, whereas there is flood dominance in the upper parts, as is typical of asymmetrical, coastal tidal currents. The general absence of tidal-bundle sequences and rarity of current ripples on reactivation surfaces in medium-scale cross strata is an indication of strongly asymmetrical tidal currents where either the flood or ebb current is dominant during deposition.

Some of the sandstone bodies indicate the influence of wave currents or combined currents lower down, but predominantly unidirectional currents higher up. Interpretation of the origin of these sandstone bodies depends on their lateral transition to the other types of sandstone bodies, as observed in nearby outcrops of coeval strata (e.g., Stevens Mountain Quarry, Figure 20). Accordingly, these bodies are interpreted as channel-mouth bars that were prograding into a storm-wave dominated sea. Such bars may have been on the seaward side of tidal inlets (i.e. ebb-tidal deltas) associated with estuaries or barred coastlines, or associated with tide-influenced deltaic distributaries (Johnson and Friedman, 1969; Miller and Woodrow, 1991; Bridge and Willis, 1994). Landward-directed medium-scale cross strata may be associated with flood-tidal currents or may represent wave-formed swash bars. Ripple marks on dune/bar slip faces indicate periods of tidal slack water or reduced tidal currents.

The thinnest sandstone bodies dominated by swaley-hummocky cross strata are interpreted as more distal parts of channel-mouth bars that were dominated by storm waves and associated currents. The lack of mud suggests deposition above fairweather wave base. The occurrence of load casts near the base of these sandstone bodies suggests rapid deposition of sand on mud, as is common offshore from deltaic distributaries.

The shelly and pebbly strata at the top of the sandstone bodies are evidence of relatively strong shoreward-directed currents, possibly due to flood tides, "storm tides", or asymmetrical shoaling-wave currents. They appear to be associated with abandonment of the channel-mouth bar, relative reduction in sand supply, and marine transgression.

The sparse fauna, low degree of bioturbation, and dominance of *Skolithos* ichnofacies in the sandstones is typical of sandy deposits in coastal areas. Large, vertical meniscate burrows are similar to those reported in fluvial and coastal deposits elsewhere (Thoms and Berg, 1985; Miller, 1979; Bridge et al., 1986) and some may be due to upward escape of bivalves. The brachiopod-

bivalve fauna is typical of Devonian nearshore communities (McGhee and Sutton, 1985; Sutton and McGhee, 1985).

The shales with interbedded sandstones are interpreted as nearshore marine deposits formed below fairweather wave base (details in Bridge and Willis, 1994). Sandstones were formed during storms by either wave currents or combined wave-unidirectional currents, whereas mudstones represent fairweather deposits or those accumulated below storm wave base.

Description of upper part

The lower Oneonta Formation (Figure 6, meters 53-83) comprises red, green and gray mudstones with subordinate red to gray sandstones. The mudstones range from fissile and relatively unbioturbated to intensely disrupted with blocky texture, slickensided clay-lined surfaces, horizons of calcareous nodules, and rare pseudoanticlines. Desiccation cracks, root casts and burrows are pervasive. The distinctive trace fossil *Spirophyton* is present but hard to find. Sandstone stratasets are sharp based, cm to dm thick sheets and lenses. The thinner ones have small-scale cross strata with wave- or current-rippled tops. Thicker ones tend to have medium-scale cross strata or planar strata at their bases. Centimeter-diameter, vertical meniscate burrows (*Beaconites*) are common, and root casts and calcareous concretions may occur at the tops of the sandstone stratasets. Groups of several sandstone stratasets with intervening mudstone may be arranged into meter-thick upward-fining or upward-coarsening sequences (e.g., Figure 6, 58-60 m). Two 4 to 6 meter thick sandstone bodies occur at the top of the sequence (Figure 6, 74-83 m). These have erosional bases (lined with intraformational shale clasts, plant fragments, and rarely the non-marine bivalve *Archanodon*) and large-scale inclined strata, that are channel filling in places (meters 80-83). Internal structures are medium-scale cross strata (mainly low angle), planar strata, and cm-diameter, meniscate vertical burrows.

Interpretation of upper part

Disrupted mudstones represent floodbasin deposits. Blocky textures, desiccation cracks, calcareous concretions and pseudoanticlines indicate repeated wetting and drying and formation of ped structure typical of calcareous vertisols. Fissile siltstones indicate relatively less bioturbation but repeated exposure, and may represent relatively high deposition rates and/or hypersalinity in ephemeral lakes. *Spirophyton* in fissile siltstones suggests more permanent standing water, possibly brackish (Miller, 1979; Miller and Johnson, 1981). Wave-rippled lenses indicate periodic wave activity. The thinner sandstones with unidirectional sedimentary structures indicate periodic sand deposition during floods, either as individual sheet-flood deposits within the floodbasin, or associated with levees or crevasse splays. Coarsening-upward sequences indicate progradation of levees or crevasse splays. Root casts and calcareous concretions in and above the tops of these units indicate reduction in deposition rate and soil formation. The thick sandstone bodies are interpreted as the deposits of river-channel bars and fills, with some tidal influence possible.

60

Discussion of meter-scale sequences in coastal deposits of the Catskill clastic wedge

Meter-scale sequences were interpreted by Bridge and Willis (1994) to record changes in relative sea level related to processes such as lateral migration, abandonment and filling of tidal channels; progradation of channel mouth bars and tidal flats; and filling of coastal bays. These sequences are parasequences using the terminology of Van Wagoner et al. (1988, 1990) and Mitchum and Van Wagoner (1991). As average Givetian deposition rates were very approximately 0.1 mm/yr, meter-scale sequences represent 10^4 to 10^5 years on average.

Sharp-based coastal sandstone bodies similar to those in the Schoharie Valley have been ascribed to deposition on prograding strandplains cut by estuaries or tidal inlets, and to wave-formed offshore bars or shoals (references in Bridge and Willis, 1994). Sandstone bodies with swaley-hummocky cross strata overlain by angle-of-repose cross strata have been interpreted as beach and shoreface deposits, their sharp bases being related to wave-current erosion during relative sea-level fall and so-called forced regression. The coarse grained strata on the tops of these sandstone bodies were taken as so-called transgressive lags associated with relative rise in sea level. In contrast, Bridge and Willis (1994) explained the sharp bases of some of the sandstone bodies as due to rapid progradation of storm-wave modified channel-mouth bars that formed rapidly as a result of channel diversion. A beach face origin of the sandstone bodies was considered unlikely due to absence of: (1) characteristic seaward dipping planar laminae; (2) alongshore directed cross strata interbedded with landward directed cross strata and planar strata typical of ridge and runnel systems; (3) eolian cross strata. Although beach deposits can be eroded during marine transgressions, and by tidal inlets, universal removal seems unlikely. The apparent absence of beach deposits in both transgressive and regressive sequences along a shoreline that clearly experienced strong storm waves is probably related to high deposition rates of sand and mud near the mouths of a complex of channels. Thus channel switching is a viable mechanism for producing the meter-scale alternations of channel-related sandstone bodies and mudstones. Upward-fining sequences representing filling of coastal bays and/or progradation of tidal flats could be formed in areas away from active channels, perhaps landward of abandoned channel-mouth bars (shoals) that were being reworked by wave currents.

Estuaries and sand barriers with muddy bays on their landward sides are expected in coastal areas during relative sea level rises (references in Bridge and Willis, 1994). Although there is evidence for washovers from sandy coastal shoals, there is no clear evidence for barrier beaches. Furthermore, no evidence was found for ravinement during regressions and estuarine filling during transgressions. The lack of evidence for muddy intertidal channel deposits with large-scale inclined heterolithic bedding, and for tidal-bundles in cross-stratified sands, indicates that the North Sea tidal flats may not be good analogues for these deposits (contra McCave, 1968; Johnson and Friedman, 1969). The strongly asymmetrical, ebb-dominated currents possibly record the dominance of river flow during deposition.

Other Givetian and Frasnian coastal and marine deposits in New York and Pennsylvania are broadly similar to those exposed in the Schoharie Valley, and interpreted depositional environments have several features in common: (1) sandy, tide-influenced channels; (2) shallow bays and tidal flats where mud and sand were deposited; (3) rarity of beaches; (4) storm-wave
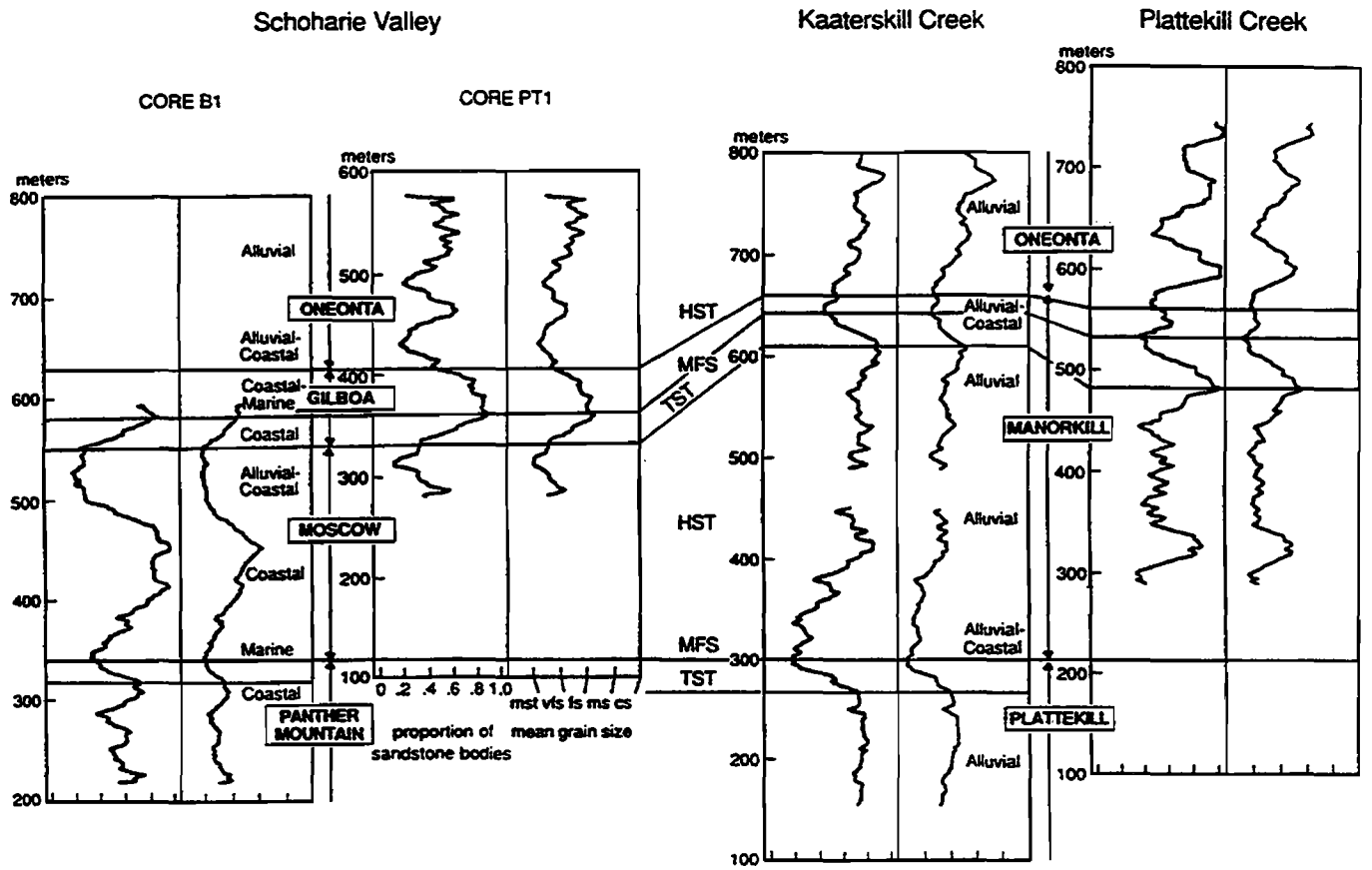
Figure 8.   Correlation of Schoharie Valley Formations with those in Kaaterskill and Plattekill Creeks (from Bridge and Willis, 1994). TST = Transgressive Systems Tract. MFS = Maximum Flooding Surface. HST = Highstand Systems Tract.

domination of the marine shelf (references in Bridge and Willis, 1994). Much of the variability in the deposits from different areas could be explained within the context of a wave- and tide-influenced deltaic coastline. Meter-thick sequences similar to those in the Schoharie Valley but in the Frasnian part of the Catskill clastic wedge have been interpreted to reflect eustatic sea-level changes associated with Milankovich climatic cycles (Van Tassell, 1987). Such an interpretation is considered unlikely here. Such an allocyclic control could only be justified if sequences could be traced laterally for distances greater than would be expected for individual delta lobes, and indeed across the whole basin. However, correlation of sequences for more than a few hundred meters has proved difficult in these types of rocks (Miller and Woodrow, 1991; Duke and Prave, 1991).

Discussion of 100-meter scale sequences in coastal and fluvial deposits of the Catskill clastic wedge

The Gilboa and Oneonta Formations in the Schoharie Valley can be correlated biostratigraphically with fully marine strata to the west and fluvial strata to the east (Figures 3 and 8). The correlations are approximate because the resolution of biostratigraphic zones is on the order of a million years at best. McCave (1969) associated mudstone-dominated fluvial sequences with marine transgressions based on the assumption that rising sea level would lead to increased rate of floodplain aggradation and higher preservation potential of overbank mudstones. This concept has been used by others more recently (e.g., Shanley and McCabe, 1993; Wright and Marriott, 1993). However, floodplain aggradation rate is only one of several controls on proportion of channel-belt deposits in alluvial successions (Mackey and Bridge, 1995). Within the 100-meter scale sequences represented by the Manorkill and lower Oneonta Formations, the mean grain size and proportion of channel-belt sandstones, and the size of individual channels, increase upward (Willis and Bridge, 1988). These trends were interpreted by Willis and Bridge (1988) to record progradation of seaward-fining distributive fluvial systems. Dating of these strata is not accurate enough to determine if the upward increase in channel-sandstone proportion is related to decreasing accomodation space and sediment accumulation rate in the way suggested by Shanley and McCabe (1993). However, by analogy with the Miocene Siwalik strata in the Himalayan foredeep, high proportions of channel-belt sandstone bodies are associated with high subsidence and deposition rates, increasing channel sizes, and progradation of megafans (Willis, 1993; Khan et al., 1997; Zaleha, 1997).

McCave (1969, 1973) and Johnson and Friedman (1969) postulated that thin marine limestones (e.g.,Tully) were deposited during marine transgressions, because sea-level rise would cause trapping of sand and mud near the coast, starving deeper marine areas of sediment. In contrast, Brett and Baird (1985, 1986, 1990) interpreted such limestones to represent shallowing and sediment starvation-winnowing events following sea-level lowstands. According to Brett and Baird (1990), the upper Moscow Formation is represented in marine areas by a Type 2 sequence boundary that is overlain by the lower Tully Limestone (Figure 3). No corresponding erosion surface has been recognized in coeval coastal deposits. The upper Tully Limestone apparently rests on a transgressive erosion surface (Brett and Baird, 1990), and may therefore correlate with the transgressive lower Gilboa Formation in Schoharie Valley (Figure 3). However, relative sea-level changes are not necessary congruent in different parts of foreland basins, such that cross-basin correlation of regressive or transgressive strata does not necessarily imply coeval events.

Many authors favor eustatic sea-level changes as the main control on the large-scale sequences (references in Bridge and Willis, 1994). The transgressive deposits of the Gilboa Formation are associated with a widely accepted eustatic sea-level rise that can be recognized worldwide (House, 1983; Johnson et al., 1985). However, eustatic sea-level changes must be moderated by tectonically induced changes in subsidence and uplift rates and sediment supply. To establish whether eustasy or tectonism is the dominant control on sequence development in foreland basins, it is necessary to establish the ages of sequences, and the relative thickness of transgressive and regressive deposits, in different areas of the basin (Jordan and Flemings, 1991). It is very difficult to know if rising and falling sea level are coeval or otherwise in different parts of the marine basin, because of dating limitations. Also, it is very difficult to predict the timing and rate of deposition in different parts of the basin in relation to tectonic uplift of the adjacent mountains and development of the peripheral bulge. Jordan and Fleming's (1991) model suggests that the thicker regressive strata relative to transgressive strata in this region points to a tectonic control of some of the large-scale sequences.

References

Arnott, R.W. D. and Southard, J.B., 1990, Experimental study of combined-flow bed configurations in fine sands, and some implications for stratification: Journal of Sedimentary Petrology, v. 60, p. 211-219.

Bishuk, D., Applebaum, R. and Ebert, J.R., 1991, Storm-dominated shelf and tidally- influenced foreshore sedimentation, Upper Devonian Sonyea Group, Bainbridge to Sidney Center, New York: New York State Geological Association Field Trip Guidebook, 63rd Annual Meeting, Oneonta, p. 413-462.

Boersma, J.R. and Terwindt, J.H.J., 1981, Neap-spring tide sequences of intertidal shoal deposits in a mesotidal estuary: Sedimentology, v. 28, p. 151-170.

Boothroyd, J.C. 1978. Mesotidal inlets and estuaries, in Davis, R.A., ed., Coastal Sedimentary Environments: Springer-Verlag, p.287-360.

Boyd, R. and Penland, S., 1988, A geomorphic model for Mississippi delta evolution: Gulf Coast Association of Geological Societies, Transactions, v. 38, p. 443-452.

Boyd, R., Suter, J. and Penland, S., 1989, Sequence stratigraphy of the Mississippi delta: Gulf Coast Association of Geological Societies, Transactions, v. 39, p. 331-340.

Brett, C.E. and Baird, G.C., 1985, Carbonate-shale cycles in the Middle Devonian of New York: an evaluation of models for the origin of limestone in terrigenous shelf sequences: Geology, v. 13, p. 324-327.

Brett, C.E. and Baird, G.C., 1986, Symmetrical and upward shallowing cycles in the Middle Devonian of New York and their implications for the punctuated aggradational cycle hypothesis: Paleoceanography, v. 1, p. 431-445.

Brett, C.E. and Baird, G.C., 1990, Submarine erosion and condensation in a foreland basin: examples from the Devonian of Erie County, New York: New York State Geological Association Field Trip Guidebook, 62nd Annual Meeting, Fredonia, p. A1-A56.

Bridge, J.S., Gordon, E.A. and Titus, R.C., 1986, Non-marine bivalves and associated burrows in the Catskill magnafacies (Upper Devonian) of New York State: Palaeogeography, Palaeoclimatology, Palaeoecology, v. 55, p. 65-88.

Bridge, J.S. and Willis, B.J., 1994, Marine transgressions and regressions recorded in Middle Devonian shore-zone deposits of the Catskill clastic wedge. Geological Society of America Bulletin, v. 106, p. 1440-1458.

Cacchione, D.A., Drake, D.E., Grant, W.D. and Tate, G.B., 1984, Rippled scour depressions on the inner continental shelf off central California: Journal of Sedimentary Petrology, v. 54, p. 1280-1291.

Cheel, R.J. and Leckie, D.A., 1992, Coarse-grained storm beds of the Upper Cretaceous Chungo Member (Wapiabi Formation), Southern Alberta, Canada: Journal of Sedimentary Petrology, v. 62, p. 933-945.

Coleman, J.M. and Prior, D.B., 1982, Deltaic environments, in Scholle, P.A. and Spearing, D., eds., Sandstone Depositional Environments: American Association of Petroleum Geologists, p. 139-178.

Cooper, G.A., 1930, Stratigraphy of the Hamilton Group of New York: American Journal of Science, 5th ser., v. 19, p. 116-134, 214-236.

Cooper, G.A., 1933, Stratigraphy of the Hamilton Group of eastern New York: American Journal of Science, 5th ser., v. 26, p. 537-551.

Cooper, G.A., 1934, Stratigraphy of the Hamilton Group of eastern New York: American Journal of Science, 5th ser., v. 27, p. 1-12.

Cooper, G.A. and Williams, J.S., 1935, Tully Formation of New York: Geological Society of America Bulletin, v. 46, p. 781-868.

Craft, J.H. and Bridge, J.S., 1987, Shallow-marine sedimentary processes in the Late Devonian Catskill Sea, New York State: Geological Society of America Bulletin, v. 98, p. 338-355.

Dalrymple, R.W., 1984, Morphology and internal structure of sandwaves in the Bay of Fundy: Sedimentology, v. 31, p. 365-382.

DeMowbray, T. and Visser, M.J., 1984, Reactivation surfaces in subtidal channel deposits, Oosterschelde, southwest Netherlands: Journal of Sedimentary Petrology, v. 54, p. 811-824.

Dennison, J.M., 1985, Catskill Delta shallow marine strata, in Woodrow, Dl., and Sevon, W.D., eds., The Catskill Delta: Geological Society of America Special Paper 201, p. 91-107.

Dennison, J.M. and Ettensohn, F.R. (editors), 1994, Tectonic and eustatic controls on sedimentary cycles: SEPM Concepts in Sedimentology and Paleontology, v. 4.

Dennison, J.M. and Head, J.W., 1975, Sea level variation interpreted from the Appalachian Basin Silurian and Devonian: American Journal of Science, v. 275, p. 1089-1120.

Dott, R.H., Jr. and Bourgeois, J., 1982, Hummocky stradfication: significance of its variable bedding sequence: Geological Society of America Bulletin, v. 93, p. 663-680.

Duke, W.L., 1990, Geostrophic circulation or shallow marine turbidity currents? The dilemma of paleoflow patterns in storm-influenced prograding shoreline systems: Journal of Sedimentary Petrology, v. 60, p. 87S883.

Duke, W.L., Arnott, R.W. and Cheel, R.J., 1991, Shelf sandstones and hummocky cross stratification: New insights on a stormy debate: Geology, v. 19, p. 625-628.

Duke, W.L. and Prave, A.R., 1991, Storm- and tide -influenced prograding shoreline sequences in the Middle Devonian Mahantango Formation, Pennsylvania, in D.G. Smith, G.E. Reinson, B.A. Zaitlin and R.A. Rahmani., eds., Clastic Tidal Sedimentology: Canadian Society of Petroleum Geologists Memoir 16, p. 349-370.

Ettensohn, F.R., 1985, Controls on development of Catskill Delta complex basin-facies, in Woodrow, D.L. and Sevon, W.D., eds., The Catskill Delta: Geological Society of America Special Paper 201, p. 65-75.

Fitzgerald, D.M., 1984, Interactions between the ebb-tidal delta and landward shoreline, Price Inlet, South Carolina: Journal of Sedimentary Petrology, v. 54, p. 1303-1318.

Fletcher, F. U., 1963, Regional stratigraphy of Middle and Upper Devonian nonmarine rocks in southeastern New York, in Shepps, V. C., ed., Symposium on Middle and Upper Devonian Stratigraphy of Pennsylvania and Adjacent States: Pennsylvania Geological Survey Bulletin G-39, p. 25-41.

Fletcher, F. U., 1967, Middle and Upper Devonian clastics of the Catskill Front, New York: New York State Geologists Association Guidebook 39, New Paltz, p. C1-C23.

Gordon, E. A. and Bridge, J. S., 1987, Evolution of Catskill (Upper Devonian) river systems: intra- and extrabasinal controls: Journal of Sedimentary Petrology, v. 57, p.234-249.

Halperin, A. and Bridge, J.S., 1988, Marine to non-marine transitional deposits in the Frasnian Catskill clastic wedge, south-central New York, in McMillan, N.J., Embry, A.F., Glass, D.J., eds., Devonian of the World, v. II: Canadian Society of Petroleum Geologists, p. 107-124.

Hayes, M.A. and Kana, T.W., 1976, Terrigenous clastic depositional environments: Technical Report No. 11-CRD, Coastal Research Division, University of South Carolina.

House, M. R., 1983, Devonian eustatic events: Proceedings of the Ussher Society, v. 5, p. 99-123.

House, M.R., 1985, Correlation of mid-Paleozoic ammonoid evolutionary events with global sedimentary perturbations: Nature, v. 313, p. 17-22.

Howard, J.D. and others, 1975, Estuaries of the Georgia Coast, U.S.A. Sedimentology and Biology: Senckenbergiana maritima, v. 7, p. 1-307.

Howard, J.D. and Reineck, H.E., 1981, Depositional facies of high-energy beach-tooffshore sequence: comparison with low-energy sequence: American Association of Petroleum Geologists Bulletin, v. 65, p. 807-830.

Hunter, R.E. and Clifton, H.E., 1982, Cyclic deposits and hummocky cross-stratification of probable storm origin in the Upper Cretaceous rocks of the Cape Sebastian area, southwestern Oregon: Journal of Sedimentary Petrology, v. 52, p. 127-143.

Johnson, J.G., Klapper, G. and Sandberg, C.A., 1985, Devonian eustatic fluctuations in Euramerica : Geological Society of America Bulletin, v. 96, p. 567-587.

Johnson, K.G. and Friedman, G.M., 1969, The Tully clastic correlatives (Upper Devonian) of New York State: a model for recognition of alluvial, dune (?), tidal, nearshore (bar and lagoon), and offshore sedimentary environments in a tectonic delta complex: Journal of Sedimentary Petrology, v. 39, p. 451-485.

Jordan, T.E. and Flemings, P.B., 1991, Large-scale stratigraphic architecture, eustatic variation, and unsteady tectonism: a theoretical evaluation. Journal of Geophysics Research, v.96, p. 6681-6699.

Khan, I.A., Bridge, J.S., Kappelman, J. and Wilson, R., 1997, Evolution of Miocene fluvial environments, eastern Potwar Plateau, northern Pakistan. Sedimentology, v. 44, p.221-251.

Leckie, D.A. and Krystinik, L.F., 1989, Is there evidence for geostrophic currents preserved in the sedimentary record of inner to middle-shelf deposits?: Journal of Sedimentary Petrology, v. 59, p. 862-870.

Mackey, S.D. and Bridge, J.S., 1995, Three dimensional model of alluvial stratigraphy: theory and application. Journal of Sedimentary Research, v. B65, p.7-31.

McCave, I.N., 1968, Shallow and marginal marine sediments associated with the Catskill complex in the Middle Devonian of New York, *in* Klein, G. deV, ed., Late Paleozoic and Mesozoic continental sedimentation, northeastern North America: Geological Society of America Special Paper 106, p. 75-108.

McCave, I.N., 1969, Correlation of marine and nonmarine strata with example from Devonian of New York State: American Association of Petroleum Geologists Bulletin, v. 53, p. 155-162.

McCave, I.N., 1973, The sedimentology of a transgression: Portland Point and Cooksburg members (Middle Devonian), New York State: Journal of Sedimentary Petrology, v. 43, p. 484-504.

McGhee, G.R. and Sutton, R.G., 1985, Late Devonian marine ecosystems of the Lower West Falls Group in New York: Geological Society of America Special Paper 201, p. 199-209.

Miller, M.F., 1979, Paleoenvironmental distribution of trace fossils in the Catskill deltaic complex, New York State: Palaeogeography, Palaeoclimatology, Palaeoecology, v. 28, p. 117-141.

Miller, M.F. and Johnson, K.G., 1981, *Spirophyton* in alluvial-tidal facies of the Catskill deltaic complex: possible biological control of ichnofossil distribution: Journal of Paleontology, v.55, p.1016-1027.

Miller, M.F. and Woodrow, D.L., 1991, Shoreline deposits of the Catskill deltaic complex, Schoharie Valley, New York, in Landing, E. and Brett, C.E., eds., Dynamic stratigraphy and depositional environments of the Hamilton Group (Middle Devonian) in New York State, Part II: New York State Museum Bulletin Number 469, p. 153-177.

Mitchum, R.M. and Van Wagoner, J.C., 1991, High-frequency sequences and their stacking patterns: sequence-stratigraphic evidence of high-frequency eustatic cycles: Sedimentary Geology, v. 70, p. 131-160.

Myrow, P.M. and Southard, J.B., 1991, Combined-flow model for vertical stratification sequences in shallow marine storm-deposited beds: Journal of Sedimentary Petrology, v. 61, p. 202-210.

Nottvedt, A. and Kreisa, RD., 1987, Model for the combined-flow origin of hummocky cross stratification: Geology, v. 15, p. 357-361.

Penland, S., Boyd, R. and Suter, J.R., 1988, Transgressive depositional systems of the Mississippi delta plain: a model for barrier shoreline and shelf sand development: Journal of Sedimentary Petrology, v. 58, p. 932-949.

Rickard, L.V., 1975, Correlation of the Silurian and Devonian rocks in New York State: New York State Museum and Science Service, Geological Survey Map and Chart Series, no. 24.

Rickard, L.V., 1989, Stratigraphy of the subsurface lower and middle Devonian of New York, Pennsylvania, Ohio and Ontario: New York State Museum Map and Chart Series no. 39.

Sha, L.P. and DeBoer, P.L., 1991, Ebb-tidal delta deposits along the west Frisian Islands (The Netherlands): processes, facies architecture and preservation, in D.G. Smith, G.E.

Reinson, B.A. Zaitlin, and R.A. Rahmani, eds., Clastic Tidal Sedimentology: Canadian Society of Petroleum Geologists Memoir 16, p. 199-218.

Shanley, K. W. and McCabe, P.J., 1993, Alluvial architecture in a sequence stratigraphic framework: a case history from the Upper Cretaceous of southern Utah, USA. In: Flint, S. & Bryant, I.D. (eds.) The geological modeling of hydrocarbon reservoirs and outcrop analogues. International Association of Sedimentologists Special Publication 15, p.21-56.

Southard, J.B., Lambie, J.M., Federico, D.C., Pile, H.T. and Weidman, C.R., 1990, Experiments on bed configurations in fine sands under bidirectional purely oscillatory flow, and the origin of hummocky cross-stratificadon: Journal of Sedimentary Petrology, v. 60, p. 1-17.

Sutton, R.G. and McGhee, G.R., 1985, The evolution of Frasnian marine 'communitytypes' of south-central New York: Geological Society of America Special Paper 201, p. 211-224.

Sutton, R.G., 1963, Correlation of Upper Devonian strata in south-central New York, in Shepps, V.C., ed., Symposium on Middle and Upper Devonian stratigraphy of Pennsylvania and adjacent states: Pennsylvania Geological Survey Bulletin G39, p. 87-101.

Sutton, R.G., Humes, E.C., Nugent, R.C. and Woodrow, D.L., 1962, New stratigraphic nomenclature for Upper Devonian of south-central New York: American Association of Petroleum Geologists Bulletin, v. 46, p. 390-393.

Swift, D.J.P., Figueiredo, A.R., Freeland, G.L. and Oertel,, G.F., 1983, Hummocky cross stratification and megaripples: a geological double standard?: Journal of Sedimentary Petrology, v. 53, p. 1295-1317.

Terwindt, J.H.J., 1981, Origin and sequences of sedimentary structures in inshore mesotidal deposits of the North Sea: International Association of Sedimentologists Special Publication No. 5, Blackwell, Oxford, p. 51-64.

Thoms, R.E. and Berg, T.M., 1985, Interpretation of bivalve trace fossils in fluvial beds of the basal Catskill Formation (Late Devonian), eastern U.S.A, in Curran, H. A., ed., Biogenic structures; their use in interpreting depositional environments: S.E.P.M. Special Publication 35, p. 13-20.

Van Tassell, J., 1987, Upper Devonian Catskill Delta margin cyclic sedimentation: Brallier, Scherr, and Foreknobs Formations of Virginia and West Virginia: Geological Society of America Bulletin, v. 99, p. 414-426.

Van Wagoner, J.C., Mitchum, R.M., Campion, K.M. and Rahmanian, V.D., 1990, Siliciclastic sequence stratigraphy in well logs, cores and outcrop: A.A.P.G. Methods in Exploration Series No. 7, 55p.

Van Wagoner, J.C., Posamentier, H.W., Mitchum, R.M., Vail, P.R., Sarg, J.F., Loutit, T.S. and Hardenbol, J., 1988, An overview of the fundamentals of sequence stratigraphy and key definitions, in Wilgus, C.K. et al., ads., Sea level changes: an integrated approach: S.E.P.M. Special Publication 42, p. 39-45.

Willis, B.J., 1993, Evolution of fluvial systems in the Himalayan foredeep through a two kilometer-thick succession in northern Pakistan: Sedimentary Geology, v. 88, p.77-121.

Willis, B.J. and Bridge, J.S., 1988, Evolution of Catskill River systems, New York State, in McMillan, N.J., Embry, A.F., Glass, D.J., eds., Devonian of the World, vol. II: Canadian Society of Petroleum Geologists, p. 85-106.

Woodrow, D .L. and Nugent, R. C. , 1 963 , Facies and the Rhinestreet Formation in south-central New York, in Coates, D.R., ad., Geology of south-central New York: New York State Geological Association, 35th Annual Meeting, Field Trip Guidebook, p. 59-76.

Wright, V.P. and Marriott, S.B., 1993, The sequence stratigraphy of fluvial depositional systems: the role of floodplain sediment storage: Sedimentary Geology, v. 86, p.203-210.

Zaleha, M.J., 1997, Intra- and extrabasinal controls on fluvial deposition in the Miocene Indo-Gangetic foreland basin, northern Pakistan. Sedimentology, v.44, p. 369-390.

Appendix: Road log for Schoharie Valley field trip

Travel from Binghamton to Oneonta on I88. Take exit 15 in Oneonta and head east on NY23 towards Grand Gorge. Approximately 3 miles past Grand Gorge, turn left down a gravel road towards Hardenburgh Falls. Cross the bridge over Bear Kill and park. Walk east down track on north side of the creek to exposures adjacent to the bridge. **Stop 1: Hardenburgh Falls**.

Return to NY23 and turn left (east) towards Prattsville. Travel approximately 1.5 miles to the bridge that crosses Schoharie Creek. Turn sharply left (north) immediately after crossing the bridge and proceed along the road that goes along the eastern side of Schoharie Reservoir. Travel approximately 6 miles as far as Gilboa-West Conesville Central School. Turn right immediately past the school, travel to the back of the school and park near the playing fields. Walk southeast to the far corner of the playing fields and find the trail leading up the hillside to the quarry (about 10 to 15 minutes walk). **Stop 2: Stevens Mountain Quarry**.

Return to the main road by the school, turn left and travel south for approximately one mile to the bridge over Manorkill. Park on the south side of the bridge and find the trail leading down to the reservoir. **Stop 3: Manorkill Falls**.

Travel north approximately 1.5 miles (past the school again) and cross Schoharie Creek at Gilboa. The display of tree trunk casts is on the left (south) side of the road. **Stop 4: Gilboa**.

Continue on this road for about 1 mile until it meets NY30. Turn left (south) on NY30 and travel approximately 1 mile until the road starts to climb up the west side of Pine Mountain. Park at the base of the hill near the first outcrops. **Stop 5: Grand Gorge, Route 30**.

The Palisades Sill, New York and New Jersey
Trip A5 - New York State Geological Association Annual Meeting
1998

H. R. Naslund
Department of Geological Sciences
SUNY-Binghamton
Binghamton, NY 13902-6000
(Naslund@Binghamton.EDU)

General Geology of the Palisades Sill: The Palisades sill is a Mesozoic tholeiitic intrusion approximately 300 m thick, that extends in outcrop for 80 km in a north-south direction along the western side of the lower Hudson river (Fig. 1, Walker, 1969), and may connect under cover with the Rocky Hill and Lambertville sills to the south for a total strike length of 150 kms (Husch, 1992). The east-west extent of the sill is unknown, but if it were circular in plan view it would represent over 1750 km^3 of magma. Field relations, petrography, and petrology have been described by a number of authors (Lewis, 1908; F. Walker, 1940; K. Walker 1969; K. Walker, et al., 1973; Shirley, 1987; Husch, 1990, 1992; Steiner et al., 1992).

The Palisades sill has an extensive differentiation sequence from Mg-rich gabbro at its base to Fe-rich diorite at approximately the 250 m level. The roof sequence, although much thinner than the floor sequence, is increasingly differentiated from the roof downwards (Fig. 2). The main constituents of the sill are plagioclase and pyroxene (augite, orthopyroxene,and pigeonite), which together make up over 90% of the primary phases; olivine, amphibole, ilmenite, magnetite, and minor amounts of biotite are additional phases. Igneous layering within the sill is restricted to thin (cm-scale), faint layers best seen on weathered outcrops. Calculated solidification times for the sill are on the order of 1000 years (Shirley, 1987; Gorring & Naslund, 1995).

Mineral compositions vary from the base of the sill upwards (and from the roof downwards) reflecting the increasing differentiation of the Palisades magma (Fig. 3). Plagioclase compositions vary from An_{78} to An_{28}; augite from
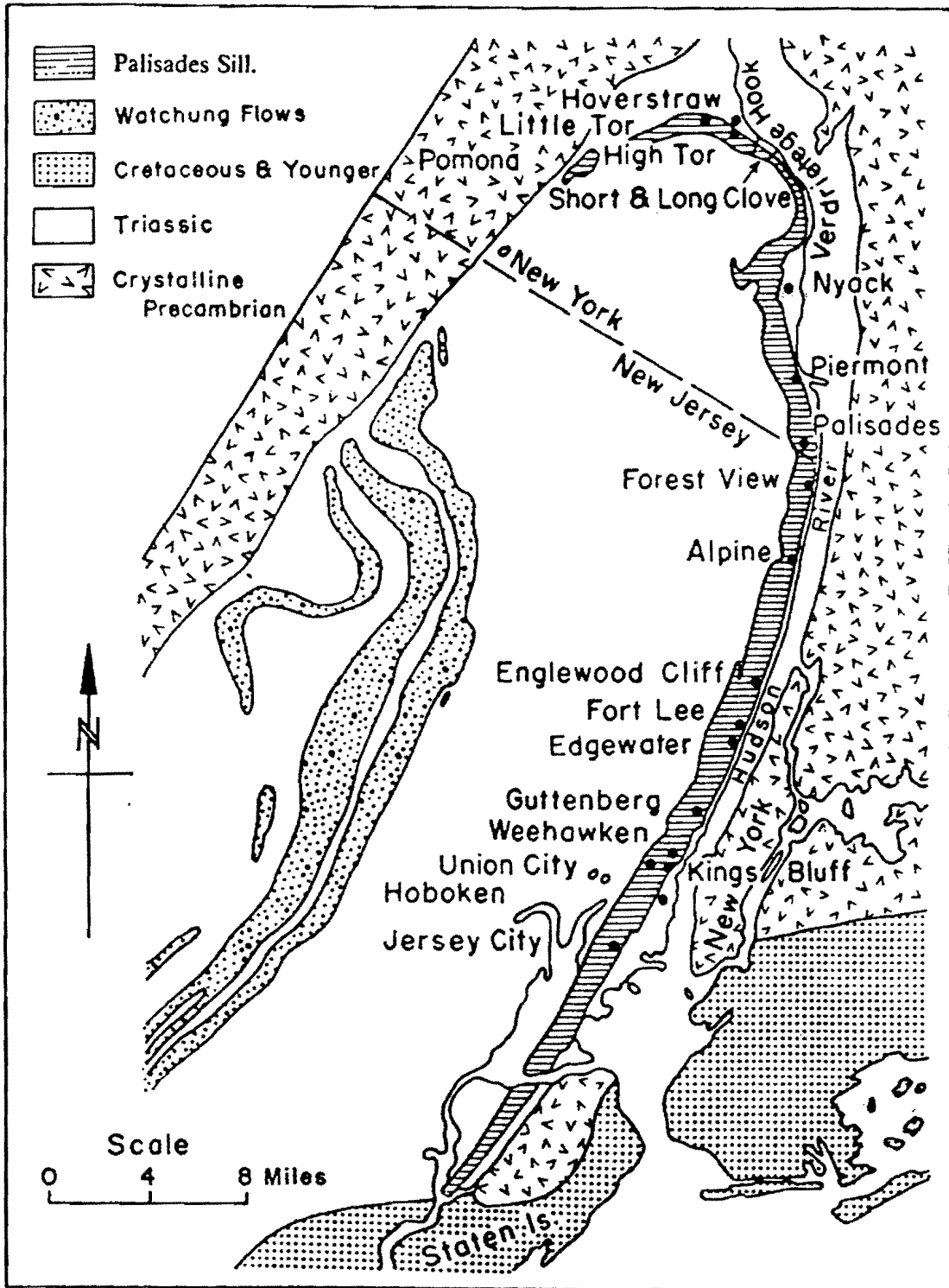
Fig. 1 Map showing the present outcrop pattern of the Palisades sill (from Walker, 1969).
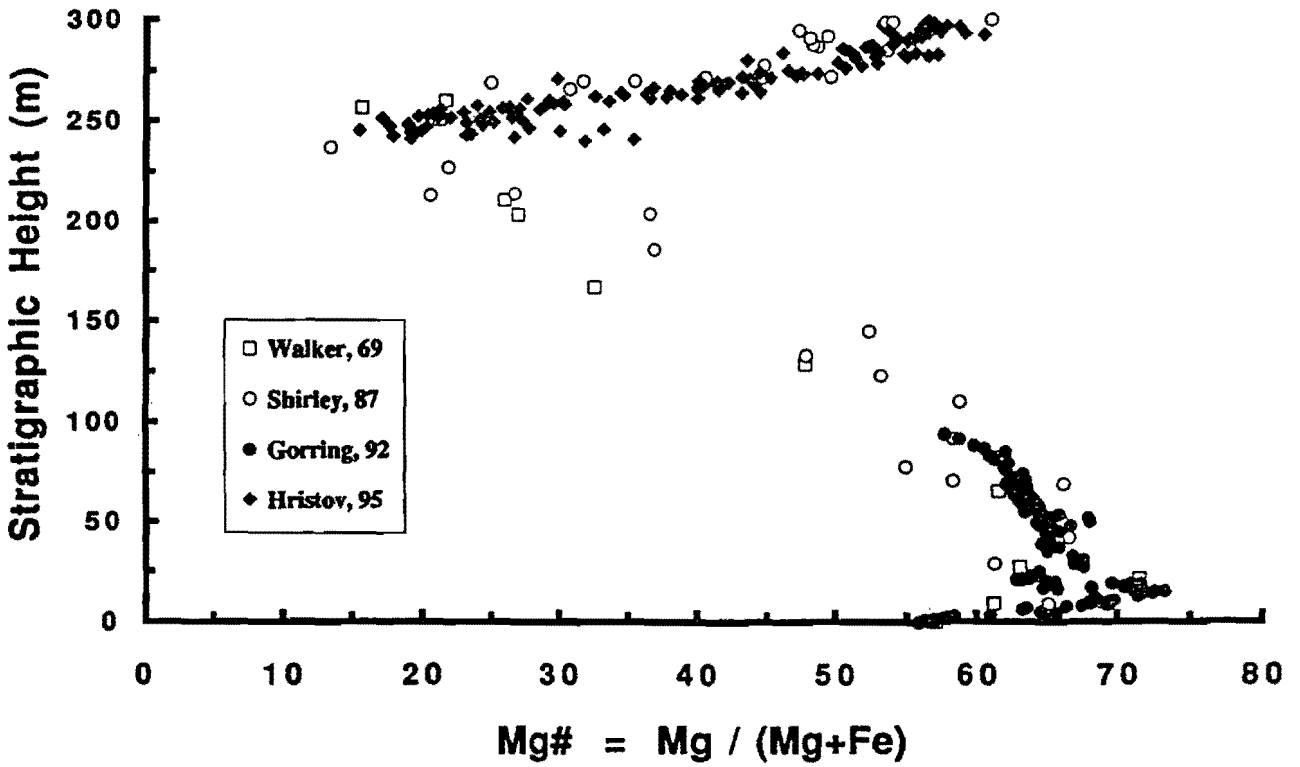
Figure 2 - A plot of Mg# vs. stratigraphic height for the Palisades sill section in Fort Lee, NJ. Data points are from Walker (1969), Shirley (1987), Gorring (1992), and Hristov (1995).
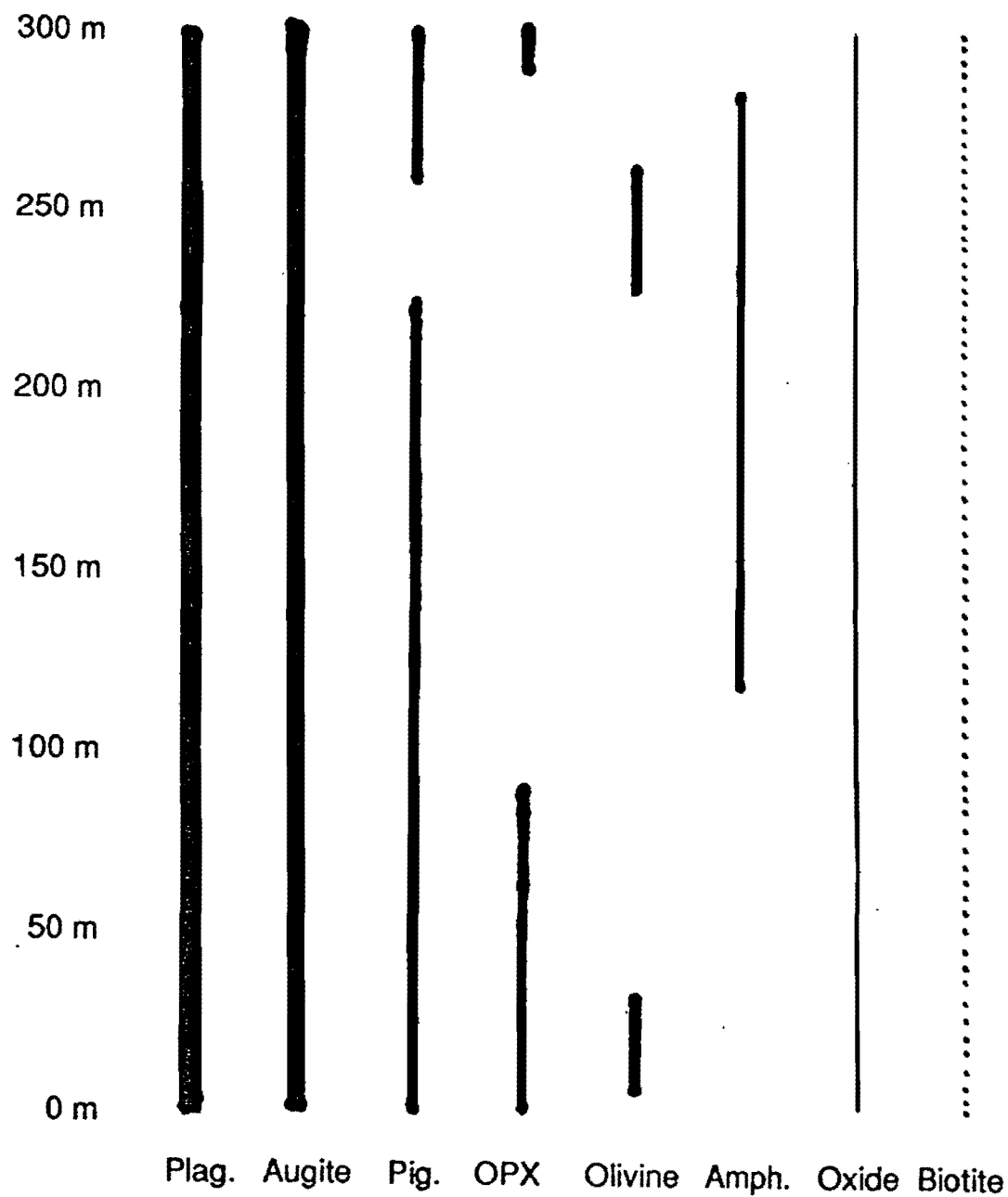
Fig. 3 Distributions of the major mineral phases of the Palisades sill vs. stratigraphic height in the sill (modified from Walker, 1969). Heavy lines indicate abundant phases, light lines indicate less abundant phases, and dotted lines indicate trace phases. Plag = plagioclase; Pig = pigeonite; OPX = orthopyroxene; Amph = amphibole.

$Wo_{38}En_{51}Fs_{11}$ to $Wo_{38}En_{10}Fs_{52}$; pigeonite from $Wo_8En_{54}Fs_{38}$ to $Wo_{12}En_{34}Fs_{54}$; orthopyroxene from $Wo_4En_{78}Fs_{18}$ to $Wo_3En_{55}Fs_{42}$ and from $Wo_3En_{34}Fs_{63}$ to $Wo_4En_{26}Fs_{70}$; and olivine from Fo_{77} to Fo_{55} and from Fo_{13} to Fo_5 (Walker, 1969; Walker et al., 1973; Gorring, 1992; Hristov, 1995). The plagioclase, pyroxenes, and olivine of the sill are all strongly compositionally zoned (Walker, 1969; Gorring, 1992; Hristov, 1995) with augite typically zoned 20 to 25% in Mg# (Mg# = Mg/[Mg+Fe]) from core to rim, orthopyroxene 15 to 20% in Mg# from core to rim, and plagioclase in excess of 25 An% within crystal cores, with rims up to 50 An% poorer than cores. Many individual grains have relatively homogeneous central cores that make up 25 to 75% of the area surrounded by strongly zoned rims.

The base of the sill is sharply defined by a very fine-grained to glassy, phenocryst-free chilled margin against the country rock. Above the chilled margin, the grain size gradually increases upward in the sill from ~2 mm to over 10 mm at the 250 m level. The lower 2.5 m of the sill is a fine grained, compositionally homogeneous, dolerite which appears to represent liquid solidified in situ with no significant addition or loss of crystals. Approximately 10m above the base of the sill is the well known olivine-rich horizon which is thought to have formed during the emplacement of the magma as a result of initial magma inhomogeneities, or the nearly simultaneous emplacement of two magmas of contrasting compositions. Geochemical data suggest that there were at least two additional pulses of magma injected into the chamber at the 27m and 45m levels. These later pulses are marked by small but abrupt regressions in the generally decreasing Mg/Fe trend, abrupt increases in Ni, Cr, and modal orthopyroxene, increases in the $Cr_2 O_3$ contents of augite and orthopyroxene, and abrupt decreases in grain-size (Gorring & Naslund, 1995).

Shirley (1987) has modeled the effects of intercumulus melt migration and compaction in the partially solidified Palisades sill. His model suggests that the rocks originally accumulated on the floor of the magma chamber along with 50 to 60% interstitial magma. Some of this interstitial liquid was subsequently forced upward through the crystal mush by compaction, reducing the final proportion of "trapped" liquid to between 40 and 50 %.

Steiner et al. (1992) present a "cumulus-transport-deposition" model for the

crystallization of the Palisades sill based on a section through the sill in Upper Nyack, NY. The model proposes that "crystals collect in convection cells or like environments at deep levels within the sheet" and are then subsequently "remelted, resorted, and/or recrystallized during epizonal emplacement due to: magma decompression, shallow level flow differentiation, and magma-wall rock interactions" (Steiner et al., 1992). In this model the first 2.5% crystallization is dominated by olivine (olivine : plagioclase : augite, 100 : 0 : 0), the next 20.5% by augite (16 : 34 : 50), and the next 26% by plagioclase (10 : 60 : 30). The substitution of orthopyroxene for olivine in the model does not significantly affect the overall fit with the observed Palisades trends; the first crystallization episode (0-2.5% crystallization) has a better fit using olivine; the second and third episodes (2.5-23% and 23-49%), however, have better fits using orthopyroxene (Steiner, et al., 1992).

Magma-chamber recharge: Overall there is a general decrease in Mg#, Cr, Ni, and modal orthopyroxene, and a general increase in grain size and modal plagioclase with increasing stratigraphic height in the sill. Petrographic and geochemical anomalies in this general trend, however, are observed at the 10 m, 27 m, 45 m, and 95 m stratigraphic levels (Figs. 4, 5, and 6).

The anomaly at 10 m is the well known olivine horizon. Sections through the horizon at both Fort Lee and Alpine had similar profiles with a gradual increase in olivine and MgO content from the 2 m level up to the lower part of the horizon at about 10 m, and a sharp decrease in olivine and MgO at the upper contact of the horizon at approximately 20 m. No abrupt lower contact was observed at either locality. Within the olivine horizon at both localities, there are two distinct maxima in olivine content separated by an interval with lower olivine and higher augite content. These maxima are clearly apparent in the trend for MgO, Ni, and Co which peak at the olivine maxima, and Cr which peaks in the augite-rich interval. Calculations based on cooling rates, crystallization rates, crystal settling rates, and magma emplacement rates suggest that the olivine horizon probably formed during the initial filling of the chamber as a result of inhomogeneity in the source magma.

The anomalies at 27 m and 45 m probably represent magma chamber recharge during which more primitive magma ponded on the floor of the magma
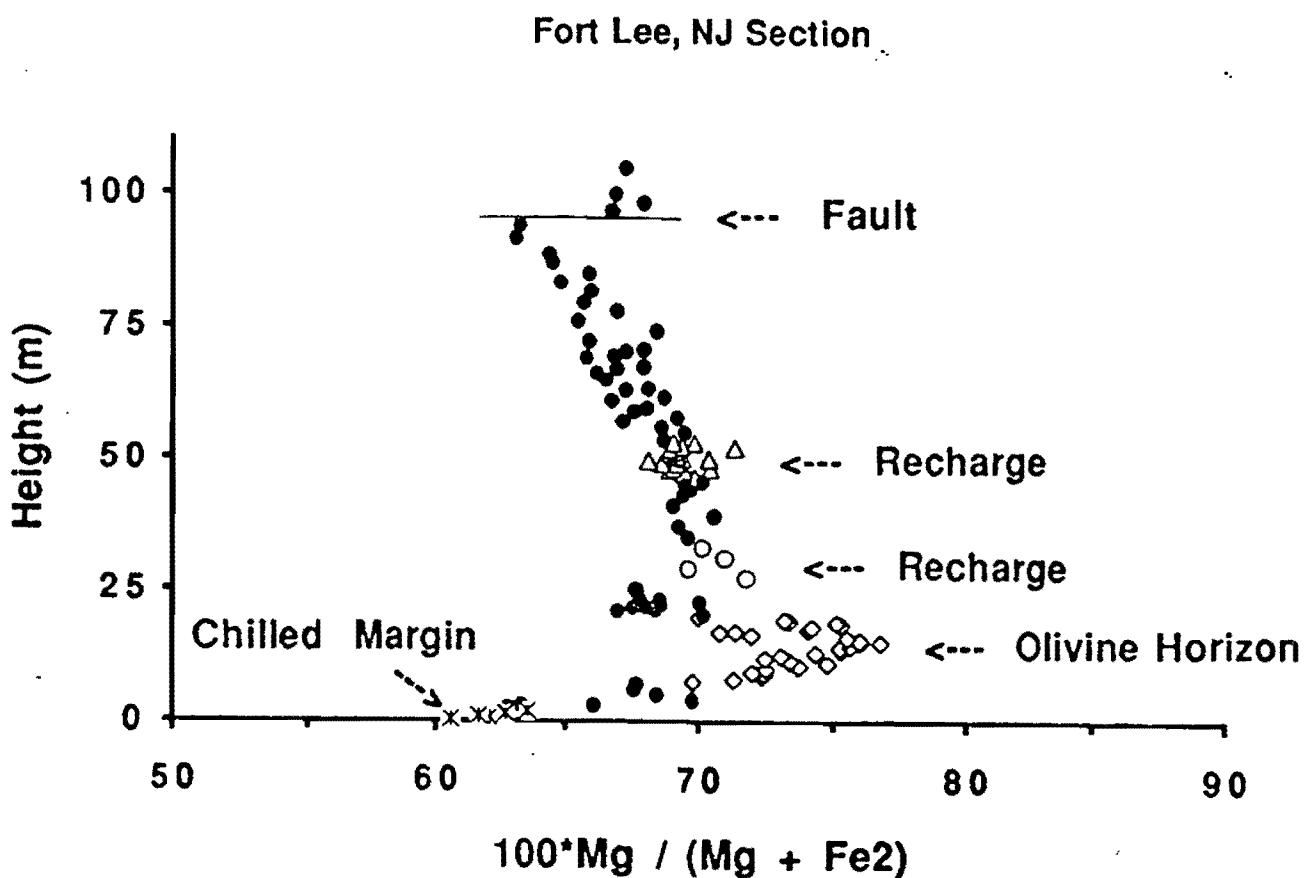
Fig. 4. Plot of Mg# vs. Stratigraphic Height for the Fort Lee, NJ section, showing the location of geochemically anomalous horizons at 10 m (open diamonds), 27 m (open circles), and 45 m (open triangles). Filled circles represent diabase samples from the sill that are not associated with geochemical anomalies, and asterisks represent chilled margin samples.

$$F' = 0.5*(Fe+Mg) + 2*Ca + 3*Na$$
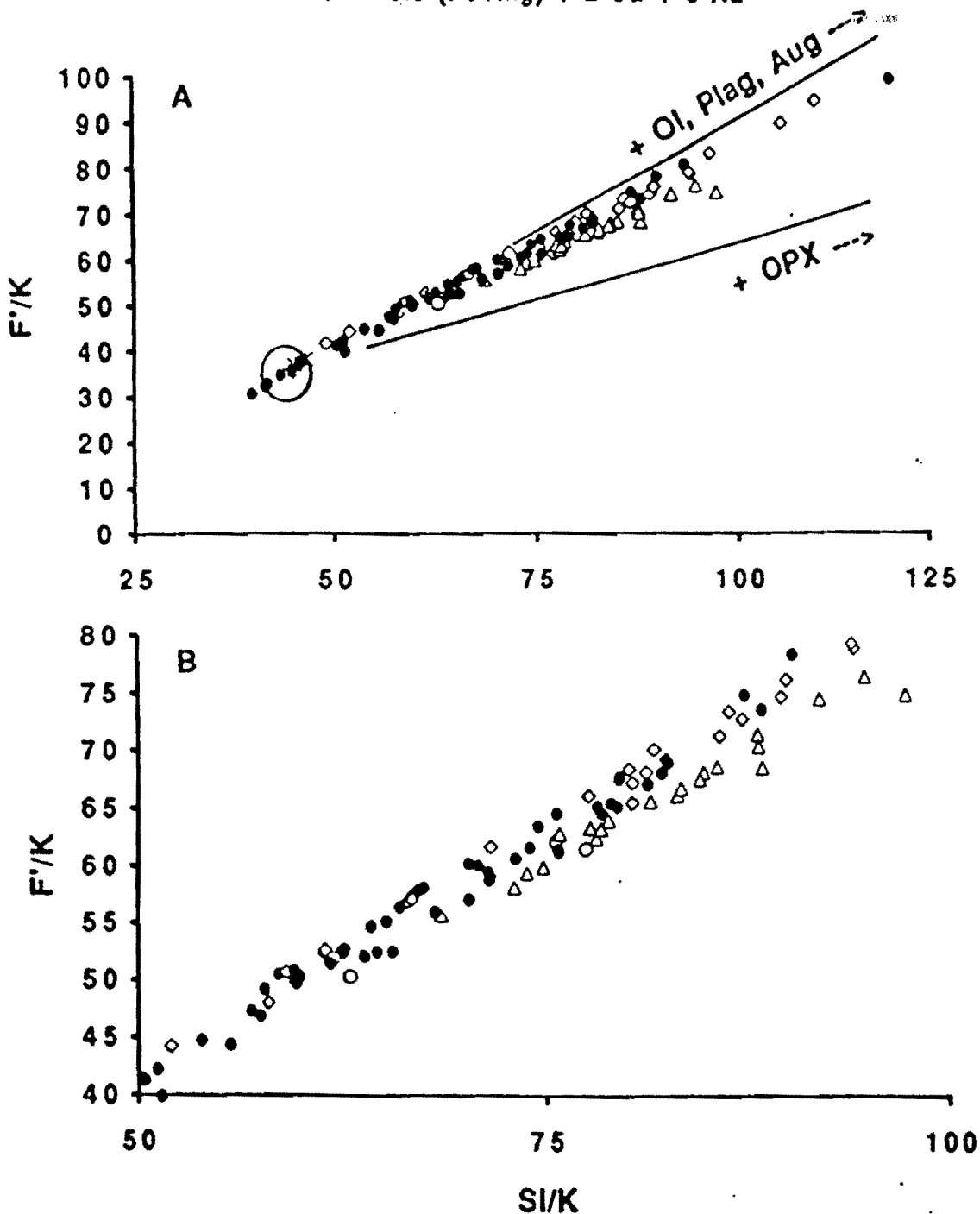
Fig. 5a. Pearce Element Plot of F'/K vs. Si/K where $F' = 0.5*(Fe+Mg) + 2*Ca + 3*Na$ for the Fort Lee, NJ section. The fractionation of olivine, augite, or plagioclase will cause a linear trend with a slope of 1.0, the fractionation of orthopyroxene will cause a linear trend with a slope of 0.5, and the fractionation of Fe-oxides will cause a linear trend with a slope of ∞. The plot assumes an augite of composition $Ca.67(Fe, Mg)1.33Si2O6$. The six chilled margin samples are circled. Symbols as in Figure 4.

Fig. 5b. Enlargement of the central part of 5a showing the separate trend for samples from the anomalous horizons at 27 and 45 m.
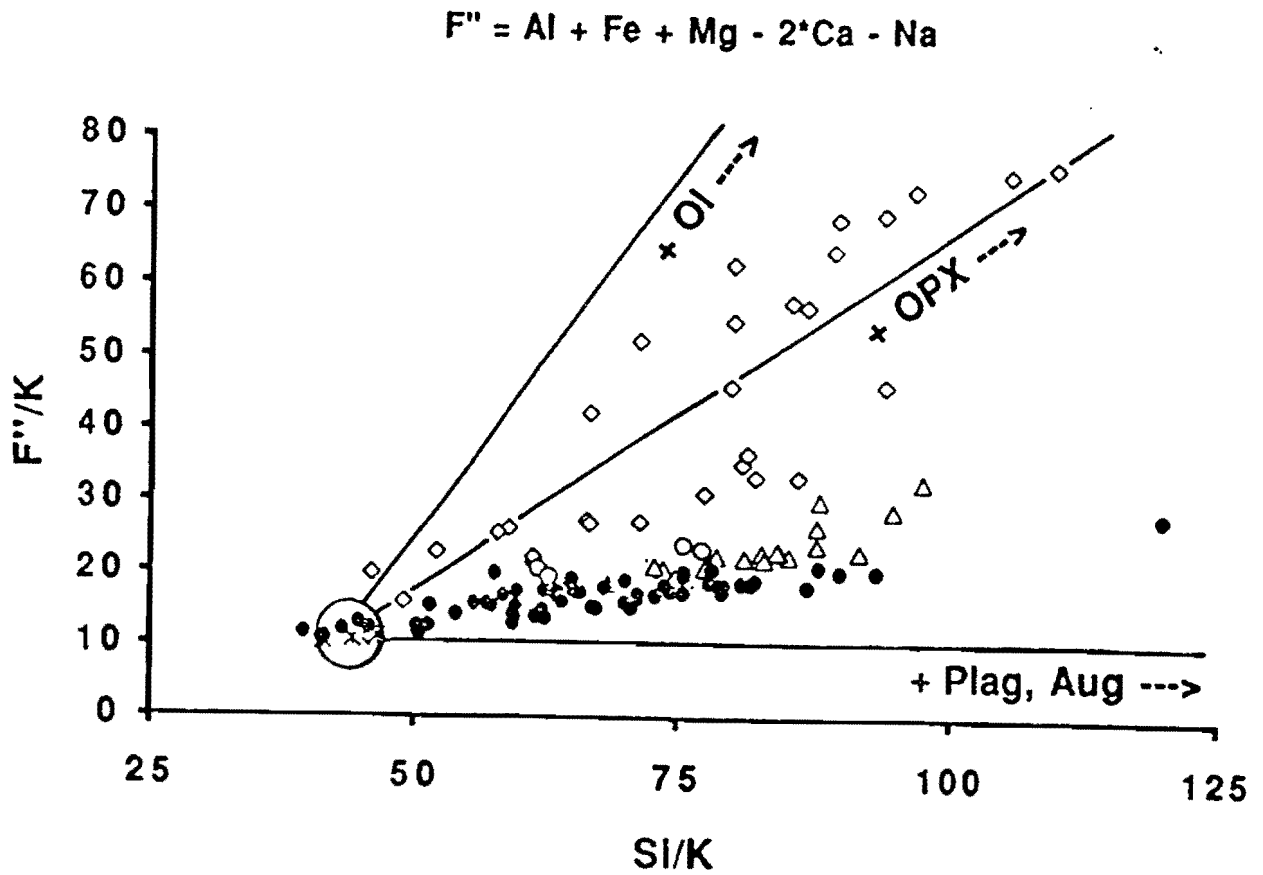
Fig. 6. Pearce Element Plot of F"/K vs. Si/K where F" = Al + Fe + Mg - 2*Ca - Na for the Fort Lee, NJ section. The fractionation of augite or plagioclase will cause a linear trend with a slope of 0.0, the fractionation of orthopyroxene will cause a linear trend with a slope of 1.0, and the fractionation of olivine will cause a linear trend with a slope of 2.0. Symbols as in Figure 4.

78

chamber and/or hybridized with the resident magma in the chamber. Both horizons are marked by abrupt but narrow intervals of increased Mg# and Cr contents, and higher percentages of cumulus orthopyroxene. The anomaly at 45 m is marked by an abrupt decrease in grain size for plagioclase and augite, and was observed in both the George Washington Bridge section and the Ross Dock section indicating that it extends for at least 500 m laterally. The anomaly at 95 m, which had been identified by a previous investigator as a recharge horizon, is the result of normal faulting.

Diabase samples from the roof sequence appear to represent nearly 100% solidified ("trapped") liquid from which plagioclase, augite, and orthopyroxene have been lost. In this regard they are a complement to the floor samples which appear to be where these minerals have accumulated. Minor geochemical anomalies in the roof section at 296m, 293m, and 283m, appear to correlate with the anomalous horizons in the floor sequence at 10m, 27m, and 45m, respectively.

Layering: Although the sill appears to be homogeneous on a hand specimen scale, faint Cm-scale layering is visible on some weathered surfaces. Two 20-Cm rhythmically layered sequences have been examined in detail; one section from the 10 m level, and another from the 70 m level (Fig. 7). Although layering is only faintly visible in outcrop, both sections have significant modal variations in the form of layers 1 to 3 cm thick. Layer boundaries are gradational, and parallel to the dip of the sill. In the section at 10 m: plagioclase varies from 35 to 55%; augite from 20 to 45%; hypersthene from 5 to 25 %; olivine from 0 to 10 %; and opaques from 1 to 10%. In the section at 70 m: plagioclase varies from 45 to 60%; augite from 35 to 50%; and opaques from 3 to 10%. Layers defined by variations in the more abundant phases (plagioclase and pyroxene) do not correlate with layers defined by the less abundant phases (olivine and opaques).

The well known olivine horizon of the Palisades sill is a layer of olivine-rich dolerite ranging from 1 to 10 m in thickness. It is located 10 to 13 m above the basal contact of the sill and is traceable for over 40 km along strike (Walker, 1969). The origin of this unit has been debated for almost 100 years, and was cited by Bowen (1928, p.71) as a classic example of crystal settling. Recent
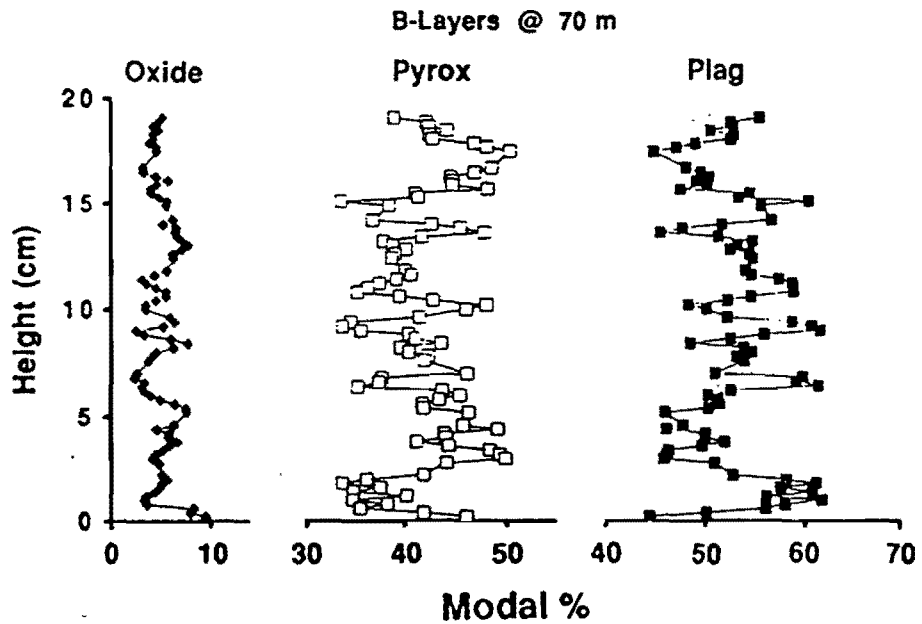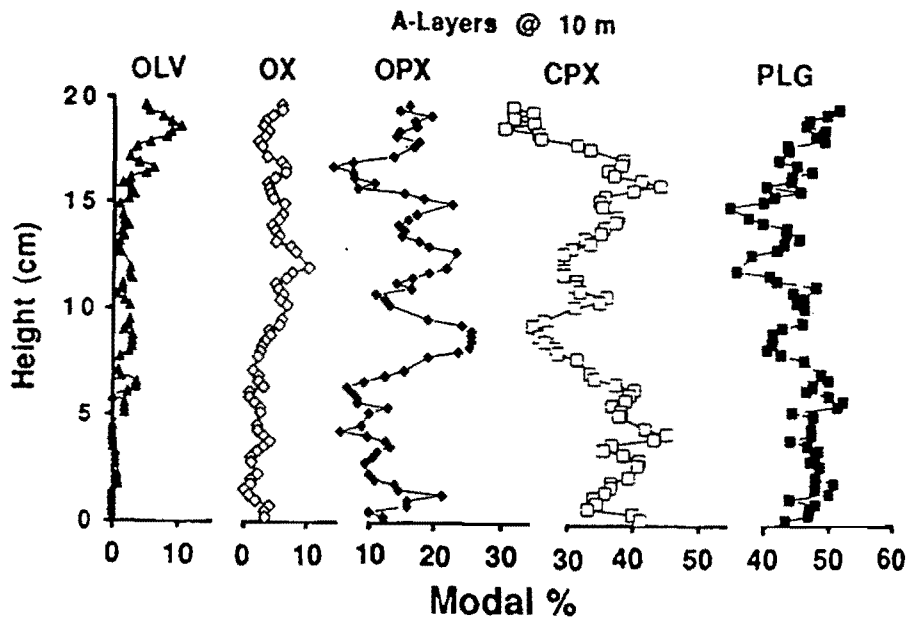
Fig. 7 Modal variation in layered sequences at the 10 m (A layers) and 70 m (B layers) stratigraphic levels.

interpretations, however, argue against gravity settling, suggesting instead that the olivine horizon is the result of either a separate pulse of olivine-rich magma (Husch, 1990) or an initially inhomogeneous magma (Gorring and Naslund, 1995). Both interpretations suggest that olivine was concentrated in the olivine-rich zone by flow segregation. Irregular cm- to m-scale layering within the olivine horizon appears to be the result of minor variations in the degree of flow segregation. Geochemical evidence from the lower part of the Palisades Sill indicates that, although plagioclase/augite and augite/orthopyroxene ratios are relatively constant, olivine/(plagioclase+pyroxene) in the olivine horizon is quite varied, suggesting that the olivine has been mechanically sorted (Gorring and Naslund, 1995). In figure 5, where olivine, plagioclase, and augite cause similar fractionation trends, samples from the olivine horizon plot along with samples from the main part of the sill. In figure 6, where the effects of olivine fractionation are separated from the effects of plagioclase and augite fractionation, samples from the olivine horizon plot as a wide scatter above the trend from the main part of the sill, indicating that the olivine horizon contains variable amounts of accumulated olivine.

Coats (1936) was probably the first to point out that crystals of differing sizes and densities tend to sort themselves in crude layers as they consolidate under the force of gravity. The forces responsible for this sorting are not well understood, but seem to be related to a self-organization of particles according to their drag coefficients in a viscous fluid. At a number of horizons within the lower part of the sill, weak, irregular, sub-horizontal layers are present. These layers appear to be similar to those postulated by Coats.

In the roof sequence of the sill, numerous pods and stringers of coarser-grained diabase form irregular grain-size layers. These are probably the result of auto injection of differentiated melts into the roof sequence.

The first 50 % solidification: A number of geochemical modeling techniques have been developed to explain the compositional variations observed in igneous rock suites. Five of these techniques have been used to model the first 50% solidification of the Palisades sill: (1) Rayleigh fractionation of excluded elements (Henderson, 1975); (2) incremental subtraction of the observed rock sequence from an initial magma composition (Morse, 1979,

1981; Naslund, 1989); (3) a least-squares-fit mass-balance calculation (Bryan, Finger & Chayes, 1969; Wright & Doherty, 1970; Bryan, 1986); (4) Pearce element ratio analysis (Pearce, 1968, 1990; Nichols & Russell, 1990); and (5) a liquid-line-of-descent calculation (the CHAOS program, Nielsen, 1985, 1988). Each of these methods requires assumptions about the differentiation process, and provides a set of relationships compatible with those assumptions.

Two methods were used to calculate the average "trapped" liquid content for the first 50% solidification of the Palisades sill. The two methods, however, are not entirely independent, in that both are based on the average content of excluded elements in the Palisades diabase, and both are dependent upon the choice of an initial liquid composition. The estimated average "trapped" liquid by these two methods ranges from 68% to 77%. The two preferred estimates are very similar; mass balance calculations, based on the average variation for ten major elements, yielded an average "trapped" liquid content of 75.6 %; a value of 76.7% was calculated from Rayleigh fractionation of TiO_2. Rayleigh fractionation of P_2O_5 and K_2O suggest slightly lower trapped liquid contents (~68%).

Geochemical modeling by Shirley (1987) estimated 40 to 50% "trapped" liquid. This estimate, however, was based on a Palisades bulk composition in the Fort Lee section that was richer in excluded trace elements than the chilled margin by a factor of 1.5x. The Palisades bulk composition in the Fort Lee section calculated by averaging analyzed samples over uniform thickness intervals is also richer in TiO_2, K_2O, Na_2O, and Fe_2O_3 (total iron) than the chilled margin, and is unlike any other magmas in the Eastern North America Mesozoic magma province (Whittington, 1988; Puffer & Philpotts, 1988; Puffer, 1992) (Table 1). It is likely that the sandwich horizon in the Fort Lee section is thicker than the intrusion-wide average (Figure 8). Mass balance calculations suggest that the bulk composition in the Fort Lee section can be obtained from a mixture of 73% chilled margin and 27% sandwich horizon. Shirley's (1987) estimate of 40-50% "trapped" liquid would be 60-75% if the excluded element content of the chilled margin was used for the initial magma in his calculations instead of the bulk composition calculated by summation.

Three relatively independent methods were used to determine the trend of magma differentiation and the fractionated mineral assemblage represented by

Table - 1

Estimated initial Palisades magmas and selected ENA magmas

	1	2	3	4	5	6	7	8	9	10	11	12	13	14
	CM f	CM r	BU*	BU	HTiQT	HFeQT	LTiQT	HFO	LFO	OMB	P-1	P-2	P-3	HMB
SiO2	52.5	52.8	53.3	53.5	51.5	52.2	51.4	47.5	49.2	51.5	52.7	51.7	50.9	49.8
TiO2	1.137	1.026	1.633	1.671	1.128	1.130	0.756	0.585	0.600	1.163	1.114	1.065	0.816	1.444
Al2O3	14.2	14.3	13.8	13.9	14.3	14.1	14.9	14.4	16.9	14.4	14.1	14.4	15.6	13.5
Fe2O3 t	11.1	11.0	12.5	12.5	11.7	13.7	11.7	12.6	10.3	11.0	12.5	13.2	11.5	16.0
MnO	0.177	0.163	0.178	0.178	0.191	0.218	0.199	0.188	0.170	0.162	0.213	0.195	0.184	0.252
MgO	7.47	7.28	6.19	5.78	7.47	5.48	7.40	12.19	8.94	7.84	5.92	6.13	7.72	5.67
CaO	10.25	10.39	8.85	8.86	10.74	9.78	10.75	10.47	11.27	10.80	9.72	7.12	10.18	10.39
Na2O	2.07	2.07	2.36	2.41	2.14	2.49	2.22	1.79	2.11	2.46	2.97	5.10	2.70	2.30
K2O	0.865	0.674	1.034	1.057	0.665	0.634	0.478	0.258	0.390	0.486	0.648	0.942	0.357	0.404
P2O5	0.142	0.202	0.202	0.207	NR	NR	NR	0.089	0.140	0.142	0.132	0.143	0.092	0.192
sum	100.0	100.0	100.0	100.0	99.8	99.8	99.8	100.0	100.0	100.0	100.0	100.0	100.0	100.0
Mg#	57.0	56.6	49.6	47.9	55.9	44.1	55.6	65.7	63.1	58.5	48.5	47.8	57.0	41.2

1 - 4 Estimated Palisades magmas: floor chilled margin, roof chilled margin, bulk composition, bulk composition without olivine horizon.

5 - 7 ENA magma types: high-Ti quartz tholeiite, high-Fe quartz tholeiite, low-Ti quartz tholeiite (Puffer and Philpotts, 1988)

8 - 9 ENA magma types: low-Fe olivine tholeiite, high-Fe olivine tholeiite (Whittington, 1988)

10-14 Whatchung basalts: Orange Mountain, Preakness 1, Preakness 2, Preakness 3, Hook Mountain (Puffer, 1992)

Fe2O3 t = Fe2O3 + 1.11*FeO; Mg# = Mg/[Mg+Fe] in cation %; NR = not reported
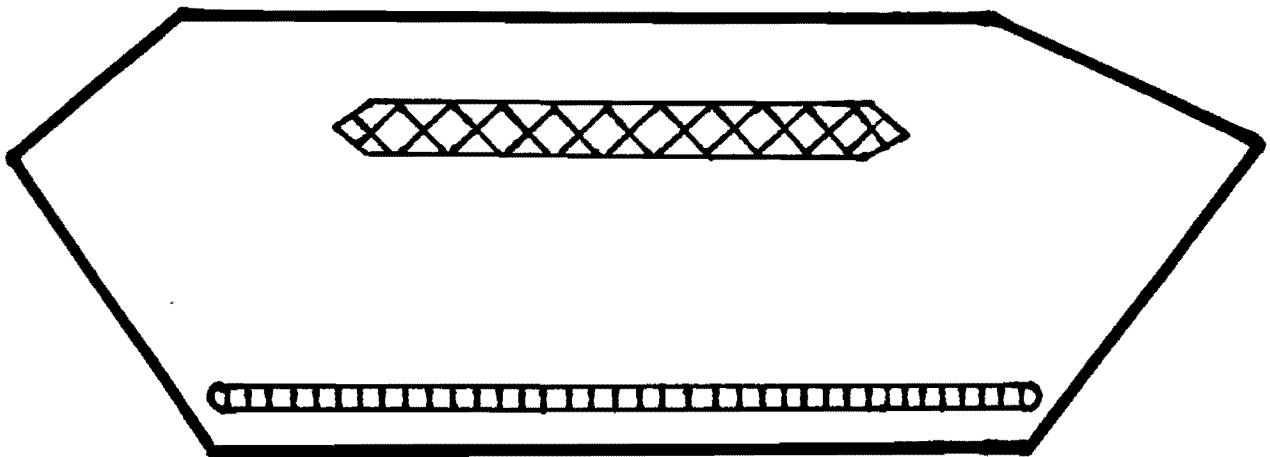
Lateral Pinch Outs
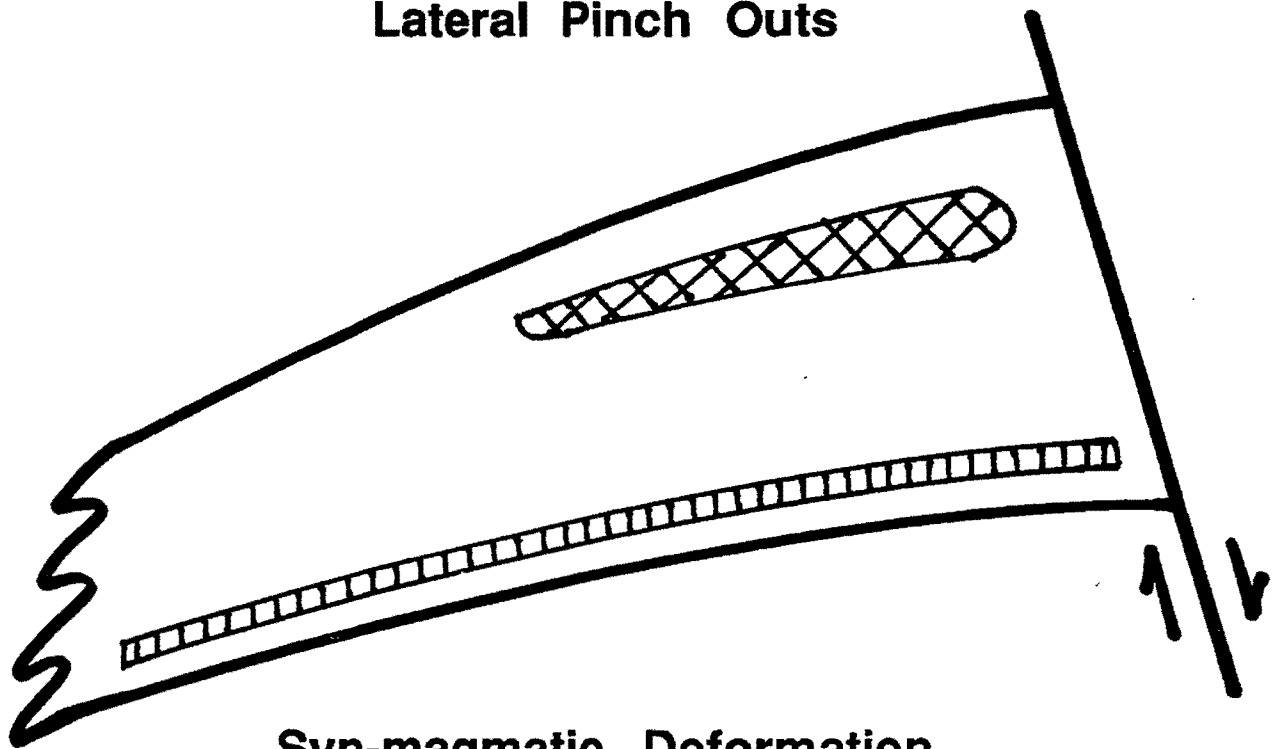
Syn-magmatic Deformation

Figure 8 – Two possibilities thatcould explainwhy the Fort Lee section
of the Palisades sill is more iron-rich than the chilled margin.
Cross hatched pattern = iron-rich Sandwich horizon; vertical
ruled = olivine horizon.

the initial 50% solidification of the Palisades sill. All three methods indicate that the composition of the Palisades magma was enriched in TiO_2, K_2O, P_2O_5, Fe_2O_3 (total iron), and MnO, and depleted in MgO as differentiation proceeded. SiO_2 remained relatively constant (<1% change) over the first 50% solidification of the sill in all three models. These models suggest that the Palisades sill fractionated a crystal assemblage dominated by plagioclase (43-58%), augite (24-30%), and orthopyroxene (19-27%), with the percentage of plagioclase and the ratio augite/orthopyroxene increasing as differentiation proceeded over the first 50% solidification. Similar results were obtained by Steiner et al. (1992) for the section in Upper Nyack, NY, where their cumulus-transport-deposition model calculated 46.1% plagioclase, 36.8% augite, and 17.1% olivine or orthopyroxene fractionation for the first 49% crystallization, with similar increases in plagioclase and augite / (olivine or orthopyroxene) with increasing crystallization.

Although, the magmas at the roof and floor appear to have fractionated similar mineral assemblages, the compositional differences between the roof and floor sequences suggests that the roof sequence has lost early formed minerals while the floor sequence has gained them. The floor sequence diabases fit reasonably well a model in which the fractionated mineral assemblage and the percent "trapped" liquid change as crystallization proceeds in accord with the proportions calculated by mass balance. The roof sequence, however, has much lower Mg#s and fits best a model in which the roof sequence diabases represent approximately 95% "trapped" liquid, but in which the liquid has undergone approximately 50% differentiation (i.e. crystals have settled out of the magma at the roof into the lower part of the chamber).

Implications for the crystallization of magma chambers:
Geochemical models for the Palisades sill suggest that the initial solidification of the sill was accompanied by approximately 25% fractionation of a crystal assemblage dominated by plagioclase, augite, and orthopyroxene. Compositional variations within the roof and floor sequences appear to be related to similar fractionation assemblages, but between 66 and 90% of the differentiation recorded in the roof sequence, as indicated by excluded element enrichment and Mg# depletion, is the result of crystal accumulation at the floor.

Although heat loss through the roof of the intrusion presumably exceeded heat loss through the floor, the floor sequence is approximately 5 times thicker than the roof sequence. These results require a mechanism for transferring crystals from the roof to the floor, and/or heat and differentiated magma from the floor to the roof.

A number of recent papers have discussed the dynamics of heat transfer during cooling in sheet-like magma chambers; some have concluded that convection is vigorous (Sparks, Huppert & Turner, 1984; Brandeis & Jaupart, 1986; Martin, Griffiths & Campbell, 1987; Sparks, 1990; Huppert & Turner, 1991; Worster, Huppert & Sparks, 1993), some have concluded that convection is weak or absent (Helz, 1987; Marsh, 1988, 1989a, 1989b, 1990, 1991; Gibb & Henderson, 1992), and some have concluded that heat (or heat loss) is transferred by plumes (Brandeis & Jaupart, 1986; Helz, 1987; Marsh, 1988, 1989a, 1989b). The Palisades sill is important in this debate because, with a thickness of 300 m, it is thicker than most of the sheet like bodies with D- or S-shaped profiles that show little evidence for the settling of crystals formed in-situ, or any evidence for post emplacement convection (Gibb & Henderson, 1992), but is smaller than most gabbroic intrusions that have clearly differentiated in-situ, and therefore, must have undergone convection or some other form of internal heat and mass transfer.

The Palisades data fit best a model in which heat loss at the roof results in crystallization adjacent to the upper solidification front, with plumes of cool, crystal-rich magma continuously detaching from the roof zone and settling to the floor where they remain and eventually solidify. Owing to the fact that pyroxene is richer in MgO than magma with which it is in equilibrium, crystallization at the roof results in a situation where both the fractionated crystal assemblage and the residual magma are denser than the underlying, unfractionated magma. This will result in the development of a "convection half-cell" in which there is steady downward flow of cool, crystal-rich magma from the roof zone, but no return upward flow. As plumes detach from the upper crystallization front, some of the interstitial liquid in the crystal-liquid mush is extracted from the plume to fill the void behind the plume. This is a process similar to that proposed by Marsh (1996) for liquid extraction from detached solidification fronts at a later stage of crystallization (55 to 60% crystals). Such a model allows the roof

sequence magma to evolve as though it was fractionating 30 to 50% early formed crystals, while the roof sequence diabases appear to represent 90 to 95% "trapped" liquid, and allows the floor zone to accumulate at five times the rate at which the roof zone accumulates, even though the majority of the heat loss occurs at the roof and the floor zone diabases contain only about 25% accumulated crystals. It is probably more than a coincidence that the percent of crystals added to the floor sequence is the same as the percent of entrained crystals proposed by Marsh (1989a) for the limit between a crystal suspension and a crystal mush. Plumes that arrive at the floor with less than approximately 25% entrained crystals are likely to be displaced upward by the later arrival of denser plumes. Plumes with 25% or more entrained crystals, however, once attached to the floor, are unlikely to move regardless of where the majority of the heat loss in the intrusion is occurring, or how the density of the overlying magma changes. Indeed, the presence of a thick floor sequence with approximately 25% accumulated crystals, may provide a indication of plume driven cooling in other sills (Fig 9).

The final 50 % solidification: Studies of lava lakes have suggested that compositional and thermal transfer can occur in magma bodies through vapor migration, and diapiric melt transfer (Helz, 1987). McBirney (1980) suggested that plumes of buoyant melt generated at crystallization fronts can rise through a magma and collect under the chamber roof to produce zoned magmas. In thick section of the Holyoke flood basalt differentiated liquid separated from the partially crystallized basalt after ~33% crystallization and migrated upward to form segregation sheets of coarser grained diabase (Philpotts, et al., 1996). Similar pods and sheets of coarse-grained diabase are common in the Palisades sill in the crystallization interval from 50% to 100% solidified. Preliminary examination of this part of the sill suggests that during the later stages of crystallization of the Palisades sill, this may have been the dominant differentiation process.

Irvine (1980) suggested that heat and chemical components can be transferred though cumulate rocks by the upward migration of interstitial liquids through the porous crystal-liquid mush. Such a process results in extensive mineral-melt reequilibration, or "infiltration metasomatism". The segregation of

87

Model For Palisades Crystallization:

Roof Contact

Heat Loss and Crystallization

Plumes of Crystals and Liquid

Accumulation of Plumes

Crystal-Magma Mush

Solid Diabase

Floor Contact
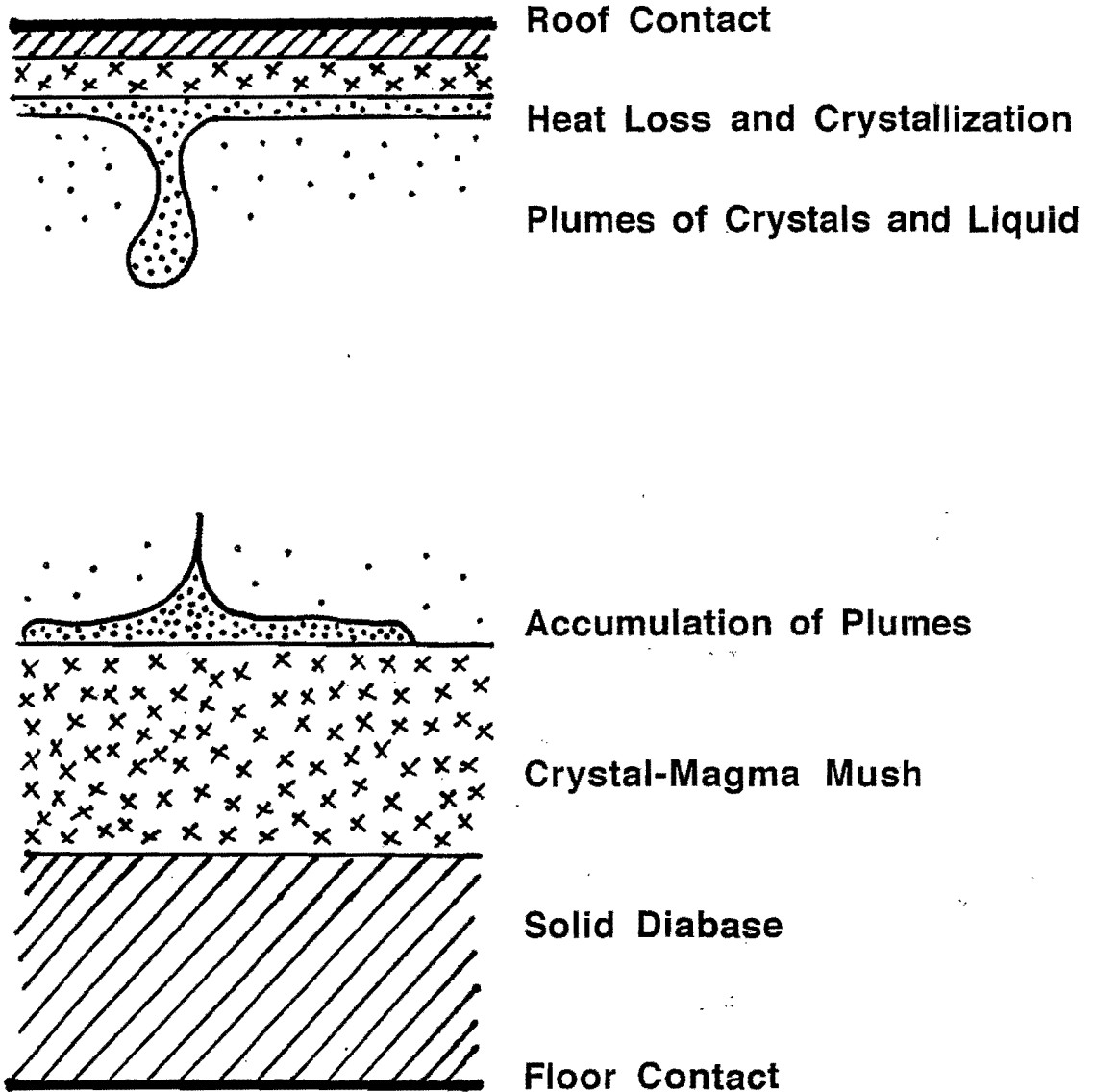
Figure 9 - Crystallization Model for the Palisades sill.

coarse grained diabase pods and lenses in the Palisades sill may have occurred through such a process of interstitial melt migration. This process has been modeled for the Palisades sill by Shirley (1987) who demonstrated that the process could qualitatively explain some of the features of the general Palisades differentiation trend. His study, however, lacked the detailed sampling necessary to confirm the model.

In the Skaergaard intrusion the roof-zone sequence is enriched in SiO_2, TiO_2, K_2O, P_2O_5, and Zr relative to the floor sequence (Naslund, 1984) suggesting that the magma at the roof of the Skaergaard chamber was compositionally zoned relative to that at the floor, or that components were added to the roof sequence by upward migration through the crystal-liquid mush. In the Palisades sill, the roof-zone sequence is enriched in Na_2O, K_2O, Al_2O_3, TiO_2, FeO, Zn, Ba, and Zr relative to the floor-sequence. In both intrusions, plagioclase in the roof-sequence has lower K_2O contents than plagioclase in the floor-sequence, in spite of the fact that, the host rocks at the roof are richer in K_2O (Naslund, 1984 and unpublished data). This relationship suggests a concentration of volatiles and increased P_{H2O} in the roof-zones of these intrusions. An additional similarity between the Palisades and the Skaergaard is that both have significantly coarser grain-sizes in their roof sequences relative to their respective floor sequences. This is probably a reflection of a slower advance of the crystallization front at the roofs of the chambers, but might also be influenced by an increased volatile content at the roof.

References cited

Brandeis, G. & Jaupart, C. 1986. On the interaction between convection and crystallization in cooling magma chambers. *Earth and Planetary Science Letters* **77**, 345-61.

Bryan, W. B. 1986. Linked evolutionary data arrays: a logical structure for petrologic modeling of multisource, multiprocess magmatic systems. *Journal of Geophysical Research* **91**, 5891-900.

Bryan, W. B., Finger, L. W. & Chayes, F. 1969. Estimating proportions in petrographic mixing equations by least-squares approximation. *Science* **163**, 926-7.

Coats, R. R., 1936., Primary banding in basic plutonic rocks, *Journal of Geology* **44**, 407-419.

Gibb, F. G. F. & Henderson, C. M. B. 1992. Convection and crystal settling in sills.*Contributions to Mineralogy and Petrology* **109**, 538-45.

Gibb, F. G. F. & Henderson, C. M. B. 1996. The Shiant Isles Main Sill: structure and mineral fractionation trends. *Mineralogical Magazine* **60**, 67-97.

Gorring, M. L. 1992. *The petrology and geochemistry of the lower 105M of the Palisades Sill, New Jersey,* MA Thesis, State University of New York at Binghamton, 167 pp.

Gorring, M. L., and Naslund, H. R., 1991. Geochemical and petrographic signatures of magma chamber recharge in the Palisades Sill, NJ-NY, *EOS* **72**, 315.

Gorring, M. L., and Naslund, H. R., 1991. A detailed petrologic investigation of the olivine horizon within the Palisades sill, NJ-NY, *Geol. Soc. Amer. Abstr. w. Progr.* **23**, A270.

Gorring, M. L. & Naslund, H. R. 1995. Magma Chamber Recharge in the Lower part of the Palisades sill. *Contributions to Mineralogy and Petrology* **119**, 263-76.

Helz, R. T. 1987. Differentiation behavior of Kilauea Iki lava lake, Kilauea Volcano, Hawaii: an overview of past and current work. In *Magmatic Processes: Physicochemical Principles*, Special Publication No. 1 (ed B. O. Mysen), pp. 241-58. The Geochemical Society.

Henderson, P. 1975. Geochemical indicator of the efficiency of fractionation of the Skaergaard intrusion, East Greenland. *Mineralogical Magazine* **40**, 285-91.

Hristov, L. G. 1995. *Petrogenesis of the Roof Zone - Palisades Sill, New Jersey.* MA Thesis, State University of New York at Binghamton, 112 pp.

Hristov, L.G., and Naslund, H.R., 1994. Petrogenesis of the roof zone of the Palisades sill, NY-NJ, *Geol. Soc. Amer. Abstr. w. Progr.* **26**, no. 2, 24.

Huppert, H. E. & Turner, J. S. 1991. Comments on "On convective style and vigor in sheet-like magma chambers" by Bruce Marsh. *Journal Petrology* **32**, 851-4.

Husch, J. M. 1990. Palisades sill: Origin of the olivine zone by separate magmatic injection rather than gravity settling. *Geology* **18**, 699-702.

Husch, J. M. 1992. Geochemistry and petrogenesis of the Early Jurassic diabase from the central Newark basin of New Jersey and Pennsylvania. In *Eastern North America Mesozoic magmatism*, Special Paper 268 (eds J. H. Puffer and P. C. Ragland), pp. 169-92. Geological Society of America.

Irvine, T. N. 1970. Heat transfer during solidification of layered intrusions, part I, sheets and sills. *Canadian Journal of Earth Sciences* **7**, 1031-61.

Irvine, T. N. 1980. Magmatic infiltration metasomatism, double-diffusive fractional crystallization, and adcumulus growth in the Muskox intrusion and other layered intrusions, in, *Physics of Magmatic Processes*, (ed Hargraves, R.B.), Princeton University Press, Princeton, NJ, 325-383.

Langmuir, C. H. 1989. Geochemical consequences of in situ crystallization. *Nature* **340**, 199-205.

Lewis, J. V. 1908. The Palisades diabase of New Jersey. *American Journal of Science* **26**, 155-62.

Mangan, M.T., Marsh, B.D., Froelich, A.J., & Gottfried, D., 1993, Emplacement and Differentiation of the York Haven Diabase Sheet, Pennsylvania, *Journal of Petrology* **3 4**, 1271-1302.

Marsh, B. D. 1988. Crystal capture, sorting, and retention in convecting magma. *Bulletin of the Geological Society of America* **1 0 0**, 1720-37.

Marsh, B. D. 1989a. Magma chambers. *Annual Reviews of Earth and Planetary Science* **1 7**, 439-74.

Marsh, B. D. 1989b. On convective style and vigor in sheet-like magma chambers. *Journal of Petrology* **3 0**, 479-530.

Marsh, B. D. 1990. Crystal capture, sorting, and retention in convecting magma: reply. *Bulletin of the Geological Society of America* **1 0 2**, 849-50.

Marsh, B. D. 1996. Solidification fronts and magmatic evolution. *Mineralogical Magazine* **6 0**, 5-40.

Marsh, B. D. 1991. Reply. *Journal of Petrology* **3 2**, 855-60.

Martin, D., Griffiths, R. W. & Campbell, I. H. 1987. Compositional and thermal convection in magma chambers. *Contributions to Mineralogy and Petrology* **9 6**, 465-75.

McBirney, A. R. 1980. Mixing and unmixing of magmas, *Journal of Volcanology and Geothermal Research* **7**, 357-371.

Morse, S. A. 1979. Kiglapait geochemistry I: systematics, sampling, and density. *Journal of Petrology* **2 0**, 555-90.

Morse, S. A. 1981. Kiglapait geochemistry IV: the major elements. *Geochimica et Cosmochimica Acta* **4 5**, 461-79.

Naslund, H.R., 1984, Petrology of the Upper Border Series of the Skaergaard intrusion, East Greenland, *Journal of Petrology* **2 5**, 185-212.

Naslund, H. R. 1989. Petrology of the Basistoppen sill, East Greenland: calculated magma differentiation trend. *Journal of Petrology* **3 0**, 299-319.

Naslund, H.R., Hristov, L.G., and Gorring, M.L., 1992. Cm-scale modal layering in the Palisades sill, NY NJ, USA. *Geol. Soc. Amer. Abstr. w. Progr.* **2 4**, A86.

Naslund, H.R., 1993. Application of Pearce element ratio analysis to the lower 100m of the Palisades sill, NY-NJ, USA. *Geol. Soc. Amer. Abstr. w. Progr.* **2 5**, no. 2, 67.

Naslund, H.R., and Hristov, L.G., 1995. Differentiation of the Palisades sill, NY-NJ, USA *Proceedings of the Magmatic Processes Conference*, Mineral. Soc. & Volc. Studies Group, University of Sheffield, **2 0**.

Naslund, H.R., and Hristov, L.G., 1995. Geochemical modeling of the Palisades sill, *Geol. Soc. Amer. Abstr. w. Progr.* **2 7**, no. 1, 71.

Nicholls, J. & Russell, J. K. 1990. Pearce element ratios - An overview, example and bibliography. In Theory *and application of Pearce element ratios to geochemical data analysis,* Short Course Notes 8 (eds C. R. Stanley and J. K. Russell), pp. 11-22. Geological Association of Canada.

Nielsen, R. L. 1985. EQUIL.FOR: a program for the modeling of low-pressure differentiation processes in natural mafic magma bodies. *Computers and Geoscience* **1 1**, 531-46.

Nielsen, R. L. 1988. A model for the simulation of combined major and trace element liquid lines of descent. *Geochimica et Cosmochimica Acta* **5 2**, 27-

38.

Pearce, T. H. 1968. A contribution to the theory of variation diagrams. *Contributions to Mineralogy and Petrology* **19**, 142-57.

Pearce, T. H. 1970. Chemical variations in the Palisade sill. *Journal of Petrology* **11**, 15-32.

Pearce, T. H. 1990. Getting the most from your data: Applications of Pearce element ratio analysis. In Theory *and application of Pearce element ratios to geochemical data analysis,* Short Course Notes 8 (eds C. R. Stanley and J. K. Russell), pp. 99-130. Geological Association of Canada.

Philpotts, A. R., Carroll, M. & Hill, J. M. 1996. Crystal-mush compaction and the origin of pegmatitic segregation sheets in a thick flood-basalt flow in the Mesozoic Hartford Basin, Connecticut. *Journal of Petrology* **37**, 811-836.

Puffer, J. H. 1992. Eastern North American flood basalts in the context of the incipient breakup of Pangea. In *Eastern North America Mesozoic Magmatism,* Special Paper 268 (eds J. H. Puffer and P. C. Ragland), pp. 95-118. Geological Society of America.

Puffer, J. H. & Philpotts, A. R. 1988. Eastern North America quartz tholeiites: geochemistry and petrology. In *Triassic-Jurassic Rifting* (ed W. Manspeizer), pp. 578-605. Elsevier, New York.

Shirley, D.N. 1987. Differentiation and compaction in the Palisades sill, New Jersey. *Journal of Petrology* **28**, 835-65.

Sparks, R.S.J., Huppert, H.E. & Turner, J.S. 1984. The fluid dynamics of evolving magma chambers, *Philosophical Transactions of the Royal Society, London* **A-310**, 511-34.

Sparks, R.S.J. 1990. Crystal capture, sorting, and retention in convecting magma: discussion. *Bulletin of the Geological Society of America* **102**, 847-8.

Steiner J. C., Walker R. J., Warner R. D., & Olsen T. R. 1992. A cumulus-transport-deposition model for the differentiation of the Palisades sill. In *Eastern North America Mesozoic magmatism,* Special Paper 268 (eds J. H. Puffer and P. C. Ragland), pp. 193-218. Geological Society of America.

Walker, F. 1940. The differentiation of the Palisades diabase, New Jersey. *Bulletin of the Geological Society of America* **51**, 1059-106.

Walker, K. R. 1969. *The Palisades Sill, New Jersey: A reinvestigation,* Geological Society of America Special Paper 111, 178 pp.

Walker, K. R., Ware, N. G. & Lovering, J. F. 1973. Compositional variations in the pyroxenes of the differentiated Palisades Sill, New Jersey. *Bulletin of the Geological Society of America* **84**, 89-110.

Whittington, D. 1988. Chemical and physical constraints on petrogenesis and emplacement of ENA olivine diabase magma types. In *Triassic-Jurassic Rifting* (ed W. Manspeizer), pp. 557-577. Elsevier, New York.

Worster, M. G., Huppert, H. E. & Sparks, R. S. J. 1993. The crystallization of lava lakes. *Journal of Geophysical Research* **98**, 15891-901.

Wright, T. L. & Doherty, P. C. 1970. A linear programming and least squares method for solving petrologic mixing problems. *Bulletin of the Geological Society of America* **81**, 1995-2008.

A4 - Roadlog

Mileage is broken up into three parts: (1) Binghamton to the Palisade Interstate Park Headquarters; (2) From the Park Headquarters to Fort Lee NJ (3) From Fort Lee to Binghamton, New York.

Binghamton, New York to the Palisades Interstate Park Headquarters:

0.0   Leave from the Parking lot at Binghamton University, turn right and proceed out the main campus entrance.

0.4   Turn Right on Vestal Parkway, Rt. 434

3.4   Follow the road as it turns left over the Susquehanna River and get into the right lane.

3.6   Turn right onto Rt. 363 following signs for Interstate 81.

5.3   Turn right onto Interstate 81 south. Watch the merge lane onto 81 South, traffic enters from the left.

9.3   Get in the left hand lane and take route 17 east.

138   Take exit to route 6 through Harriman Park.

144   Take the Palisades Parkway south.

169   Take exit 2 off of the Palisades Parkway. Turn left and then left again passing under the Parkway. Follow signs to the Palisades Interstate Park Headquarters.

From the Park Headquarters to Fort Lee, New Jersey:

0.0   **Stop 1** - Park in the parking lot at the headquarters building and walk down the road (away from the parkway, towards the river) about 0.1 miles to the second set of outcrops on the left. This is about the 70m stratigraphic level in the sill. The rock here is a two pyroxene diabase with weak modal layering. Plagioclase abundances vary from 45% to 60 % and pyroxene varies from 35% to 50 % from layer to layer. The Palisades diabase is, in general, a rather featureless rock. This horizon is one of two in the sill that has poorly developed rhythmic layering.

93

Along the length of the central part of the sill similar layering is found at the 70 m level near the top of the cliff face. At stop 6 we will see another example of this layering.

Return to cars at Park headquarters and drive down the road to the river past the stop 1 outcrop. Go slowly and watch for bikers.

0.6 **Stop 2 -** Leave flashers on and stay on the right side of the road to avoid traffic. Remind students to stay out of the roadway. Well developed rhythmic layering is present below the olivine horizon at the 10m stratigraphic level. The main layering "signal" is in the orthopyroxene which varies from 10% to 25%. Texturally the orthopyroxene is ophitic to poikilitic at this level.

Proceed down the road and turn right at the circle to drive south along the river. If the road is closed return to the Palisades parkway heading south and get off at exit 1 (Hudson Terrace). Turn left at the stop sign and proceed down to the river to rejoin the roadlog at the base of the cliff (mileage 5.6) and proceed south along the river. As you drive along the river you are at a level below the Palisades sill in arkoses of the Stockton formation.

7.4 The circle above Ross landing boat dock. Note the crude columnar jointing in the diabase above the circle. If you desire an additional stop: above the steps under the roadway at the circle, in the second buttress of outcrops to the north, flow banding is present within the olivine horizon. Watch for poison ivy !!! Continue south from the circle along the river.

7.6 **Stop 3 -** Chilled margin (if the road is blocked you can see similar contact relations by walking south from the circle). Note the minor stair steps in the lower contact and the contact metamorphism of the arkose below the sill. The sill here has a uniform composition for 3 m in from the very fine grained chilled margin. Note that in places it is hard to tell the difference in hand specimen between hornfels sediments below the sill and the Palisades fine-grained chilled margin.

Proceed south under the George Washington Bridge. A phytosaur

94

(Clepsysaurus Rutiodon) was found in the Stockton arkose below the bridge.

8.2　**Stop 4** - Just before the park entrance there is a classic undercut outcrop of the olivine horizon. Although is looks really rotten you can see fresh olivine in it.

　　　Proceed south to the entrance on Bergen County route 505. Turn right (north and proceed up the hill.

8.6　**Stop 5** - The entrance to Fort Lee Historic Park. Drive in or park on the street and walk in. The first outcrops inside the park along the entrance road have sub-horizontal, irregular, plagioclase-rich layers. These appear to be layers of the type theorized by Coats (1936) to have formed by settling and compaction of a crystal mush within a viscous fluid.

　　　From the park entrance turn right on Bergen county route 505. Mileages assume you parked on the street and did not drive in which would add ~0.2.

8.8　Just after you pass under the interstate turn left on Merkel past the Toll Gate Motel (hourly rates available). After 1 block Merkel runs into N. Central. Turn left and circle around onto Bridge Plaza North. After two blocks turn right on Hudson St. and park.

9.0　**Stop 6.** - Outcrop with the best rhythmic layering in the Sill is located around the corner you just passed on Bridge Plaza North. This is again at the 70 m level in the sill. This layering is very regular suggesting a mechanism involving changing conditions of crystallization at the crystal/magma interface rather than layering due to compaction processes.

　　　Continue west on Bridge Plaza North to mileage 9.5, take the middle of three lanes. Turn left on Fletcher, stay in the right hand lane and after crossing over the interstate bear slightly to the right down the hill on Edwin.

9.8 **Stop 7** - Park in front of the NJ dept. of transportation lot. Outcrops of coarse, iron-rich "sandwich horizon" are exposed to the left of the cemetery entrance.

Proceed on Edwin to the stoplight, turn left and then left again on Fletcher. As you pass back over the interstate stay in the right lane and take the first right onto 80/95 west/south. Stay in the right hand lane and watch for traffic entering from the right.

11.2 **Stop 8** - Just after you pass under an impressive high bridge pull over on the shoulder. Park with your flashers on and **stay off of the roadway. Be careful, if the police come, be polite and they will probably ask you to leave.** Cross over the guard rail and look at the upper contact of the sill. Lots of interesting vein minerals and some grain-size layering. The roof rocks below this level (back before the bridge you just passed under) contain segregations of coarse-grained gabbro injected as dikes and sills.

From Fort Lee, New Jersey to Binghamton, New York:

0 Proceed west on I-80 through the Delaware Water Gap.

93 Proceed north on I-380.

121 Proceed north on I-81.

180 Stay in left lane on Route 17 west.

184 Turn right onto 201 south.

185 Take first right at circle and cross the Susquehanna River. Follow signs to route 434 east and SUNY.

186 Turn right into SUNY campus.

B1 - Workshop on Stratigraphic Interpretation of Drill Core Samples

John Bridge and Scott Jarvis, Binghamton University

High quality cores from Schoharie Valley, New York will be examined. Techniques for recognizing sedimentary facies and interpreting depositional environments in core samples will be discussed. Participants should read section A-4 of the guidebook to familiarize themselves with the stratigraphy and sedimentary structures present in the Schoharie Valley.

Sunday October 4th - 9:00 to 12:00

Room 162, Science 1, Binghamton University

Field trip/Workshop B2
Environmental Geophysics

Jeff Barker
Dept. of Geological Sciences and Environmental Studies
Binghamton University

This workshop will include short demonstrations of a variety of geophysical methods commonly applied to environmental hazard assessment problems. We will carry out seismic refraction and reflection surveys, electrical resistivity sounding and profiling as well as a microgravity survey at an abandoned dump/landfill in the Village of Endicott. The dump is located in a former wetland in the flood plain of the Susquehanna River. Aerial photos from 1937 show streams and meander bends at the site. Industrial and municipal waste was dumped there until 1977, when the dump was closed and later capped. The structure and composition of the cap are known, but the content and extent of the waste beneath is largely unknown. The primary water well for the Village of Endicott is located about 600 m east of the dump and is contaminated with vinyl chloride and other volatile organics. Purge wells and air strippers have been installed to remediate water contamination. Ground water flow models indicate the dump is the source of contamination.

Most of the common geophysical methods were developed for oil and mineral exploration, but are now widely used in environmental applications. This is because they are remote sensing methods; they do not require drilling or surface exposures. We have been allowed access to the dump site for a Masters-level feasibility study of the use of various environmental geophysical methods. We are also using the site for an undergraduate/graduate course in environmental geophysics. During the field trip, we will collect data, but will not have time for data processing and analysis. We will demonstrate the primary seismic methods: refraction and common midpoint reflection methods. We will also use electrical resistivity, but in sounding and profiling configurations. We will make a few gravity measurements and discuss the strategies for doing a full gravity survey of such a site. Other methods could be used, but the equipment is not available for the field trip.

Site Location Map
704008   Endicott Village Landfill and Wellfield
NYSDOT Planimetric Quadrangle(s):
ENDICOTT
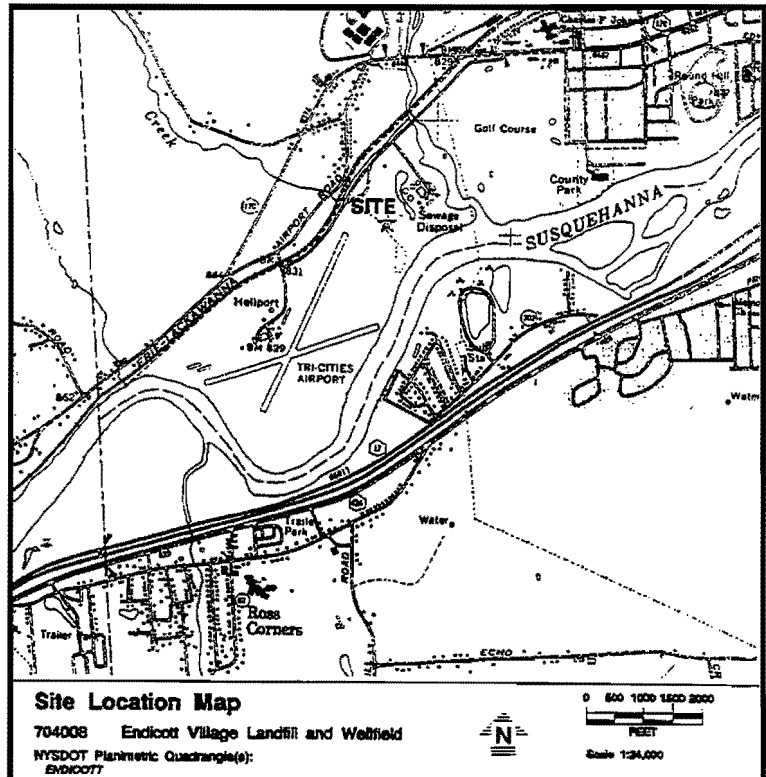
Magnetic methods could be quite useful in a municipal dump experiment to locate metallic waste. Ground-penetrating radar is becoming an invaluable tool in shallow geological, archeological and environmental problems. However, if the cap of the landfill is predominantly clay, this will shield deeper materials from the electromagnetic waves, making ground-penetrating radar useless for this purpose.

Background

1)   Seismic Refraction. A seismic "walk-away experiment" is usually the first seismic data collection effort, intended mostly as a reconnaissance of our site. We set up geophones along a line, with shot points at each end. The shot points are moved away from the geophones (we "walk away") rather than moving the geophones away from the shot point. Our equipment consists of a Geometrics Strataview 24-channel seismograph, geophones, cables, and a "Roll-along switch box" which selects sets of 24 from the 48 geophones we will lay out. We will use a sledge hammer source on each end of the line of geophones, and if possible, will fire a buffalo gun source (a blank 12-gauge shotgun shell detonated at the bottom of an augured hole) from a shotpoint off the edge of the dump. The figure below illustrates an experiment with 2-meter geophone spacing. We will use 1-meter spacing and will have additional shot points located 48 meters from each end. Using the Roll-along switch box allows us to record a 48-channel refraction profile even though our seismograph can record only 24 channels at a time.
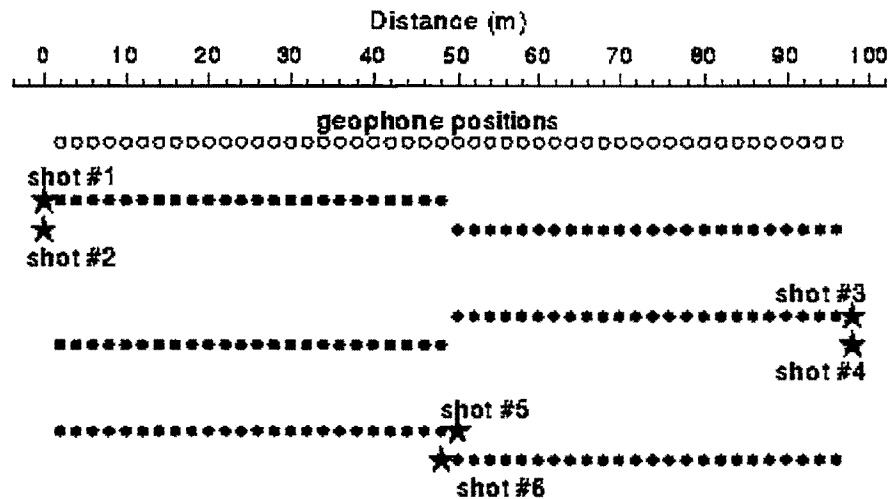
Interpretation is the standard seismic refraction approach. We will be trying to determine the seismic velocity and thickness of a set of horizontal (or not) layers. We won't see much of detailed lateral variations in structure; that's what seismic reflection is for. In addition to determining a layered velocity structure, we will want to identify the air wave and ground roll, and to estimate the wavelength of the ground roll in order to avoid spatial aliasing.

For two horizontal layers of constant velocity, find V_1 and V_2 by fitting straight lines to the beginnings of the arrivals on the time vs. distance plots (velocity is change in

distance divided by change in time). Extrapolate the line for the faster layer back to zero distance to measure the intercept time, T_2. Then the thickness of the top layer (or depth to the top of the second layer) is $h_1 = \dfrac{T_2}{2} \dfrac{V_1 V_2}{\sqrt{V_2^2 - V_1^2}}$ (in m if V is in m/sec and time is in sec).

For three layers, measure the velocities of all three layers as above, and the thickness of the top layer. Also extrapolate the line for the third layer to zero distance and measure its intercept time, T_3. Then the thickness of the second layer (which must be added to the thickness of the first to get depth to the third) is

$$h_2 = \left(\frac{T_3}{2} - h_1 \frac{\sqrt{V_3^2 - V_1^2}}{V_3 V_1} \right) \frac{V_3 V_2}{\sqrt{V_2^2 - V_1^2}}.$$ You can continue this way for multiple layers, but

the equation for each successive layer becomes more complicated and depends on the results from upper layers.

For two layers in which the interface between the two dips, the velocity of the top layer should be the same from either direction, but the lower-layer velocity will apparently be faster in the up-dip direction (V_{2U}) than in the down-dip direction (V_{2D}). The dip is $\delta = \frac{1}{2}\left[\sin^{-1}(V_1/V_{2D}) - \sin^{-1}(V_1/V_{2U})\right]$. The intercept times will vary as well, so if the intercept time in the up-dip direction is T_{2U}, the thickness at this end is

$$h_{1U} = \frac{T_{2U} V_1 V_{2U}}{2 \cos\delta \sqrt{V_{2U}^2 - V_1^2}}.$$ Simply replace U with D to get the thickness at the other end.

2) <u>Seismic Reflection</u>. Much of our effort will be in seismic reflection surveys. We will use "Common Midpoint Profiling" (CMP) which gives us multiple samples of reflections from each point at depth. This requires a great deal of processing, and it is difficult to draw conclusions from the raw (field) data. But, the result is a seismic section which looks very much like a depth section, except that the vertical axis is time, not depth. In a CMP survey, the shot (only sledge hammer blows this time) is placed at the end of a line of geophones. After each shot, the shot point and every geophone point is shifted by the same amount (e.g. 1 m). To make this easier, we will use a "Roll-along switch box", which allows us to lay out 48 geophones, but select any set of 24 for each shot. After 24 shots, we pick up the first 24 geophones and shift them to the end of the line (and shift the cables), and continue.

Since reflections occur at approximately the midpoint between shot point and geophone, the spatial sampling of the reflector will be half the geophone interval, and the multiplicity (or "fold") will be up to 12 at any point. In the following diagram, S denotes the shot point, g denotes the geophones, and ^ shows the reflection point (midpoint) for each shot-geophone pair. Below this is the fold, or the number of reflections recorded at each midpoint after the entire experiment is completed. At the ends, the fold increases from 1, but beyond the 12th shot point, the fold remains constant at 12. Part of our processing will be to collect the data together into "common midpoint gathers" and add or "stack" the data for each reflection point. This stacking improves the signal-to-noise ratio and helps us exclude arrivals that are not the reflections of interest (e.g. headwaves, multiple reflections, surface waves, airwave).

```
S g g g g g g g g g g g g  g  g  g  g  g  g  g  g...
 ^^^^^^^^^^^^^^^^^^^^^^^^^^

 S g g g g g g g g g g g g g  g  g  g  g  g  g  g  g...
  ^^^^^^^^^^^^^^^^^^^^^^^^^^

  S g g g g g g g g g g g g g  g  g  g  g  g  g  g...
   ^^^^^^^^^^^^^^^^^^^^^^^^^^^

   S g g g g g g g g g g g g g  g  g  g  g  g  g...
    ^^^^^^^^^^^^^^^^^^^^^^^^^^^^

              ...

          S g g g g g g g g g g...
           ^^^^^^^^^^^^^^^^^^^^^

           S g g g g g g g g g...
            ^^^^^^^^^^^^^^^^^^^^

 112233445566778899111111111111111111111111111...
 0011222222222222222222222222...
```

3) <u>Electrical Resistivity</u>. DC Electrical resistivity methods are commonly used for determining depth to the water table or bedrock. This is because the electrically conductive properties vary greatly between dry soil or gravel, saturated soil or gravel, and bedrock. Basically, water enhances electrical conductivity (reduces electrical resistivity), and the presents of salts can enhance this even more. Thus, electrical resistivity surveys are ideal for mapping contaminant plumes which contain ionized compounds.

The equipment and field methods are extremely simple. Four electrodes are placed into the ground. Current is applied from a battery to the outer two electrodes. Voltage and current are measured across the inner two electrodes. If the electrodes are spaced equally with a distance A between each electrode (a Wenner configuration), the apparent resistivity at the center is $\rho = 2\pi A \dfrac{V}{I}$. If A is measured in meters, the units of apparent resistivity are ohm-meters.

The first experiment will be electrical resistivity *sounding*. In this case, we use a set of cables with electrical contacts at distances of 0.5, 1, 2, 4, 8, 16, 32 meters from the center. The cables are connected to a switch box which allows us to select sets of 4 electrodes, the spacing between which increase by a factor of two each time. Once the electrodes are attached to the cables, it is a fairly quick matter to record apparent resistivity for electrode spacings (A) of 0.5, 1, 2, 4, 8, 16, 32 meters. As the spacing is increased, the portion of the subsurface which is "sampled" by a significant amount of current becomes greater, extending from the surface to increasing depth. Since the actual resistivity of the subsurface materials varies with depth (e.g. at the water table or at bedrock), the apparent resistivity we measure is essentially an average of the properties from the surface down to some depth. Thus, in addition to the predictable change in resistivity with spacing (A), there will be a variation due to the actual resistivity of subsurface materials. If we plot the apparent resistivity vs. spacing (usually on a log-log plot), we can interpret the variations for actual resistivity and depth.

Once the resistivity and depth of a target of interest (e.g. the water table) are determined, we can set up electrodes with a fixed spacing appropriate for that depth, and increment which set of four electrodes are measured each time. In this way, we can

measure apparent resistivity along a *profile* horizontally. Variations in depth of the target (e.g. shallower water table) or in the actual resistivity of the material at that depth (e.g. increased concentration of ionized contaminants), will appear as horizontal variations in apparent resistivity.

Electrical resistivity, as with gravity, magnetic and electromagnetic methods, are potential fields methods. This means that what we measure at the surface is the integral or net effect of all of the sources or physical properties within a volume beneath the survey. There are naturally trade-offs between the position, depth and extent of the source which generates a measured anomaly. Data processing and forward modeling can help in interpretation, but there will always be some ambiguity in the results. On the other hand, the physical properties of the material which affect electrical resistivity, gravity and magnetic measurements cannot be determined by any other remote means, and are often the most direct indication of contaminants or properties of environmental concern.

4) <u>Gravity</u>. Finally, we will make a few measurements of gravity to illustrate how a gravity survey of the site is done. Gravity data must be "reduced" to remove as many known effects as possible so that we see the effects of density "anomalies" at depth. These include:

a) *Drift and tides*: The Earth's gravity oscillates on a 12-hour period due to tidal effects, and the gravimeter slowly drifts due to thermal and mechanical effects internal to the gravimeter. To account for both of these, we re-occupy and re-measure gravity at a base station every 30-40 minutes. To make the correction, note the time of each measurement, and the change in gravity between successive base-station measurements, then linearly interpolate the drift correction to be removed from the other measurements. Graphically, this may be done as below, but you can also do this using a spreadsheet or calculator:
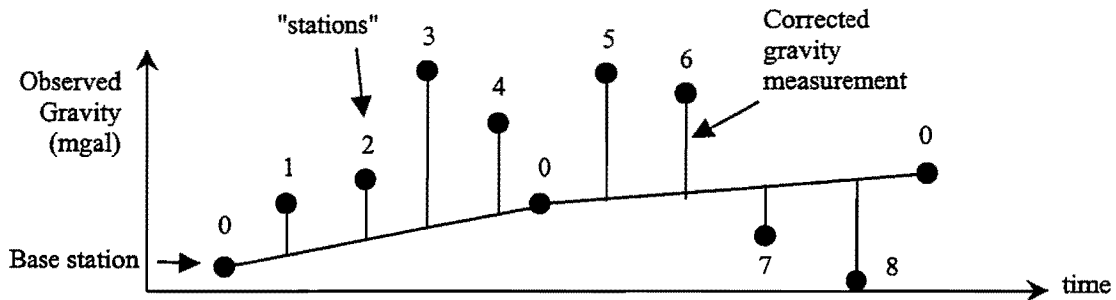
b) *Latitude correction*. Earth's gravity is least at the equator and greatest at the poles due to rotation (that's why there is an equatorial bulge). Any survey covering a significant N-S distance must account for this. The degree of variation depends on the latitude, but at our latitude (approx. 42^0N), this is 0.809 mgal/km. We will be interested in gravity anomalies of about 0.1-1.0 mgal across our site. However, the dump covers a N-S distance of about 500 m, so the latitude effect will be about 0.4 mgal, about the size of the effects we are looking for. Note that on E-W survey lines, no latitude correction is

102

necessary unless you want to combine these data with other lines at different N-S positions (for contouring of the gravity anomalies). The latitude correction is subtracted from observed (drift-corrected) data (assuming distance N is considered positive).

c) *Free-air correction*. Earth's gravity decreases with distance away from the Earth's center (with elevation). To account for this, we add a correction of 0.309 mgal/m. Thus, since we are interested in anomalies at the 0.1-0.2 mgal level, it is necessary to measure elevation to an accuracy of about 1/3-2/3 m. If we intend to combine our survey results with others for a regional gravity map, we would need to choose a common datum for each of these surveys (e.g. sea level). For a local survey, however, we can simply choose a convenient datum, such as the lowest elevation in the survey area. Ordinarily, it is necessary to accurately survey for elevation, however due to the engineering of the dump cap, this information is already available.

d) *Bouguer correction*. The Free-air correction ignores the mass of the material between the measurement and the datum. In order to account for this, we estimate the average density of the material between the surface and the datum and correct for the gravity due to an infinite slab with this density. If your datum is sea level, you would want to choose an average density for continental crust (e.g. 2.65 g/cm^3). If your datum is the lowest point in your survey, you will want to choose a density appropriate for the surficial materials (e.g. 2.0 g/cm^3 for wet gravels or 1.5 g/cm^3 for dry alluvium). Whatever you choose, the gravity anomalies you determine will be due to density variations with respect to that assumed density. The Bouguer correction is subtracted from your measured (and corrected so far) gravity according to 0.042 ρ h mgal/m (where

ρ is density in g/cm^3). For $\rho = 2.0 g / cm^3$, this is 0.084 h mgal/m (a relatively small effect).

e) The Bouguer gravity anomaly is the result of applying all these corrections. After correcting for drift and tides to get "observed gravity", the Bouguer gravity is $g_b = g_{obs} - dg_{lat} + dg_{FA} - dg_B$. This is what you usually see in maps of "gravity" or "gravity anomalies", and represents the effects of density variations within the survey area. The dump is likely to be characterized as a shallow zone of low relatively density. We can use this to map the subsurface distribution of waste, and perhaps to estimate its total mass.

f) A remaining correction is the *Terrain correction*. This is important in the vicinity of mountains or valleys, but it is difficult to do. The "standard procedure" involves overlaying a template on a topographic map and estimating average elevations within various distance and azimuth bins. In our study area, rather than doing this, you should simply be aware that gravity measurements close to the hills will contain an effect of those hills. The effect (of either hills or valleys) is to subtract from actual gravity (hills pull up, valleys don't pull down as much), so the terrain correction is an addition to observed gravity. There is little topographic relief in the immediate vicinity of the dump, so we can neglect this correction.

Directions to the Village of Endicott dump. From campus, follow Rt. 434 west to "4 corners" in Vestal (the third light beyond the Rt. 26 underpass). Turn right, cross the bridge into Endicott, turn left at Main Street (Rt. 17C and 26). From outside of the area, follow Rt. 17, exit on Rt. 26 north to Endicott. Take the cloverleaf exit to Rt. 17C west

(Main Street). Continue west on Rt. 17C past several lights until you see the En-Joie Golf Course on your left (site of the recent BC Open). There may be road construction on this portion of Rt. 17C. Turn left beyond the golf course (before crossing a railroad bridge), and follow the road toward the Triple Cities Airport. Turn left at the first (and only) street immediately after crossing a creek. Park on the road shoulder or in the large, paved area of the highway department facility. The workshop will be just beyond the paved area.

Cornwall-Type Iron Ores of Pennsylvania
Trip B3 - New York State Geological Association Annual Meeting
1998

H. R. Naslund
Department of Geological Sciences
SUNY-Binghamton
Binghamton, NY 13902-6000
(Naslund@Binghamton.EDU)

Introduction: Magnetite-apatite ore deposits are important ores of iron in many parts of the world. They can be classified into two major groups: a) high-Ti, high -P magnetite-apatite-ilmenite deposits (Nelsonites) associated with anorthosites; and b) low-Ti, variable-P magnetite +/- apatite deposits (Kiruna type ores) principally associated with volcanic rocks. The origin of the first type is generally accepted to be magmatic, with liquid immiscibility between silicate magma and iron-titanium-phosphorous-oxide magma the most commonly cited process (Philpotts, 1967; Kolker, 1982; Barton & Johnson, 1996). The origin of the Kiruna-type, however, has been a matter of controversy, with both magmatic and hydrothermal origins proposed. The Cornwall-type deposits of Pennsylvania, may be considered as an apatite-poor variety of these Kiruna-type deposits.

Many of these Kiruna-type deposits, contain originally-horizontal, laterally-extensive, stratified, iron oxide-rich units. These stratified iron oxide deposits do not appear to have formed by the same mechanism in all localities, indeed there may be a variety of mechanism that would lead to units with similar appearances. Such mechanisms might include: (1) magmatic ignimbrites, airfall ash, lavas, or sills; (2) sedimentary exhalative, lateritic, or detrital deposits, and (3) hydrothermal replacement, veins, or phreatic surface venting of hydrothermal systems. These various types of deposits should present different field relationships, textural characteristics, and trace element compositions, in accord with their mechanism of formation.

Stratified iron oxide ores have been described from El Laco, Chile

(Henríquez and Martin,1978, Nyström and Henríquez,1994); the Chilean Cretaceous Iron Belt (Travisany et al.,1995); Kiruna, Sweden (Nyström and Henríquez,1994); Cerro Mercado, Mexico (Swanson, et al., 1978; Lyons, 1988); Vergenoeg, South Africa (Crocker, 1985); and the Bafq Mining District, Iran (Förster and Jafarzadeh, 1994). In all of these localities the authors have interpreted them as pyroclastic iron ore. Similar stratiform deposits in the Missouri Iron District have been interpreted as replacement of volcanic tuff (Snyder, 1969; Ridge,1972; Panno and Hood, 1983), or as hematite tuff produced by the venting of a fumarolic system into a lake (Nold,1988; Hauck,1990). Stratified magnetite ores of the Cornwall-type are associated with a series of diabase sills in the Newark and Gettysburg Triassic rift basins. Cornwall-type deposits are characterized by laterally extensive, banded to massive magnetite ores with only traces of apatite, located adjacent to the upper contact of diabase sills. They are generally hosted in limestone or marble country rock, but locally they are hosted in the diabase sills or in clastic sediments or gneissic country rock. The Cornwall-type ores have been interpreted as hydrothermal replacement deposits (Smith, 1931; Tsusue, 1964; Lapham & Gray, 1973; Eugster & Chou, 1979).

The recent discoveries of the enormous Cu-Au-U-REE hematite breccias at Olympic Dam in Australia (Roberts & Hudson, 1983; Oreskes & Einaudi, 1990, 1992; Haynes, et al., 1995), and the giant REE iron oxide deposit at Bayan Obo, China (Argall, 1980; Wang, 1981; Wei & Shangguan, 1983; Bai & Yuan, 1983) have made iron oxide-apatite deposits of the Kiruna type of considerable economic interest for commodities other than iron. Indeed, many Kiruna type deposits are associated with near-by Cu, Au, U, or REE mineralizations (Crocker, 1985; Kisvarsanyi, 1990; Hauck, 1990; Einaudi & Oreskes, 1990; Marikos, et al., 1990; Vivallo, et al., 1993, 1994, 1995a, 1995b; Espinoza, et al., 1994; Förster and Jafarzadeh, 1994; Rojas & Henríquez, 1994; Foose & McLelland, 1995). The Cornwall type deposits are associated with minor, but recoverable amounts of Cu, Au, Ag, and Co, but no significant REE concentrations have been reported in the district.

Triassic diabase sills: At least four large diabase sills or sheets are present in the Gettysburg and Newark Basins of Pennsylvania (Figure 1).
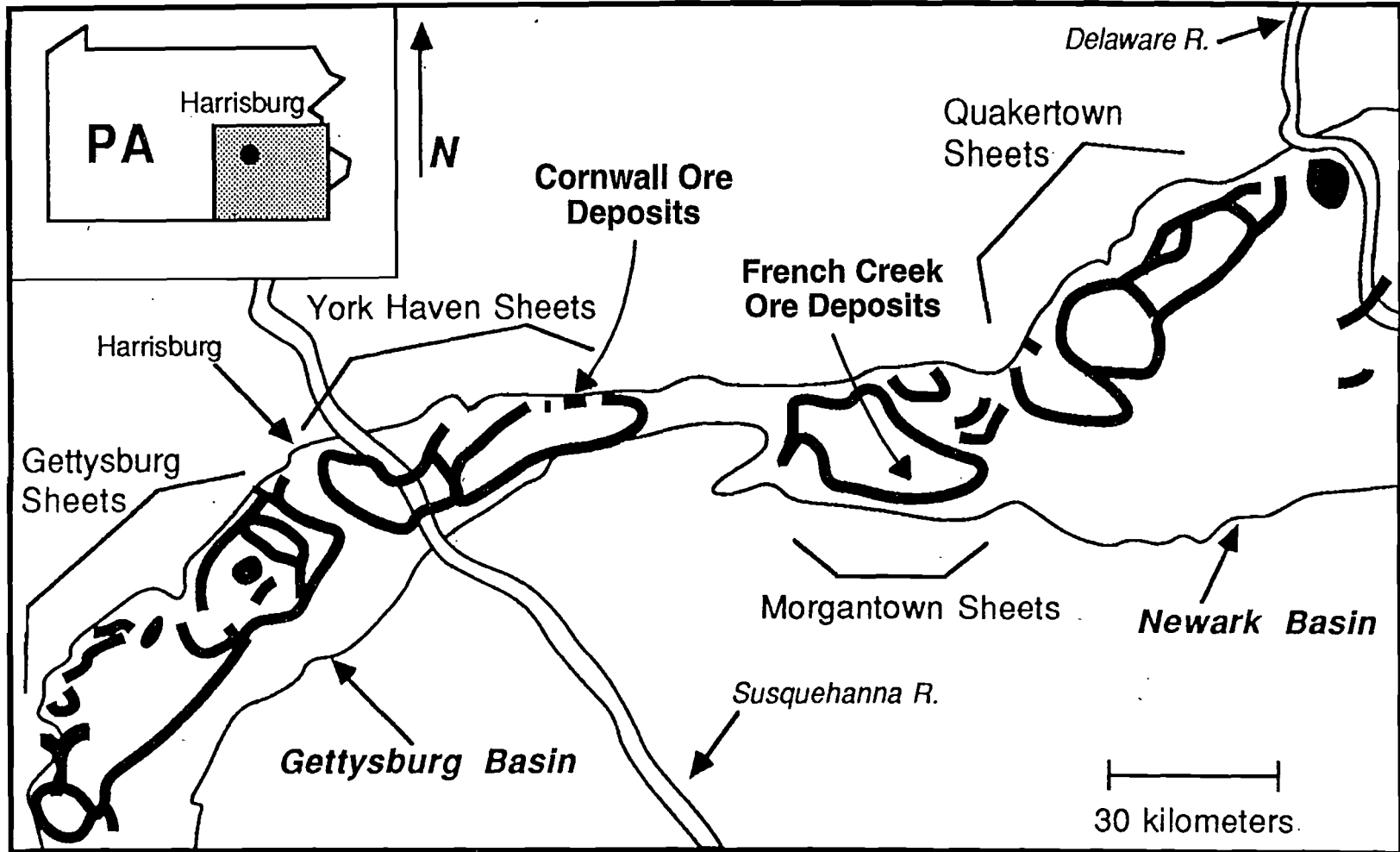
Figure 1 - Diabase sheets in the Gettysburg and Newark Basins in Pennsylvania. The locations
of the Cornwall Ore Deposits and the French Creek Ore Deposits is shown. Modified
from Mangan et al., 1993.

These are similar in age, bulk composition, and mode of emplacement to the more famous Palisades Sill of New York and New Jersey. The sheets outcrop as a series of rings or saucers in which the center of the sheets are covered and the inwardly dipping edges of the sheets are exposed at the surface. Iron ores of the Cornwall type are associated with all four of these major sheets in Pennsylvania. These Cornwall-type deposits were a major source of iron ore from the 1700's to the early 1900's, and played a prominent role in the Revolutionary War, the Civil War, and World Wars One and Two.

These diabase sheets range from less than 100 to over 600 meters in thickness, and are laterally extensive for 30 to 60 kms along strike. Each sheet represents the intrusion of a huge volume of tholeiitic magma in excess of 1000 km^3. They are believed to represent magma generated and intruded during the initial rifting and opening of the north Atlantic in the Mesozoic. The diabase was intruded at shallow levels (<1 km) largely within a series of rift basins filled with continental shales and sandstones. In a few cases the margins of the sills cut the bounding rift basin faults and extend into the pre-Mesozoic country rocks. Although a few of the sills, like the Palisades sill, are differentiated from a magnesium-rich diabase at their base to a more iron-rich, silica-rich granophyre in their centers, most of the sills have little compositional variation from top to bottom. The diabase is characterized by an interlocking mosaic of plagioclase, augite, and low-Ca pyroxene crystals with minor amounts of interstitial olivine, ilmenite, and/or magnetite.

Cornwall District, Pennsylvania: The Triassic magnetite deposits of Cornwall Pennsylvania produced over 140 million tons of iron ore during 230 years (1742-1972) of continuous mining (Lapham & Gray, 1973). The two main ore bodies occur as lenses or pods 30-50 m thick with over 1000 m of strike length, overlying the York Haven Triassic diabase sill. The ore occurs primarily as a replacement of limestone, and commonly interfingers with unaltered limestone along the margins of the deposit (Lapham & Gray, 1973) (Figure 2). The ore is typically finely banded or layered with alternating magnetite-rich and magnetite-poor laminae. The dominant minerals are magnetite, actinolite, chlorite, and sulfides, with only minor amounts of apatite. In places the ore replaces diabase and hornfels country rock, and in one location fills a fault

cutting the diabase. Field relations at both the Cornwall mine and the Carper mine to the west, indicate that faulting occurred after diabase solidification and before ore deposition, suggesting a time lag between the solidification of the sill and the formation of the ore bodies (Lapham & Gray, 1973). It is suggested, however, that there is an inverse correlation between the amount of granophyre in the sill and the amount of ore adjacent to (above) the sill . This would suggest that magmatic processes, perhaps degassing or late stage melt migration, are genetically related to the ore-forming process.

Contact metamorphism associated with the sill attained a maximum temperature of ~600 °C, while metasomatism occurred in the range of 500 to 700° C (Lapham & Gray, 1973). On the basis of experimental studies, it has been suggested (Chou & Eugster, 1977; Eugster & Chou, 1979) that the Cornwall deposit may have originated by the precipitation of Fe carried in Cl-rich hydrothermal fluids, with the cooling of the diabase sill serving as the heat source for fluid circulation. From all the available evidence, the Cornwall deposit appears to be an example of a stratified iron oxide ore formed by hydrothermal replacement. The source of the hydrothermal solution, and the source of the iron, however is not clear. The heat source for the circulation of the fluids is also not known. There is no "missing" iron in the sill, nor any rocks near the sill that appear to have lost iron. If the sill predates the ore, as some field relations suggest, than the source of heat necessary to deposit that much iron at temperatures near 500° C is not known. Even with fluids containing 30,000 ppm dissolved iron (maximum values reported in hydrothermal brines) it would require almost all of the available heat from the sill to form the amount of known iron ore.

French Creek District, Pennsylvania: A number of small magnetite deposits are associated with the Morgantown Triassic diabase sill south of Hopewell, Pennsylvania, and were the main source of ore for the Hopewell furnace active from 1771 to 1883. Deposits include: The Elizabeth and Susie mines in St. Peters Village, the Warwick mine, the Hopewell Mine, the Jones Good Luck Mine, and the Grace Mine. Ore was concentrated in pods or layers within Biotite gneiss over lying the Diabase sill (Figure 3). In places the ore
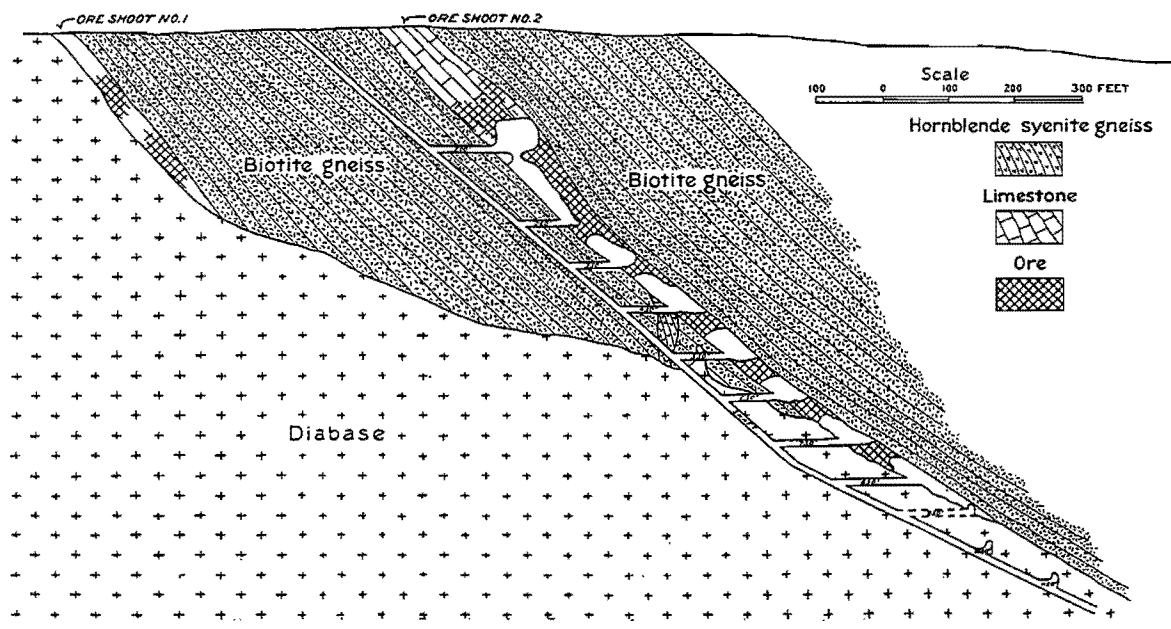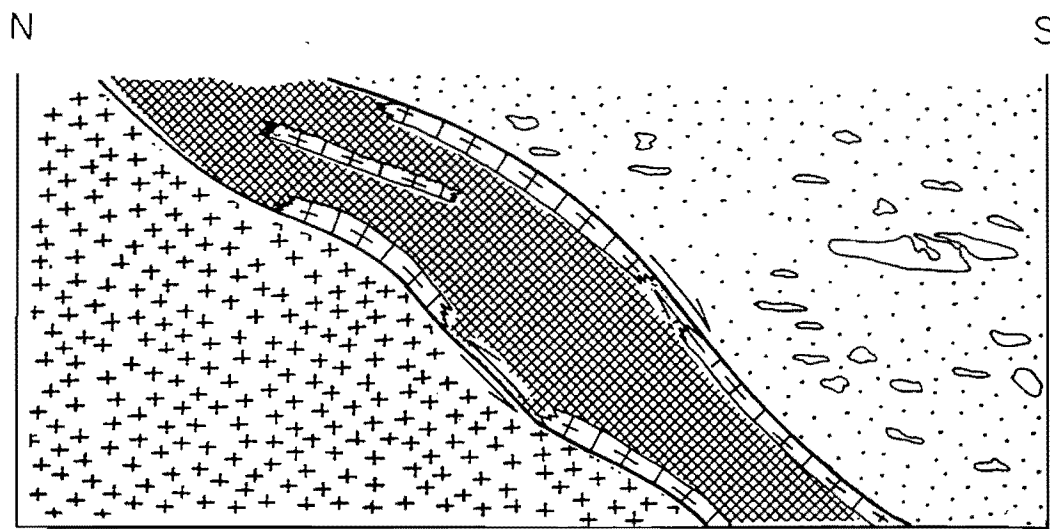
Figure 2 – Geologic cross section of the west end of the Elizabeth Mine,
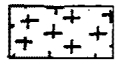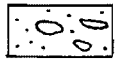St. Peters, PA, French Creek District.   From Smith (1931).

Figure 3 – Cross section through the east end of main pit, No. 3 Mine,
Cornwall District, Cornwall, PA.   From Lapham & Gray (1973).

occurs as a replacement of marble lenses within the Biotite gneiss. The last of the iron mines in St Peters village closed in 1928, although a diabase quarry has remained intermittently active until the present day. The Grace mine near Morgantown remained active until the 1970's.

Calcite-dolomite geothermometry from the Grace mine suggest a temperature of about 650° C for the formation of the veins adjacent to the deposit (Tsusue, 1964). Because the magnetite in the deposit is intergrown with serpentine, however, the magnetite was considered by Tsusue (1964) to have formed below 500° C which he considered to be the upper stability limit for serpentine. The magnetite in the ore at the Grace mine is associated with small amounts of chalcopyrite, marcasite, pyrite, pyrrotite, sphalerite, and galena, but the ore grades for commodities other than iron are not reported (Tsusue, 1964). The magnetite ores in the Elizabeth and Susie mines in St.Peters village are associated with ubiquitous pyrite and chalcopyrite, and although originally opened as a copper mine, very little Cu was produced except from a small near-surface supergene enrichment zone.

Formation of iron-rich melts and fluids: The origin of massive magnetite deposits and stratified iron-oxide ores is not well understood, and in fact, although they share a number of similarities, it is not likely that all of these deposits are produced by the same mechanism or mechanisms. Proposed origins include: (1) separation of an immiscible iron-rich melt from a silica-rich melt during cooling; (2) partial or complete melting of iron-rich crustal rocks; (3) contact metamorphism and/or replacement of wall rocks by iron-rich fluids; (4) hydrothermal vein or replacement deposits; and (5) sedimentary exhalative deposits. These mechanisms can be group into two major categories, magmatic and hydrothermal. Magmatic processes 1 and 2 above both involve the transport of iron as an extremely iron-rich magma; they differ primarily in how that magma was formed. Hydrothermal processes 3, 4, and 5 all involve the transport of iron as a dissolved component in a fluid, and differ mainly in how and where that fluid interacts with the surrounding rocks to release the dissolved iron. It is not necessary that the hydrothermal and magmatic processes are mutually exclusive. A magmatic iron ore at depth may produce a hydrothermal deposit near the surface as a result of degassing. Indeed, many

large "hydrothermal hematite deposits" are associated with large gravity and magnetic anomalies at depth that may represent magmatic magnetite (for example, Pilot Knob in Missouri and Olympic Dam in Australia).

Geochemical "signatures" of hydrothermal iron-oxide deposits: The formation of iron-apatite ores by hydrothermal fluids requires a system that can efficiently transport iron while limiting most other cations to low abundances. Experimental studies suggest that Fe can be transported in Cl-rich or Cl-poor hydrothermal solutions as Fe, Fe-Cl, or Fe-OH complexes (Chou & Eugster, 1977; Eugster & Chou, 1979; Whitney, et al., 1985; and Crerar, et al., 1985). Deposits formed by hydrothermal replacement should have trace element compositions that reflect the ease with which components are transported in hydrothermal solution, and the processes that result in their deposition in a specific environment. Such trace element signatures might include: low contents of immobile high-field strength cations (Zr, Nb, Ta, Th), high alkali contents (Na, K, Rb, Cs), and high contents of easily transported included elements (Ca, Mg, Mn, Cu, Zn, Pb). This will be in marked contrast to magmatic ores originating from differentiation and immiscibility which will have high P, Zr, Nb, Ta, Th, U, and REEs and low Na, K, Rb, Cs, Ca, and Mg. Experimental studies suggest that hydrothermal fluids fractionate geochemically similar elements differently than do magmatic processes, and as a result, hydrothermal fluid transport might produce unusual ratios for Cs/Rb, Pb/Ce, La/Ba, and LREEs/HREEs (You, et al., 1996) or Hf/Zr, and Y/Ho (Bau, 1996). Hydrothermal replacement deposits will also be likely to have specific elemental distribution patterns reflecting changing fluid compositions and temperatures, zoned from the center of a deposit towards the margins (Hemley, et al., 1992; Hemley & Hunt, 1992). Apatite in such deposits may be richer in Cl and OH, in contrast to the apatite in igneous systems which is generally F-rich.

Associated Mineral Deposits: Recently, a new ore mineralization type has been defined, and named after the type locality at the Olympic Dam deposit in Southern Australia (Roberts & Hudson, 1983; Oreskes & Einaudi, 1990, 1992; Haynes, et al., 1995). Olympic Dam type deposits are characterized by Cu, U, Au, Ag, and/or REE mineralization associated with iron oxide-apatite

deposits. This mineralization type is accompanied by magnetic and gravity anomalies that in many of the cases are caused by magnetite–apatite deposits at depth. These deposits range from small mineralized zones to "giant" ore bodies. The type locality at Olympic Dam contains 2,000 million metric tons with an average grade of 1.6% Cu, 3.5 g/ton Au, 0.06% U_3O_8 and 0.5% REE (Oreskes & Einaudi, 1990). At Olympic Dam the Cu–U–Au–Ag mineralization is hosted principally in hematite breccias that have been interpreted as a very unusual type of sediment–hosted mineralization (Robert & Hudson, 1983), or as a hydrothermal breccia complex formed by hot saline fluids mixed with cooler meteoric waters (Oreskes & Einaudi, 1990, 1992; Hayes, et al., 1995). The Olympic Dam mineralization is characterized by iron sulfides with Cu, Co, and some Au, and Ag. The REEs and U are principally associated with apatite. Au and Ag are also present in zones of siliceous hydrothermal alteration. In the Cornwall deposit average ore grades run approximately 39.4 % Fe, 1.29% S, and 0.29% Cu. Co can be recovered from the pyrite concentrate and Cu can be recovered from the Chalcopyrite concentrate. In 1953 1700 oz of Au was recovered from approximately 1.4 million tons of ore (Lapham & Gray, 1973).

References

Argall, G.O., Jr., 1980. Three iron ore bodies of Bayan Obo, World Mining, 33, 38-41.

Bai, G., & Yuan, Z.X., 1983. On the genesis of the Bai Yun Obo ore deposit, Chinese Acad. Geol. Sci. , Inst. Mineral. Deposits. Bull. 4, 1-17.

Barton, M.D. & Johnson, D.A., 1996. Evaporitic-source model for igneous-related Fe oxide-(REE-Cu-Au-U) mineralization, Geology 24, 259-262.

Bau, M., 1996. Controls on the fractionation of isovalent trace elements in magmatic and aqueous systems: evidence from Y/Ho, Zr/Hf, and lanthanide tetrad effect. Contr. Mineral. Petrol. 123, 323-333.

Chou, I.M., & Eugster, H.P., 1977. Solubility of magnetite in supercritical chloride solutions, Am. J. Sci. 277, 1296-1314.

Crerar, D., Scott, W., & Brantley, S., 1985. Chemical controls on solubility of ore-forming minerals in hydrothermal solutions, Can. Mineral. 23, 333-352.

Crocker, I.T., 1985. Volcanogenic fluorite-hematite deposits and associated pyroclastic rock suite at Vergenoeg, Bushveld complex, Econ. Geol. 80, 1181-1200.

Einaudi, M.T., & Oreskes, N., 1990. Progress towards an occurrence model for Proterozoic iron oxide deposits - a comparison between the ore provinces of south Australia and southeast Missouri, In Pratt, W.P. & Sims, P.K., (eds.) The midcontinent of the United States - permissive terrane for an Olympic Dam-type deposit?, U.S. Geol. Sur. Bull. 1932, 58-69.

Espinoza, S., Vivallo, W., & Henríquez, F., 1994. Geología y genésis de mineralización metálica en el distrito ferrífero de Cerro Imán, Copiapó, Chile. VII Congreso Geológico Chileno Vol. II, 799-802.

Eugster, H.P., & Chou, I.M., 1979. A model for the deposition of Cornwall type magnetite deposits, Econ. Geol. 74, 763-774.

Foose, M.P., & McLelland, J.M., 1995. Proterozoic low-Ti iron-oxide deposits in New York and New Jersey: Relation to Fe-oxide (Cu-U-Au-rare earth element) deposits and tectonic implications, Geology 23, 665-668.

Förster, H., & Jafarzadeh, A., 1994. The Bafq mining district in central Iran - a highly mineralized infracambrian volcanic field, Econ. Geol. 89, 1697-1721.

Hauck, S.A., 1990, Petrogenesis and tectonic setting of middle Proterozoic iron oxide-rich ore deposits - an ore deposit model for Olympic Dam-type mineralization, In Pratt, W.P. & Sims, P.K., (eds.) The midcontinent of the United States - permissive terrane for an Olympic Dam-type deposit?, U.S. Geol. Sur. Bull. 1932, 4-39.

Haynes, D.W., Cross, K.C., Bills, R.T., and Reed, M.H., 1995. Olympic dam ore genesis: a fluid-mixing model, Econ. Geol. 90, 281-307.

Hemley, J.J., Cygan, G.L.,Fein, J.B., Robinson, G.R., & D'Angelo, W.M., 1992. Hydrothermal ore-forming processes in the light of studies in rock buffered systems I: Iron-copper-zinc-lead-sulfide solubility relations, Econ. Geol. 87,1-22.

Hemley, J.J., & Hunt, J.P., 1992. Hydrothermal ore-forming processes in the light of studies in rock buffered systems II: Some general geologic applications, Econ. Geol. 87, 23-43.

Henríquez, F., & Martin, R.F., 1978. Crystal growth textures in magnetite flows and feeder dykes, El Laco, Chile, Can. Mineral. 16, 581-589.

Kisvarsanyi, E.B., 1990, General features of the St. Francis and Spavinaw granite-rhyolite terranes and the Precambrian metallogenic region of Southeast Missouri, In Pratt, W.P. & Sims, P.K., (eds.) The midcontinent of the United States - permissive terrane for an Olympic Dam-type deposit?, U.S. Geol. Sur. Bull. 1932, 48-57.

Kolker, A., 1982. Mineralogy and geochemistry of Fe-Ti oxide and apatite (Nelsonite) deposits and evaluation of the liquid immiscibility hypothesis, Econ. Geol. 77, 1146-1158.

Lapham, D. M., & Gray, C., 1973, Geology and origin of the Triassic magnetite deposit and diabase at Cornwall, Pennsylvania, Mineral Resources Report M56, Pennsylvania Geological Survey, 343p.

Lyons, J.I., 1988. Volcanogenic iron oxide deposits, Cerro de Mercado and vicinity, Durango, Mexico, Econ. Geol. 83, 1886-1906.

Mangan, M.T., Marsh, B.D., Froelich, A.J., & Gottfried, D., 1993, Emplacement and Differentiation of the York Haven Diabase Sheet, Pennsylvania, J. of Petrol. 34, 1271-1302.

Marikos, M.A., Nuelle, L.M., & Seeger, C.M., 1990. Geologic mapping and evaluation of the Pea Ridge iron ore mine (Washington County, Missouri) for rare-earth element and precious metal potential - a progress report, In Pratt, W.P. & Sims, P.K., (eds.) The midcontinent of the United States - permissive

terrane for an Olympic Dam-type deposit?, U.S. Geol. Sur. Bull. 1932, 4-39.

Nold, J.L., 1988. The Pilot Knob hematite deposit, Iron County, Missouri - a Proterozoic volcano-sedimentary iron deposit, Geol. Soc. Am. Abstr. Progr. 20, no. 7, A141.

Nyström, J.O., & Henríquez, F.,1994. Magmatic features of iron ores of the Kiruna type in Chile and Sweden: Ore textures and magnetite geochemistry, Econ. Geol. 89, 820-839.

Oreskes, N., & Einaudi, M.T, 1990, Origin of rare earth element enriched hematite breccias at the Olympic Dam Cu-U-Au-Ag deposit, Roxby Downs, South Australia, Econ. Geol. 85, 1-28.

Oreskes, N., & Einaudi, M.T, 1992, Origin of hydrothermal fluids at Olympic Dam: preliminary result from fluid inclusions and stable isotopes, Econ. Geol. 87, 64-90.

Panno, S.V. & Hood, W.C.,1983. Volcanic stratigraphy of the Pilot Knob iron deposits, Iron County, Missouri, Econ. Geol. 78, 972-982.

Parák, t., 1975. Kiruna iron ores are not "intrusive magmatic ores of the Kiruna type", Econ. Geol. 70, 1242-1258.

Philpotts, A.R., 1967. Origin of certain iron-titanium oxide and apatite rocks, Econ. Geol. 62, 303-315.

Ridge, J.D., 1972. Annotated bibliographies of mineral deposits in the Western Hemisphere, Geol. Soc. Am. Memoir 131, 1-681.

Roberts, D.E., & Hudson, G.R.T., 1983. The Olympic Dam copper-uranium-gold deposit, Roxby Downs, South Australia, Econ. Geol. 78, 799-822.

Rojas, M.G., & Henríquez, F., 1994. Contento y distribución de terras raras en apatitas del yacimiento de hierro El Algorrobo, III region, VII Congreso Geológico Chileno Vol. II, 1177-1178.

Smith, L.L., 1931, Magnetite deposits of French Creek, Pennsylvania, Bulletin M14, Fourth Series, Pennsylvania Geological Survey, 52p.

Snyder, F.G., 1969. Precambrian iron deposits in Missouri, In Wilson, H>D>B>, (ed.), Magmatic ore deposits - a symposium, Econ. Geol. Monograph 4, 231-238.

Swanson, E.R., Keizer, R.P., Lyons, J.I., & Clabaugh, S.E., 1978. Tertiary volcanism and caldera development near Durango City, Sierra Madre Occidental, Mexico, Geol. Soc. Am. Bull 89, 1000-1012.

Travisany, V., Henríquez, F., & Nyström, 1995. Magnetite lava flows in the Pleito-melon district of the Chilean iron belt, Econ. Geol. 90, 438-444.

Tsusue, A., 1964, Mineral aspects of the Grace Mine magnetite deposit, Mineral Resources Report M49, Pennsylvania Geological Survey, 10p.

Vivallo, W., Henríquez, F., & Espinoza, S., 1993. Hydrothermal alteration and related mineralization at El Laco mining district, northern Chile. Low temperature Metamorphism, processes, Products and Economic Significance, Symposium IGCP Proyect 294, 142-146.

Vivallo, W., Espinoza, S., & Henríquez, F., 1994. Significado de la distribución del oro en menas y rocas de caja en los depósitos de hierro de los distritos Cerro Negro Norte y Cerro Imán, Chile. VII Congreso Geológico Chileno Vol. II, 926-930.

Vivallo, W., Espinoza, S., & Henríquez, F., 1995a. Metasomatismo y alteración hidrotermal en el Distrito Ferrífero Cerro Negro Norte, Copiapó, Chile. Revista Geológica de Chile 22, Nº 1, 75-88.

Vivallo, W., Espinoza, S., & Henríquez, F., 1995b. Los depósitos de hierro del tipo magnetita-apatita: geoquímica de las rocas volcánicas asociadas y potencialidad de la mena de hierro como fuente de mineralización de oro. Revista geológica de Chile 22, Nº 2, 159-175.

Wang, K.Y., 1981. Distribution characteristics of the rare earth elements in Bayanobo iron deposit, Scientia Geologica Sinica 4, 360-367.

Wei, J.Y., & Shangguan, Z.G., 1983. Oxygen isotope composition of magnetite and hematite in Baiyun Ebo iron deposit, Inner Mongolia, Scientia Geologica Sinica 3, 218-224.

Whitney, J.A., Hemley, J.J., & Simon, F.O., 1985. The concentration of iron in chloride solutions equilibrated with synthetic granite compositions: the sulfur-free system, Econ. Geol. 80, 444-460.

You, C.F., Castillo, P.R., Gieskes, J.M., Chan, L.H., & Spivack, A.J., 1996. Trace element behavior in hydrothermal experiments: Implications for fluid processes at shallow depths in subduction zones, Earth. Planet. Sci. Lett. 140, 41-52.

B3 - Roadlog

Mileage is broken up into three parts: (1) Binghamton to the Village of St. Peters, Pennsylvania; (2) St. Peters to Cornwall, Pennsylvania; and (3) Cornwall, Pennsylvania to Binghamton, New York.

Binghamton, New York to St. Peters, Pennsylvania:

0.0   Leave from the Parking lot at Binghamton University, turn right and proceed out the main campus entrance.

0.4   Turn Right on Vestal Parkway, Rt. 434

3.4   Follow the road as it turns left over the Susquehanna River and get into the right lane.

3.6   Turn right onto Rt. 363 following signs for Interstate 81.

5.3   Turn right onto Interstate 81 south. Watch the merge lane onto 81 South, traffic enters from the left.

17.9   Pennsylvania State Line

37.9   Pennsylvanian aged Cross bedded Sandstone on left.

40.3   Pennsylvanian aged Red Beds on Right.

58.7   Clark's Summit, Pennsylvania. Turn right onto Pennsylvania Turnpike (Interstate 476).

118.8 Lehigh Tunnel. Note the Valley and Ridge topography.

133.1 Take exit 33 to Routes 78, 22, and 309. Follow signs to 22 east and take the first exit onto 309 south.

136.5 Turn right South on Route 222.

140.7 Turn left, South on Route 100.

146.8 Junction with Route 29 south, continue on Route 100.

160.8 Triassic Red Beds on left.

165.2 Triassic Red Beds on Right.

172.1 Turn right on Route 23 west.

175.6 Turn right on St Peters road.

176.1 Turn right into parking lot across from St. Peters Inn.

St Peters, Pennsylvania to Cornwall, Pennsylvania:

Mileage for part 2 begins in the Parking lot across from St. Peters Inn on St. Peters Road in the Village of St Peters, Pennsylvania.

0.0 **Stop 1** - Pennsylvania Granite Corporation Quarry. Diabase is exposed in the parking lot and along the road to the south. The main point of this stop is to see the diabase that is associated with the ore deposits. Two of the largest ore bodies in this district are located 1 mile to the north of this spot. Note how unaltered and unfractured the diabase is at this location. In fact, its fresh, unfractured character is the reason there is a building stone quarry here. If the iron ores were formed from a hydrothermal system associated with the cooling of the sill, it does not appear to have affected the underlying diabase.

0.5 Turn right onto Route 23 west.

2.7 This stretch of 23 west travels on top of the diabase sill. Note the diabase stone fence on right.

3.1 Turn right on Warwick road.

3.7 Turn right on 345 north.

3.8 Turn left onto Laurel road.

4.6 Continue on gravel road.

4.8 **Stop 2** - Turn right and park cars. This is state game land open to hunters. Not a good spot to visit during deer hunting season. Proceed on foot through gate on "emergency road". Turn left at every road junction. Note the "blue conglomerate" in the float along the road. This Ordovician sediment forms the cap rock above the Cornwall deposit. Its relationship to the ore body here is not known. After about 10 minutes you will come to an open field. Follow the road to the left under the power lines. At the far edge of the trees follow the road to the left back into the woods. This is the Hopewell iron mine. Dumps are on the right, the open pit is on the left. Exposed in the walls of the pit is a quartz-feldspar pegmatite that predates the ore body, but cross cuts the host gneiss. A similar pegmatite is present in the Ore body in St. Peters village to the east. The relationship of these pegmatites to the diabase sill is not clear. In the dumps you should be able to find all the ore

118

textures present in the deposit.

4.8   Return to cars and retrace route out Laurel Road.

5.8   Turn right onto 345 south.
[3.3 miles north of this point is the Hopewell Furnace National Historic Site. Open daily 9 to 5, except national holidays. If you are with a student group and call in advance you can take a self guided tour of the old furnace for free. Otherwise it is $4. Hopewell Furnace National Historic Site, 2 Mark Bird Lane, Elverson, PA 19520. ph. 610-582-8773. If you want to show students about iron making in the 19th century, this is a better site than the Cornwall Furnace Historic Site]

5.9   Turn right at the intersection with Warwick road and continue on 345 south.

6.0   Continue to the left around the curve on 345 south. The house on right is constructed of locally quarried diabase "Pennsylvania Black granite".

6.3   Turn right onto Route 23 west.

8.6   Continue straight on Route 23 west.
[Chestnut Street (Route 82 north) in Elverson. Several of the older homes in Elverson are constructed out of "Pennsylvania Black Granite". The Jones Luck Iron Mine is located approximately 2 miles north of this point at the intersection of Route 82 and Red Hill Road. The mine is a good example of reclamation. The open pit is now a swimming lake north and east of the intersection. The only sign of the mine are some tailings piles on the north side of Red Hill Road (south side of the lake) just past the intersection.]

11.7   Turn right on Cherry Lane (Route 10) in Morgantown.

12.6   Turn right onto Route 76 west.
[About 0.5 miles north of here is the now inactive Grace Iron Mine where calcite-dolomite geothermometry in veins adjacent to the ore body suggests temperatures in excess of 650 degree C. The ore body is located at the upper contact of a diabase sheet, and is composed of magnetite and serpentine.]

17.6   Good diabase outcrops on the right.

35.0   Exit 20 to Lebanon.

35.4   Turn left on Route 72 north.

38.6   Turn right on Route 419 north.

39.5   Turn right onto Alden street, (Route 419 turns to the left) big church on your left after you turn.

39.8   Go under viaduct on Burd Coleman Road.

40.0   **Stop 3.** - Mine dump on the left. This is from the main pit of the No. 3 mine.

40.1   Turn around and continue back on Burd Coleman Road. Turn right just before the underpass on Rexmont Road.

40.6   Cornwall Iron Furnace Historic Site on the right.

40.7   Go through intersection and veer to the right on Rexmont road.

41.4   **Stop 4** - After crossing a small bridge park on the right. Return to bridge on foot and climb down into railroad cut at the south east side of the bridge (the corner closest to where you parked). Rail road cut through the diabase sill below the ore body. Outcrops of the diabase are just north of the bridge (to your right as you climb down). Outcrops of altered sediments below the diabase sill can be reached by walking south along the railroad right of way for about 200 meters.

41.7   **Stop 5** - Driveway on right. "No dumping of Refuse Allowed" Park and walk back along old railroad right of way. Slag from the iron furnace has been dumped along either side of the road. Near where you park, most of it is covered by later piles of concrete and asphalt. About 30 meters back on the right are some good chunks of furnace slag.

42.1   Turn left at intersection.

42.4   **Stop 6** - Turn into driveway on left watching for traffic. If you are in a big van it is best to back in so you will be able to see when pulling out. This is the upper part of the No. 3 mine. The contact between the ore body and the diabase is preserved on the slope to the left of the talus pile. Be careful of the talus pile, it is unstable so it is best not to climb on it. Most of this talus is probably from the underground Elizabeth mine at the to of the hill. Walk south along the road to diabase out crops across from the Historic Marker. Note how fresh it is for a rock associated with a major hydrothermal system. Walk across the street to the overlook beside the historic marker for a good view of the pit.

42.9   Turn around at the baseball diamond and head back the way you came. The main point of this detour was to drive through the old Cornwall

mining village. There are old tailings piles from the No. 4 mine behind first base if you haven't had enough of mine tailings by this point, or if you have been scared off by no trespassing signs at earlier stops.

43.7   Turn left at intersection onto Rexmont Road.

43.8   **Stop 7** - Turn left into Cornwall Iron Furnace Historic Site. Tuesday-Saturday 10-4; Sunday 12 -4; closed Monday.

Cornwall, Pennsylvania to Binghamton, New York:

Mileage for part 3 begins in the Parking lot of the Cornwall Iron Furnace Historic site in Cornwall, Pennsylvania.

0.0   Turn left on Rexmont Road at the entrance to the Cornwall Iron Furnace Historic Site.

0.5   Turn right on Burd Coleman Road and go under the Railroad Viaduct.

0.9   Turn left on Route 419.

1.8   Turn right on Route 72 north.

5.9   Limestone exposed along sidewalk in Lebanon. A similar limestone was the host rock for the Cornwall deposit.

16.9   Turn onto Interstate 81 north.

172.9 Stay in left lane on Route 17 west.

176.9 Turn right onto 201 south.

177.9 Take first right at circle and cross the Susquehanna River. Follow signs to route 434 east and SUNY.

178.9 Turn right into SUNY campus.

FIELD ILLUSTRATIONS OF GEOLOGIC FEATURES IN THE UPPER SUSQUEHANNA VALLEY AND ADJACENT MOHAWK REGION

by
DAVID M. HUTCHISON
Department of Geological and Environmental Sciences
Hartwick College
Oneonta, NY 13820

Introduction

The outcrops and surficial features observed on this trip have been selected (1) to show students the change in lower Paleozoic stratigraphy through time (2) to illustrate several sedimentary and topographic features (3) to help students gain a better understanding of the geologic framework of this area.

The trip starts at the large Upper Devonian flood plain channel behind the F.W. Miller Science Building on the Hartwick College campus in Oneonta and ends in Precambrian garnet gneiss six miles east of Canajoharie. Progressively older beds are exposed to the north because of three factors: the gentle southerly dip of the beds, the erosion by the Mohawk river and the uplift, tilting and erosion of large fault blocks associated with normal faults in the Adirondack Mountains which extend into the Mohawk Valley.

The clastic sediments are the result of the Middle Ordovician Taconian Orogeny (470-435 m.y. ago) and the Middle and Late Devonian Acadian Orogeny (385-355 m.y.ago). Both of these times of crustal unrest and uplift east of the Hudson River and in New England provided an influx of clays, silts and sands into the Ordovician and Devonian seas which occupied the area of this field trip. The carbonate rocks were deposited by these seas during periods of quiescence between orogenies.

Geologic History of the Area

(Modified from Fisher, 1965)

During Precambrian time a thick sequence of geosynclinal sediments was deposited. The geosyncline was folded and regionally metamorphosed into a mountain range during the Grenville Orogeny (1,100 m.y. ago). For the next 500 million years the area was eroded and the mountains were beveled down exposing the metamorphic rocks in roots of the eroded mountains.

By Late Cambrian time these Precambrian metamorphic rocks were covered by transgressing shallow seas which deposited the Little Falls sandy dolostones and dolostones forming a nonconformity. The Precambrian gneiss and Late Cambrian dolostone are exposed in a railroad cut six miles east of Canajoharie along the Mohawk River.

Shallow seas continued to deposit dolomitic rocks into Early Ordovician time. The Chuctanunda Creek Dolostone exposed in the gorge of Canajoharie Creek represents deposition at this time. After deposition of this dolostone the seas withdrew.

In Middle Ordovician time shallow seas again covered the area and deposited the Kings Falls and Sugar River argillaceous limestones on top of the Lower Ordovician Chuctanunda Creek Dolostone forming a disconformity. The thin beds of black shale in the limestones reflect crustal unrest many miles to the east in the area of the present Taconic Mountains. This was the beginning pulse of the Taconic Orogeny. A thick black shale, the Canajoharie Shale, which overlies the limestones represents increased unrest during the Taconic Orogeny. These Early and Middle Ordovician sediments are well exposed in the gorge of Canajoharie Creek.

During Late Middle Ordovician time there was extensive erosion of the mountains. The detritus was deposited to the west as a thick sequence of shales and sandstones which are exposed in a few scattered outcrops between Sharon Springs and Canajoharie. The best exposure is just north of Sharon Springs.

Throughout most of Silurian time this area was emergent. If there are any Silurian rocks present, they are not exposed along the field trip route.

In Early Devonian time shallow seas encroached into the area and deposited a thick sequence of limestones (Helderberg Group) which are exposed north of Cherry Valley along Route 20 east to Sharon Springs.

Later in Early Devonian time there was uplift and erosion which resulted in the deposition of the Esopus Shale and Carlisle calcareous siltstone. This uplift was followed by another period of submergence when the Onondaga Limestone was deposited. These three formations are exposed on Route 166 north of Cherry Valley .25 mile south of Route 20.

During Middle and Late Devonian time the Acadian Orogeny was taking place in New England. This mountain building episode provided a vast supply of sediments which formed the thick sequence of sandstone, siltstone and shale which are exposed between Cherry Valley and Oneonta. These sediments were deposited as part of the extensive Catskill delta and flood plain deposits.

Since Late Devonian time the area has been subjected to erosion and the development of the Mohawk River, the Susquehanna River and their tributaries. In the Pleistocene, glaciers moved into the area. The ice enlarged the river valleys and deposited morainic material in the valleys. Some of this material was reworked by later advances of the ice to form drumlins or was redeposited by meltwater to form kame terraces along the valley walls. The area is currently being drained by the Mohawk River which joins the Hudson River north of Albany and the Susquehanna River and its tributaries which flows south through Pennsylvania and enters the Atlantic Ocean in Chesapeake Bay.

References Cited

Fairchild, H. L., 1925, The Susquehanna River in New York: New York Museum and Science Service Bull., 256, pp. 78-82.

Fisher, D. W., 1965, Mohawk Valley Strata and Structures: in Hewitt, P. C. and Hall, L. M., editors. Guidebook to Field Trips in the Schenectady area, New York State Geological Association 37th Annual Meeting (also published as Educational Leaflet No. 18 by State Museum and Science Service, Albany, New York).

Fleisher, J. P., (personal communication)

LaPorte, L. E., 1967, Carbonate deposition near mean sea-level and resultant Facies mosaic: Manlius Formation (Lower Devonian) of New York State: Am. Assoc. Petroleum Geologists Bull., v. 51, p. 73-101.

Park, R. A. and D. W. Fisher, 1969, Paleoecology and stratigraphy of Ordovician carbonates, Mohawk Valley, New York, in Bird, J. M. (Ed.) Guidebook for Field Trips in New York, Massachusetts, and Vermont: 1969 New England Intercoll. Geol. Conf., Albany, New York, p. 14-1 - 14-12.

Rickard, L. V. and D. H. Zenger, 1964, Stratigraphy and Paleontology of the Richfield Springs and Cooperstown Quadrangles, New York: New York Museum and Science Service Bull. 396, 101 p.

Additional Bibliography

Friedman, G. M. and K. G. Johnson, 1966: in Shirley, M. L. editor, Deltas in their Geological Framework, Houston Geol. Soc., p. 171-188.

Johnson, K. G., 1970: in Heaslip, W. G. editor, Guidebook to Field Trips of the New York State Geological Association 42nd Annual Meeting, C-1 - C-14.

STRATIGRAPHIC SECTION OF FORMATIONS ON TRIP

(adapted from Rickard and Zenger, 1964 and Fisher, 1965)

Upper Devonian (Senecan Series)   Thickness

Oneonta Formation	200'	Stop 1
Gilboa Formation	460'	Stop 2

Middle Devonian (Erian Series)

Cooperstown Shale	410'	Drove by (after stop 2)
Portland Point Limestone	5-6'	Not observed
Panther Mountain Formation	800'	Not observed
Solsville Sandstone	290'	Not observed
Otsego Shale	260'	Not observed
Chittenango Shale	150'	Stop 5
Cherry Valley Limestone	5'	Stop 5
Union Springs Shale	25'	Stop 5
Onondaga Limestone	120'	Stop 3

Lower Devonian (Ulsterian Series)

Rickard Hill Limestone (Schoharie)	0-1'	? Stop 3 ?
- ? disconformity ? -		
Carlisle Center Shale	10-40'	Stop 3
- ? disconformity ? -		
Escopus Shale	0-20'	Stop 3
- ? disconformity ? -		
Oriskany Sandstone	0-2'	Not present
- unconformity -		

Lower Devonian (Helderbergian Series)

Kalkberg Limestone	15-50'	Stop 6
Coeymans Limestone	90-100'	Stop 7
Manlius Limestone (lower Thacher member)	30-40'	Stop 4

Upper Silurian (Cayugan Series)

Cobleskill Limestone	10-12'	Not observed
- ? disconformity ? -		
Brayman Shale	100-200'	Not observed
Vernon Shale	0-80'	Not observed
- unconformity -		

Middle Silurian (Niagaran Series)

Herkimer Sandstone	0-40'	Not observed
Kirkland Hematite	0-2'	Not observed
- ? disconformity ? -		

|		
Willowvale Shale	0-30'	Not observed
- ? disconformity ? -		
Sauquoit Formation	0-130'	Not observed
Oneida Conglomerate	0-15'	Not observed
- unconformity -		

Middle Ordovician (Mohawkian Series)

Frankfort Shale	500-800'	Just past stop 8
Canajoharie Shale	200' (?)	Stop 9
Sugar River Limestone	15'	Stop 9
Kings Falls Limestone		
- unconformity -		

Lower Ordovician (Canadian Series)

Chuctanunda Creek Dolostone	20'	Stop 9
Tribes Hill Limestone	100'	Not observed

Upper Cambrian (Croixian Series)

Little Falls Dolostone	500'	Stop 10
- unconformity -		
Precambrian gneisses	?	Stop 10
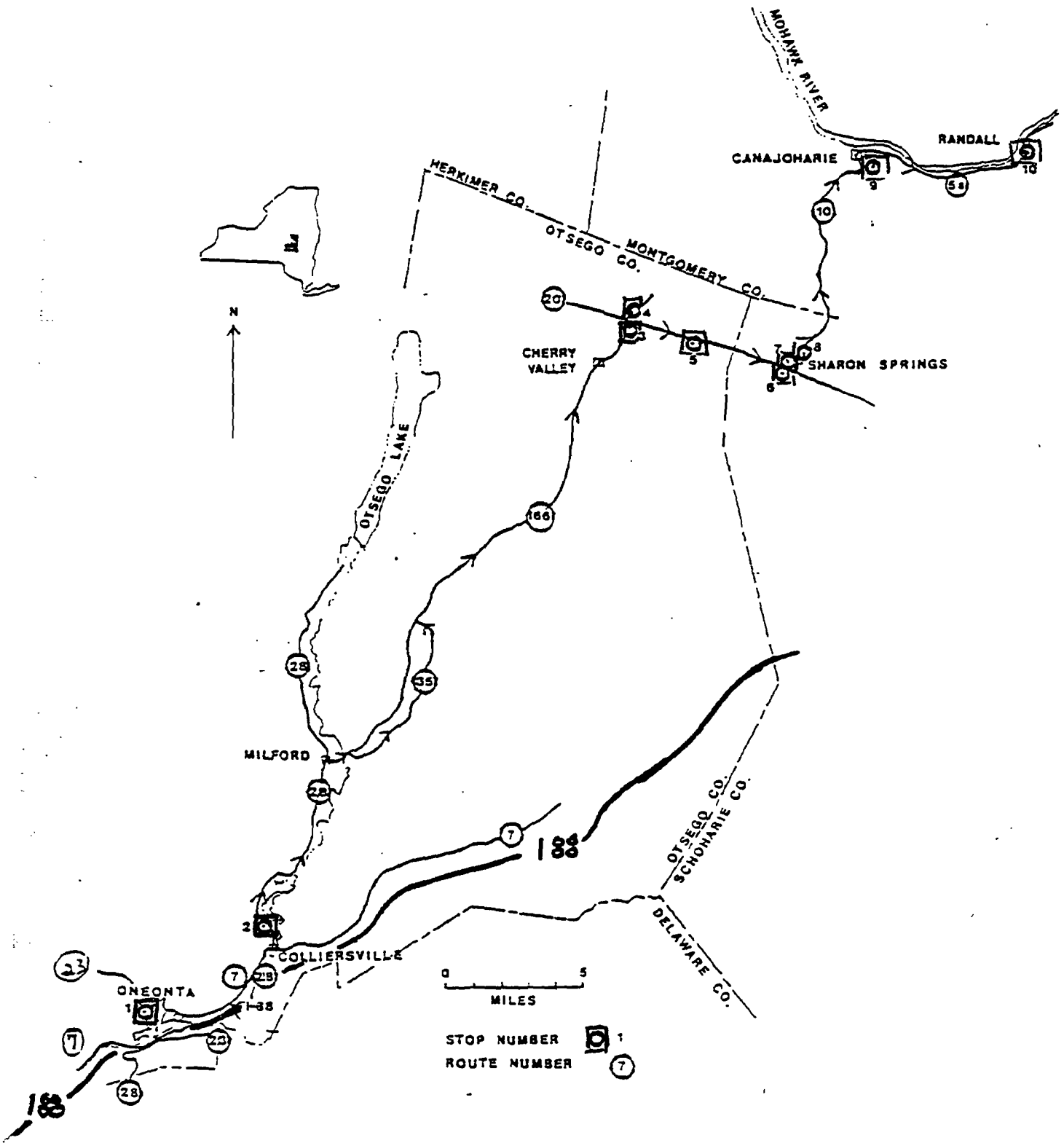
ROAD LOG

GEOLOGIC SETTING OF UPPER SUSQUEHANNA
AND ADJACENT MOHAWK REGION
Updated 8/28/98

Cumulative Mileage	Route Description
0.0	**ASSEMBLY POINT**: Upper Devonian Outcrop (250 feet long, 15 feet high) next to Miller Science Building (West end of Arnold Hall Parking Lot). Drive up main entrance (two brick pillars). Either left or right fork will bring you to Arnold Hall Parking Lot and Miller Science Building.

Departure: At 10:00 a.m. (or until group arrives from Binghamton)

Stop 1 Upper Devonian Oneonta Formation

This outcrop consists of dark grey shales, thinly bedded siltstones and sandstones. A massive sandstone which fills in part of a Devonian stream channel is well exposed for about 150 feet at the left end of the outcrop. There is an erosion surface between the underlying shale and the overlying massive sandstone. This surface which marks the bottom of the channel rises stratigraphically to the right. Interference ripple marks are exposed just below the road level. Plant materials are abundant in some layers. A few galena crystals about 1mm across have been found in the thinly bedded sandstone.

Trilobites, marine pelecypods and brachiopods of the Gilboa Formation have been found in beds stratigraphically 75 feet below this outcrop, and marine fossils are found in thinly bedded siltstones and shales stratigraphically 200 feet below stop 1. This outcrop is next to Nick's Diner on Chestnut Street. We probably will not stop here today.

A clean sandstone which shows extensive trough-type cross bedding overlies this outcrop.

Stop 1A is about 200 feet higher in elevation. Follow the road to the Ernest B. Wright Observatory.

Red mudstones and shales with root casts, worm burrows and ripple marks are exposed at the top of the hill just below the Ernest B. Wright Observatory which houses a 16" telescope.

The view down the valley is looking southeast to Mr. Utsayantha in Stamford (about 30 miles map distance). The broad U-shaped valley is the result of a Pleistocene glaciation. The Susquehanna River flows in from the north (out of your view) and through the city of Oneonta. The terraces on either side of the valley are kame terraces. Red beds are exposed near the top of the hills across the valley.

LEAVE STOP 1A AND GO BACK DOWN HARTWICK DRIVE TO WEST STREET AT THE MAIN ENTRANCE TO HARTWICK COLLEGE. (.5 miles)

TURN RIGHT (SOUTH) ON WEST STREET and continue going down hill. (For .2 miles)

TURN LEFT (EAST) ONTO CENTER STREET which is immediately past the Lutheran Church. (This is called "crash corner" for obvious reasons.)

CONTINUE ON CENTER STREET FOR .6 MILE TO WALLING AVE. TURN RIGHT (SOUTH). Walling Ave. is the first street to the right immediately after your cross Oneonta Creek at the entrance to the park.

Set Odometer Here
0.0

TURN LEFT (EAST) AT FRIENDLY ICE CREAM. You are now on Main Street and Route 7 And 28. (Stay on this road for 4.8 miles to Colliersville.)

0.1

Fox Hospital on your right.

129

1.2	Small kettle hole on right. This has been partially filled in to make a parking lot.
1.7	View to right showing kame terraces across valley.
2.3	Access to I88 (continue going straight)
3.2	On right (South) across valley gravel pit in delta Kame.
4.9	**TURN LEFT (NORTH) ONTO ROUTE 28 IN COLLIERSVILLE AT JUNCTION OF ROUTE 28 AND 7.**
5.4	Stop sign; turn left (North)
5.8	STOP 2 Stop directly next to dam at Goodyear Lake. There is parking on right (East) side of the road. The Upper Devonian Gilboa Formation with horizontal sandstones and siltstones is exposed here. The well developed flowrolls are of interest. It is apparent that these are primary structures (formed while the sediment was still "soft"), rather than secondary structures (formed after lithification), but there is some question as to Their origin. There are brachiopods, bryozoans, crinoids and pelecypods in some layers.
8.4	Outcrop of Middle Devonian Cooperstown Shale at curve in road. Good view ahead of broad U-shaped valley. The Susquehanna River flows south from its headwaters in Otsego Lake (Cooperstown) in this valley.
10.7	Spring 1998 Tornado damage on hillside to west.
13.3	**TURN RIGHT (EAST) IN MILFORD ONTO ROUTE 166.**
14.0	Cross Susquehanna River. Clays indicate a glacial Lake occupied this area. Grass now covers the glacial clays.

130

14.2	**TURN RIGHT ONTO OTSEGO COUNTY 35** and take metal bridge over Cherry Valley Creek.
14.3	Bear left at junction
18.1	Old Church on right
18.7	Westville Cemetery on left.
19.7	**TURN LEFT (WEST) AND CROSS CHERRY VALLEY CREEK.** After crossing the creek, NOTE THE EXCELLENT hummocky morainic deposits showing numerous kettle holes and knob and kettle topography.
20.6	**TURN RIGHT (NORTH) AND GO NORTH ONTO ROUTE 166.**
22.4	OTSEGO 52
29.5	Town of Roseboom. Rte 165 – Rte 66
33.1	Cherry Valley Massacre Monument
33.3	Cherry Valley – The town was settled about 1740. On November 11, 1778 over 40 people were killed by Tories and Native Americans in the infamous Cherry Valley Massacre.
33.7	Limestone Bldgs. Route #166 verge left
35.4	STOP 3 (Pull off road to left and park in Highway Department gravel and salt storage area.) Topographically this spot is a break in the Helderberg escarpment. Fairchild interpreted this as a glacial spillway formed at a time when ice filled most of the Mohawk Valley. Meltwater was blocked from draining north and "spilled over" the escarpment eroding the valley (Fairchild, 1925). Fleischer (personal communication) feels that the valley is the result of glacial scouring of a through valley.

Three formations are exposed here. The lowest formation (exposed about .1 mile down the |

road) is the Esopus Shale. This is overlain by the Carlisle Center calcareous siltstone which contains numerous worm burrows Toanurus cauda-galli (Rickard and Zenger, 1964). About .1 mile south along the road the Carlisle Center siltstone is overlain by the Middle Devonian Onandaga Limestone which contains crinoids, corals, and brachiopods.

The upper part of the Onondaga contains abundant chert. Jointing is very obvious at this outcrop.

LEAVE STOP 3 AND CONTINUE GOING STRAIGHT AHEAD AND GO UNDER ROUTE 20.

36.3

STOP 4 The Lower Devonian Manlius Formation (lower Thacher Member) crops out on the right. This laminated micrite contains some ostracods, teentaculitids and stromatoporids. Some mud cracks are present. This is the intertidal facies of LaPorte, 1967. The Coeymans Formation rests on top of the Manlius Formation.

TURN AROUND AND GO SOUTH TO ROUTE 20 EAST.

GO EAST ON ROUTE 20 FOR 2.6 MILES

TURN RIGHT OFF OF ROUTE 20 ONTO BLACKTOP ROAD AND PROCEED TO THE OUTCROP VISIBLE TO THE RIGHT.

STOP 5 Three Middle Devonian formations are exposed here. The lower most formation is the Union Springs Shale which is a black fissile shale containing calcareous concretions. There is a thin limestone near the top of the shale. This is overlain by the Cherry Valley Limestone which is about 7 feet thick and contains a cephalopod fauna. More than 100 feet of the jet-black Fissile Chittenango Shale rests on top of the Cherry Valley Limestone. At the east end (left) of the outcrop the Union Springs Shale has been broken up and sheared indicating some minor faulting.

Reset Odometer	
	RETURN TO ROUTE 20 AND CONTINUE GOING EAST.
0.0	Schoharie County Line. Reset Odometer to 0.0
1.7	STOP 6 Pull off the road and stop at down-going slope of hill. The Lower Devonian Kalkberg Limestone is exposed in a fresh outcrop. This is a medium grained thin to medium bedded limestone with abundant chert. There are numerous brachiopods, bryozoans, some corals and trilobite fragments. A 2" thick layer of bentonite is exposed near the eastern end of the outcrop (at the east end of grassy field below outcrop there is a small creek that disappears into a sink hold in the limestones.)
2.2	IN SHARON SPRINGS TURN LEFT (NORTH) AT STOPLIGHT ONTO ROUTE 10 AND PROCEED NORTH FOR .1 MILE TO OLD QUARRY NEXT TO BOWLING ALLEY.
2.3	STOP 7 (in old quarry) The Lower Devonian Coeymans Formation consists of a coarse grained, thickly bedded limestone with abundant brachiopods, crinoids and corals.
	LEAVE THE QUARRY AND PROCEED DOWN THE HILL.
2.9	STOP 8 (STOP AT PARK NEXT TO OLD (BATHS) Stop to look at springs and tufa deposits in the city park at the north end of the village of Sharon Springs. There is a strong odor of H2S from the spring water. This is probably caused by the water passing through the underlying thick black shales.
3.1	Upper Middle Ordovocian Shales and Sandstones Exposed in cliff at left.
4.9	Montgomery County Line
5.9	Two drumlins are in view to the left.

11.6	IN CANAJOHARIE TURN RIGHT AT THE FIRST STOPLIGHT ONTO MONTGOMERY STREET.
11.7	CROSS OVER CANAJOHARIE CREEK AND TURN RIGHT ONTO MOYER STREET. CONTINUE ON MOYER STREET. SIGN FOR WINTERGREEN PARK.
12.0	TURN RIGHT ONTO FLORAL AVENUE AND PROCEED TO THE TURN-AROUND AT END OF ROAD.
12.2	STOP 9 Four Lower and Middle Ordovician Formations are exposed in Canajoharie gorge. The lower most formation is the Chuctanunda Creek Dolostone. This is unfossiliferous except for the "hippopotami backs" which are dolomitized hemispherical stromatolites (algal mounds) (Park and Fisher, 1969). Large potholes have formed in the dolostone (Canajoharie is the Iroquois name for the "Pot that washes itself") (Park and Fisher, 1969).

The Middle Ordovician Kings falls and Sugar River black limestones overlay the dolostone, forming a disconformity. These limestones and the thin black shales in them contain abundant trilobite fragments, bryozoans, brachipods and crinoids.

The limestones are overlain by more than 100 feet of Middle Ordovician Canajoharie Shale. |
12.4	RETURN TO JUNCTION OF FLORAL AVENUE AND MOYER STREETS. TURN LEFT AND GO DOWN HILL.
12.7	CROSS MONTGOMERY STREET AND GO ONTO MITCHELL STREET (WHICH IS 30 FEET LEFT AND PARALLEL TO CANAJOHARIE CREEK).
12.8	CROSS RAILROAD TRACKS AND TURN RIGHT ONTO ROUTE 5S AT THE BEECHNUT FACTORY. Continue on Route 5S.

En route to the next stop note the cliffs of Upper Cambrian Little Falls Dolostone.

19.3   STOP 10 Rusty weathering Precambrian garnet gneiss exposed along the south side of the road and in railroad cut.

FOLLOW THE FOOT PATH AT THE EAST END OF THE OUTCROP TO THE RAILROAD CUT. BEWARE OF POISON IVY ALONG PATH AND AT RAILROAD CUT.

The folded Precambrian gneiss is overlain by the Upper Cambrian Little falls Dolostone. The Dolostone is brecciated for several feet above the contact with the gneiss. Apparently there was movement along the unconformity during Ordovician time when the normal faults in the Adirondack Mountains and the Mohawk River Valley were formed. There are also good exposures of the gneiss north of this outcrop across the Mohawk River along Route 5 (5.4 miles east of Palatine Bridge).

PROCEED EAST TO OBSERVE THE FAULT-LINE SCARP OF NOSES FAULT FROM THE VEHICLES.

Overpass of Route 5S over the railroad tracks. Note that west of the Noses faulty-line scarp the Mohawk Rive Valley has steep cliffs of Little falls Dolostone. These are caused by the down cutting of the Mohawk River on the upthrown western side of the fault. East of the fault-line scarp on the downthrown side of the fault-line scarp there are no cliffs.

20.3   END OF TRIP AT RANDALL.
Note: Time may not permit us to stop at all of the Stops. Depending upon the interest of the group, certain stops may be omitted.

(Total Distance 60 miles)